UNIVERSITÀ DEGLI STUDI DI PADOVA

DIPARTIMENTO DI INGEGNERIA ELETTRICA

SCUOLA DI DOTTORATO DI RICERCA IN
INGEGNERIA INDUSTRIALE
INDIRIZZO ENERGETICA
CICLO XXI

Models for the investigation of the results of MHD mode active control in RFX-mod

Direttore della scuola: prof. Paolo Bariani
Supervisori: prof. Antonio Buffa
dott. Roberto Paccagnella

Dottorando: Andrea Pizzimenti

31 gennaio 2009

Contents

Abstract

In this Ph.D. thesis we report the work performed at Consorzio RFX[1] in Padua, where a large RFP device is set to study magnetically confined plasmas for thermonuclear fusion.

Particular configurations of magnetic fields permit this confinement. The *tokamak* is been the most successful concept of toroidal machine, but alternative concepts, like *reversed field pinch* (RFP) and *stellarator*, have been developed for a commercial application (fusion power plant). All the present experiments are inductive and pulsed. ITER[2] machine will work stationary and will demonstrate the scientific and practical feasibility of thermonuclear fusion.

To reach this goal many questions have to be solved: the in-depth comprehension of transport mechanism for to achieve the better plasma confinement, equilibrium and stability; the crucial topic of magnetohydrodynamics (MHD) instability control (or *mode control*); the development of right materials for the first wall; the utilization of superconductive magnets; the problem of the plasma impurities, due to the plasma-wall interaction.

Linear MHD is a fundamental model in plasma physics and in fusion research, providing basic ideas about the system stability, the dominant modes and their spatial structure. However, strong non-linear effects are also at work and the most important is the so-called *dynamo effect*: the RFP configuration is sustained in a steady state by the generation of a plasma self-induced electric field. This *dynamo electric field* originated, in turn, from the non-linear coupling between magnetic and velocity fluctuations. There are also other interesting phenomena linked to the mode couplings. In all these cases, their exploration and the investigation of their mechanisms is an important issue in order to understand the nature of the RFP sustainment.

In the last decade, several experiments carried out and theoretical studies indicate that MHD instabilities can be stabilized by active feedback. In this work we consider feedback systems for the RFP, using a reasonably realistic geometrical description of the coils.

[1] RFX is acronym for *Reversed Field eXperiment*.

[2] The acronym means *trail* or *path*, *the way* in latin. ITER is for *International Tokamak Experimental Reactor*.

A feedback model, inspired by previously works, it is developed and applied for the $m = 0$ modes. In particular, the *sidebands effect* is taken into account, well reproduced by the model itself. In fact, owing to the limited number of active coils the field generation is affected by the coupling of different Fourier components.

Then, we propose an analysis of the experimental data obtained in the RFX-mod device in order to shed some new light on the mode coupling among magnetic perturbations. The model mentioned above permits to investigate the $m = 0$ behavior, linked to the $m = 1$ couplings. Even though several experiments have been carried out in the past in an attempt to quantitatively determine the mode coupling in RFPs, the peculiarity of this study is that the coupling is estimated by actively applying an $m = 0$ perturbation to the plasma.

Successively, a second model concerning $m = 1$ modes has been designed.

The thesis is organized in three big Sections.

In Chapter 1 a general introduction on the topic argument is provided: the energy question, the fundamental of MHD-theory, with particular consideration to plasma equilibrium and stability. In Chapter 2 we present and describe in depth the linear model developed, from the basis equations to the final relations. In Chapter 3 we present the application of the code for $m = 0$ modes, from its validation to the physical interpretation of the results, and the structure of the model for the $m = 1$ modes.

Sommario

Nella tesi di Dottorato qui presentata è illustrato il lavoro svolto presso il Consorzio RFX[3] di Padova, dove è messo a punto un grande dispositivo RFP per lo studio di plasmi magneticamente confinati per la fusione termonucleare.

Configurazioni particolari di campi magnetici permettono questo confinamento. Il *tokamak* è stato il concetto di macchina toroidale di maggior successo, ma concetti alternativi, come *reversed field pinch* e *stellarator*, sono stati sviluppati per applicazioni commerciali (centrale a fusione). Tutti gli esperimenti attuali sono induttivi e pulsati. La macchina ITER[4] lavorerà in stato stazionario e dimostrerà la fattibilità pratica e scientifica della fusione termonucleare.

Per raggiungere questo obiettivo molte questioni devono essere risolte: la comprensione approfondita dei meccanismi di trasporto per ottenere i migliori confinamento, equilibrio e stabilità di plasma; il tema cruciale del controllo della instabilità magnetoidrodinamiche (MHD) (o *controllo dei modi*); lo sviluppo dei giusti materiali per la prima parete; l'utilizzo di magneti superconduttori; il problema delle impurità di plasma, dovuto alla interazione plasma-parete.

L'MHD lineare è un modello fondamentale sia in fisica del plasma che nella ricerca sulla fusione, fornendo idee base sulla stabilità dei sistemi, sui modi dominanti e la loro struttura spaziale. Comunque, agiscono anche forti effetti non-lineari e il più importante è il c.d. *effetto dinamo*: la configurazione RFP è sostenuta in stato stazionario dalla generazione di un campo elettrico autoindotto nel plasma. Questo *campo elettrico dinamo* è originato, a sua volta, dall'accoppiamento non lineare tra fluttuazioni magnetiche e di velocità. Ci sono anche altri fenomeni interessanti legati all'accoppiamento dei modi. In tutti questi casi, la loro esplorazione e l'investigazione del loro meccanismo è una importante questione per comprendere la natura del sostenimento della configurazione RFP.

Nell'ultimo decennio, diversi esperimenti effettuati e studi teorici indi-

[3] RFX è acronimo di *Reversed Field eXperiment*.

[4] L'acronimo significa *cammino* o *percorso*, *la via* in latin. ITER sta per *International Tokamak Experimental Reactor*.

cano che le instabilità MHD possono essere stabilizzate per mezzo di feedback attivo. In questo lavoro sono considerati sistemi di feedback per RFP, usando una descrizione della geometria delle bobine ragionevole e realistica.

È stato sviluppato ed applicato un modello di feedback per i modi $m = 0$, ispirato a studi precedenti. In particolare, sono considerate e riprodotte accuratamente le *sidebands*. Infatti, a causa del numero limitato di bobine attive, la generazione del campo è influenzata dall'accoppiamento delle diverse componenti di Fourier.

È quindi proposta un'analisi dei dati sperimentali ottenuti dal dispositivo RFX-mod, per far chiarezza sull'accoppiamento dei modi delle perturbazioni magnetiche. Il modello su citato permette di investigare il comportamento dei modi $m = 0$, legati all'accoppiamento non lineare degli $m = 1$. Sebbene diversi esperimenti RFP siano stati effettuati nel passato, nel tentativo di determinare quantitativamente l'accoppiamento dei modi, la peculiarità dello studio qui presentato è che l'accoppiamento viene stimato applicando attivamente una perturbazione $m = 0$ al plasma.

Successivamente, è stato progettato un secondo modello che riguarda i modi $m = 1$.

La tesi è organizzata in tre grandi Sezioni.

Nel Capitolo 1, è fornita una introduzione generale sugli argomenti di interesse: la questione energetica, i fondamenti della teoria MHD, con considerazioni particolari su equilibrio e stabilità del plasma. Nel Capitolo 2, si presenta e descrive in profondità il modello lineare sviluppato, dalle equazioni di base alle relazioni finali. Nel Capitolo 3, è illustrata l'applicazione del codice per i modi $m = 0$, dalla sua validazione all'interpretazione fisica dei risultati, e l'intelaiatura del modello per i modi $m = 1$.

CHAPTER 1

Thermonuclear magnetic controlled fusion

1.1 The Energy problem and the Thermonuclear magnetic controlled fusion

1.1.1. Resources and energy

The energetic system is the base of the modern society as we know it in all its own social, cultural and technological aspects. This means that ensuring us the subsistence level (in fact much more than it), we can avoid to spend the most part of our time for to satisfy the primary necessities. So, we can consider as yield of the energy all the materials goods, the market goods and those cognitive and recreational. Moreover the western social model is based on the *communication* meant as the faculty to communicate in real-time the information, with all the technological development able to reach such level. This require, in turn, a wide availability and use of energetic fuels: both the use of the media and to develop, as mentioned, the projects create by a such system.

It is well known that the humankind is going through a critical and unstable period with regard the energy resources. What's more, this question belongs to a wider range of problems, like climate, food, minerals, and so on. For this motivation, the solution of the energy problem must intercept the solutions of the other problems, as much as possible, in the framework of the sustainability.

Our energy future depends of uncertain elements of technological, environmental and political nature [2]. Today, most of the worldwide electricity demand[1] is satisfied by oil (41%), natural gas (22%), coal (16%), nuclear

[1]The importance of production and distribution of the electrical energy reside in its versatility and flexibility, with the possibility to be easily transferred to great distances and in capillary way. So, the *electrical penetration coefficient*, that is the ratio of electrical

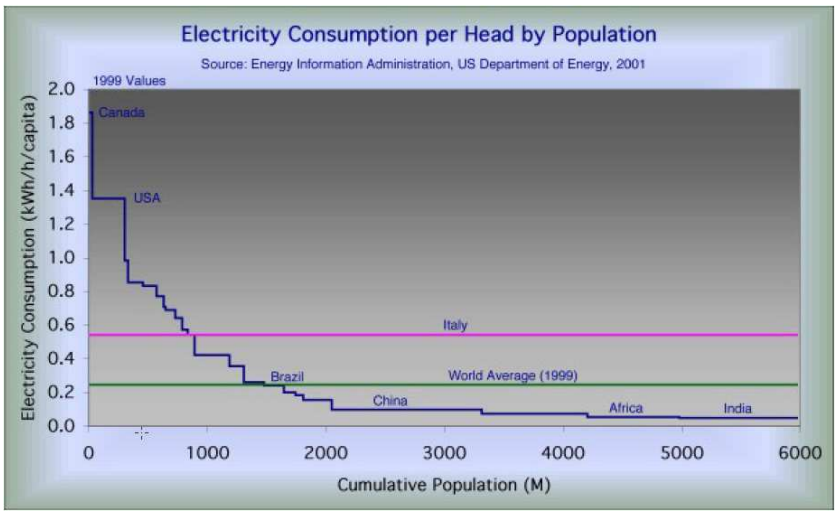

Figure 1.1: Electricity consumption per-capite in the world. From U.S. DOE site [1].

(15%) and renewables (6%). Between this technologies, only renewables and nuclear fission can limit the CO_2 emissions. The renewables, even if certainly, will contribute much more in the future, probably they will not be able to satisfy the total demand [4]. About the nuclear fission, we can say that it is a long-term energy source (at least when product by means of the breeder reactors), with known impacts to the economics and environmental cycles; but, at the end, the spread of nuclear plants depends on the public appreciation of options and alternatives.

It is well known that the curve of the exploitation of particular resource (energetics or minerals) mined in a geographical area large enough, without social or political upheavals and in free market condition, follows in time a bell-shaped curve in which the side after the maximum (that is said *Hubbert's peak*) is much more steep than the side before the peak itself (see figure 1.2). So, this exploitation will end before of the complete exhaustion for the unavoidable turn up of technological problems and, consequently, unsustainable costs. The Hubbert's peak indicates this watershed; for the oil it is estimated between the 2010 and the 2020 [5].

At the actual consumption rate and supposing to utilize only one kind of fuel for time, they can endure (upper limits): oil and natural gas $30 \div 50$ years, coal $6 \div 7$ centuries, U^{235} (fuel for conventional fission reactors) few decades, U^{238} (fuel for the breeder reactors) $10^4 \div 10^5$ years. Obviously the

energy consumption respect to the total energy consumption, give an idea of how the diffusion of the first one is related to the industrial development (for example, in Italy this number is passed from 0.241 in 1963 to 0.351 in 2003 [3]).

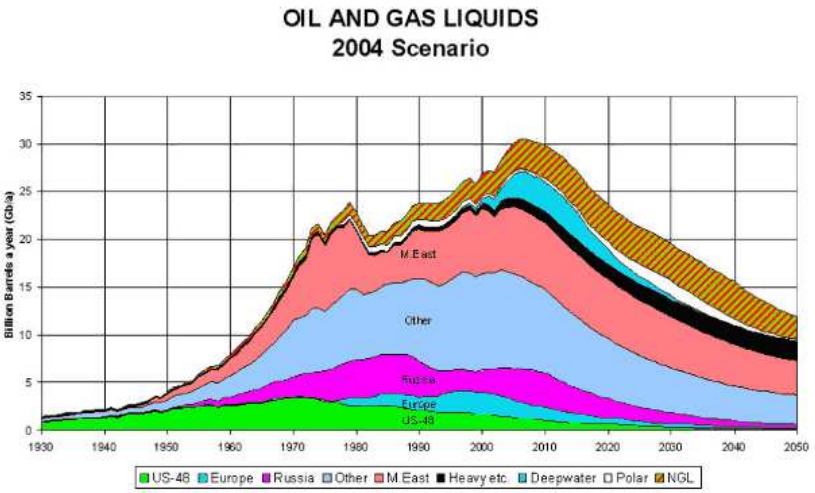

Figure 1.2: Production of oil and NGL in the 2004 scenario: the Hubbert peak, i.e the . From Aspo site [6].

renewables technologies have virtually unlimited "fuels" at one's disposal.

It is clear that this rates sketch an optimistic picture: strong economic growth in many developing countries is leading to sharp increases in energy consumption (both gross and per-capita). So, it is unrealistic to estimate supposing to utilize *only one kind of fuel for time*; rather, the estimate above can be taken as a lower limit. Also, much better use could be made of the raw materials burned that are irreplaceable for the chemical and farmaceutical industries [2][7].

Besides, the energetic consumption is tied to the mean income for person; today, the most of the mankind life in poverty whereas in the high income countries there is waste of energy. We consider the yearly use of primary energy per person: the worldwide mean, in 2002, was 1.65 toe, but with enormous disparity. In the USA this value was 8.32 toe; the mean of OECD countries[2] was 3.36 toe; in Brazil 1.07 toe; in China 0.87 toe; in India 0.48 toe; in Africa 0.63 toe [8]. Nevertheless, to eliminate the wastes of energy and a simple redistribution of the energy today consumed would be not enough, alone, to permit the development of poorest countries up to acceptable levels.

Again, the estimated demographic growth [9] will imply the foods problem and so the research of the adequate energy to produce and to distribute the food, with consequent political instabilities [2].

This raise of energy (i.e in global energy consumption) will increase the

[2]OECD is for Organization for Economic Co-operation and Development. OECD countries are: EU, Iceland, Norway, Switzerland, Czech Rep., Hungary, Poland, Slovakia, Turkey, Canada, Mexico, USA, Australia, New Zealand, Japan, South Korea.

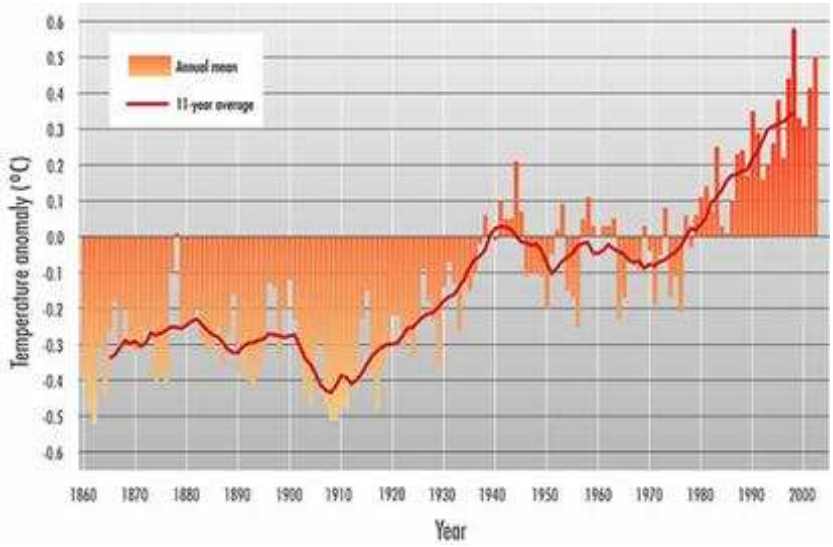

Figure 1.3: Northern hemisphere average surface temperature. From Aspo site [6].

amount of fossil fuels necessary, but with big additional environmental and supplying problems, from high pollution (and linked health problems) to climate changes [2][10][11][12]. For example, let consider the northern hemisphere average surface temperature in the last 1000 years, shown in figure 1.3, and the atmospheric CO_2 increase on a very rapid timescale, shown in figure 1.4. In particular, the steeply slope is clearly referred to the industrial revolution (see figure 1.5).

So, it is crucial to diversify the energetic sources for the production of energy (in particular electric energy), give priority to the more available fuels, to the more advanced technologies and to the sources free from altering-climate emission.[3]

Fusion energy could be one of these possibilities.

1.1.2. Thermonuclear fusion: energetic considerations

Thermonuclear fusion relates to a nuclear reaction where two light nuclei fuse into a heavier one, producing also neutrons. This is the mechanism that permit the energy production in the stars, and then their shining.

Two nuclei can fuse together if they are close enough $d \approx 10^{-13} cm$ to the point that the short-range attractive nuclear force overcomes the Coulomb repulsion among them. So, for to bring at the right distance the nuclei,

[3]For the author it is also important to consider the reduction of the consumption and of a drop of the obsessive run up of the growth, acting primarily on the life-style and on the economical system.

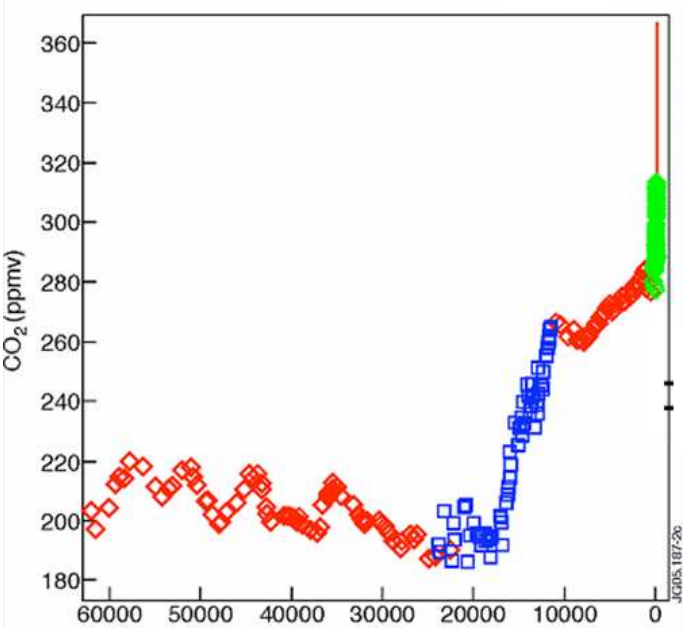

Figure 1.4: Carbon dioxide levels in atmosphere, in the last 60000 years (in the abscissa, years before present). From [2].

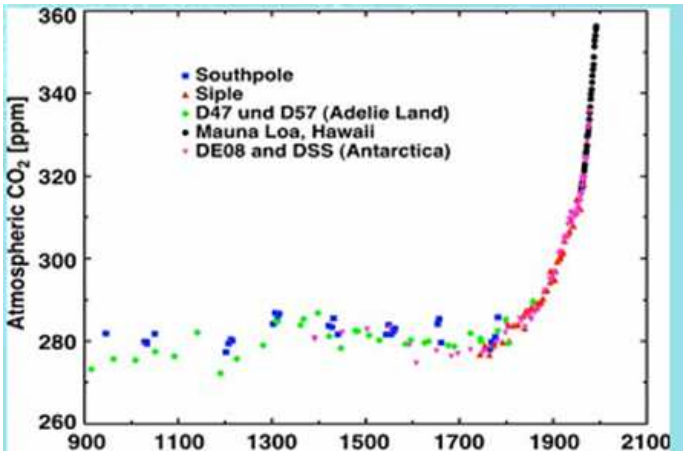

Figure 1.5: Carbon dioxide levels in atmosphere, from 900 b.c. to now. From [2].

we (or the nature, in the case of the stars) must give them enough kinetic energy. This is the main obstacle to obtain nuclear fusion; for example, the energy needed to overcome the Coulomb-wall for two hydrogen nuclei is about $0.4MeV$. But luckily the *quantum tunneling* through the Coulomb

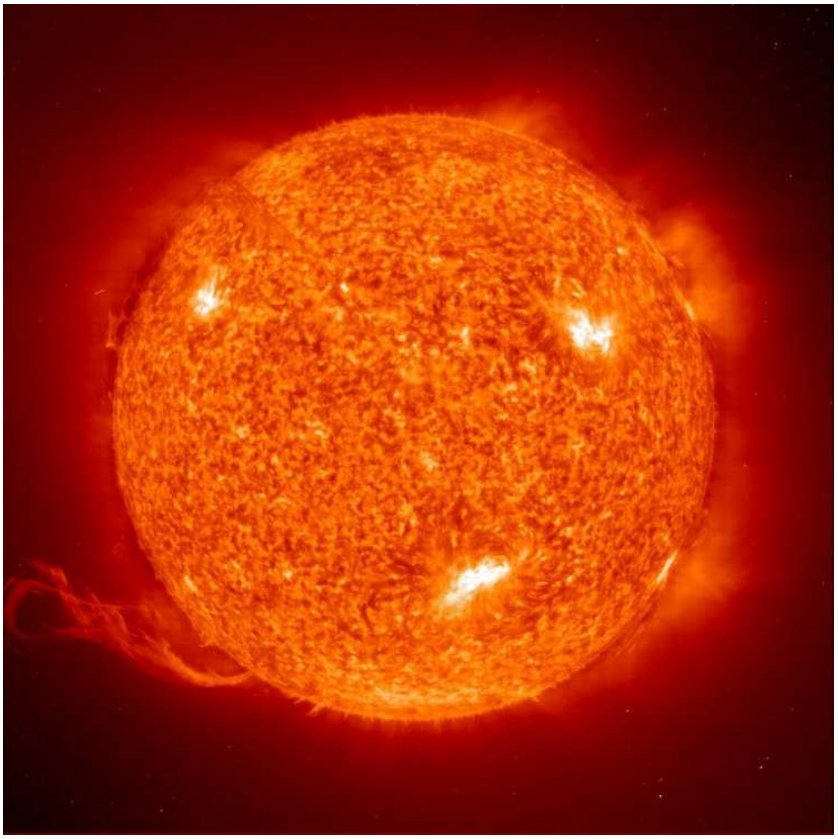

Figure 1.6: The Sun. From the NASA astronomical pictures archive [13]. For comparison, the Earth is an invisible point.

barrier makes lower temperatures possible [14].

More than 80 different fusion reactions are currently known; since the lowest Coulomb repulsion verifies for nuclei with lower atomic number, fusion reactions between hydrogen isotopes require the lowest plasma temperatures.

The fusion reactions must happened in a significant fraction and this is possible only for a sufficiently high density and temperature and for a sufficiently long time: matter is in its fourth state, i.e. the *plasma* state, a quasi-neutral ensemble of ions and electrons [14][15].

In the stars like the Sun, the reactions that permit them to burn and light are those belonging to the *proton-proton cycle* [16][17]:

$$p_1^1 + p_1^1 \rightarrow D_1^2 + e^+ + \nu + 1.44MeV \tag{1.1}$$

$$D_1^2 + p_1^1 \rightarrow He_2^3 + \gamma + 5.49MeV \tag{1.2}$$

$$He_2^3 + He_2^3 \rightarrow He_2^4 + p_1^1 + p_1^1 + 12.86MeV \tag{1.3}$$

(the third reaction is only possible at temperature above $10^7 K$).

For several decades researchers have studied the possibility of realizing analogous reactions, but controlled, on Earth, in order to produce energy for civil and peaceful purpose. The main line for to obtain this on terrestrial laboratories is the *magnetic confinement fusion*, where strong magnetic fields confine the plasma: in fact it is well known that a charged particle in a magnetic field make a spiral motion around the magnetic field lines.[4]

The most important fusion reactions for the controlled thermonuclear reactor are the following:

$$D_1^2 + D_1^2 \rightarrow He_2^3 + n_0^1 + 3.3MeV; \tag{1.4}$$

$$D_1^2 + D_1^2 \rightarrow T_1^3 + p_1^1 + 4.0MeV; \tag{1.5}$$

$$D_1^2 + He_2^3 \rightarrow He_2^4 + p_1^1 + 18.4MeV; \tag{1.6}$$

$$D_1^2 + T_1^3 \rightarrow He_2^4 + n_0^1 + 17.6MeV; \tag{1.7}$$

The total energy output is distributed between the kinetic energy of the products. The charged particles are confined by the magnetic field containing the plasma and used to heat the fuel; neutrons and the others neutral particles escape through the wall of the device and will be absorbed by a blanket. The reactions 1.4 and 1.5 trigger for temperatures higher than $\sim 20keV$, optimum at $\sim 40keV$; the reaction 1.6 triggers for temperatures higher than $\sim 30keV$; the reaction 1.7 happens at the lower trigger temperature, $\sim 5keV$, optimum at $\sim 15keV$. Another datum to utilize as terms of comparison is the equivalent electrical energy given to the produced nuclei respect to the masses of reagent nuclei. This is, for every reactions above: 98 and $94kWh/g$ for the reactions 1.6 and 1.7, 27 and $22kWh/g$ for the reactions 1.5 and 1.4, respectively.

The reaction frequency is a crucial issue. The *reaction rate* R is proportional to the density of the species involved and to the product σv, where the average is done over particles of all the possible velocities, σ is the fusion cross-section and v is the relative velocity between the reacting particles.

As example, the fusion rates of the reaction from 1.4 to 1.7, in terms of σv, are shown in the figure 1.7. In particular, we can see that the highest reaction rates at lower temperature ($E \leq 20keV$) exists for the D-T reaction and hence this is the best choice for a fusion reactor. It is important to evaluate the amount of fuels for this reaction, available on the Earth.

These are the main motivations to use, in the nuclear fusion plants, the reaction 1.7, where the main portion of the energy is released to the neutron. Although the fast fusion neutrons created lead to secondary radioactivity in

[4] Another line to pursuit nuclear fusion is the *inertial confinement fusion*, where a small quantity of solid matter is compress by means lasers (or any other high power source) that hit it from many directions. So the system is brought to the critical condition to activate the fusion reaction. For a simple introduction see [18].

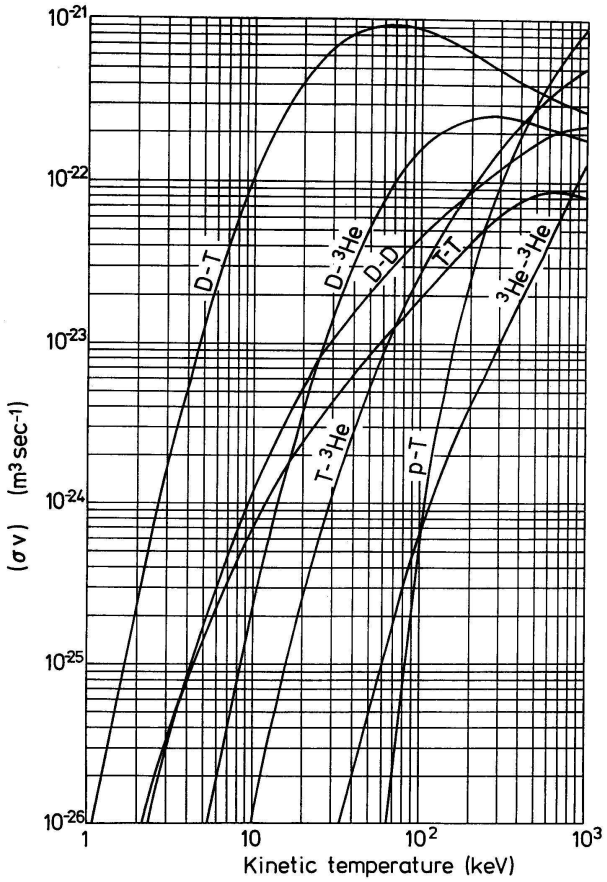

Figure 1.7: Fusion reaction rates for the main reactions interesting the controlled thermonuclear reactors. From [19].

the materials surrounding the plasma, this must be considered an advantage: neutrons don't carry electric charge and so are not held back by the magnetic field. Penetrating the confinement vessel, they can hand over their energy to a moderator.

According to the expression for the *Gamow factor*[5], it is only a small fraction of highly energetic particles that are reacting, and then lost through fusion. This tail is repopulated by scattering collisions (that in the other hand cause diffusion and particle losses from the vessel) and so the plasma approach a Maxwellian distribution: this is an essential characteristic of thermonuclear fusion [20].

The 0.0015% of of hydrogen atoms in water is deuterium: since the total amount of water is estimated in $\sim 10^{13} tonnes$, deuterium resources

[5]The Gamow factor gives the quantum probability for penetrating the Coulomb wall; it is proportional to $exp(-cost/\sqrt{E_{kin}})$.

are practically endless. Today is easily pay for $1 euro/g$ [2][20].

Tritium is a radioactive isotope of hydrogen with half-life of 12.3 years, following the reaction $T_1^3 \rightarrow He_2^3 + \beta^- + \bar{\nu_e}$ and so it occurs in nature in negligible quantity. But we can obtain tritium from the lithium, in accordance with the reactions:

$$Li_3^6 + n_0^1 \rightarrow T_1^3 + He_2^4 + 4.6MeV \tag{1.8}$$

$$Li_3^7 + n_0^1 \rightarrow T_1^3 + He_2^4 + n_0^1 - 2.5MeV \tag{1.9}$$

The reaction 1.9 is endothermic and generates a neutron that permits the continuation of the breeding reaction. This is the motivation why is conceived a lithium blanket on the vacuum vessel of fusion reactors: in order to provide the necessary tritium source for a long, virtually unlimited, period of time. In fact the lithium is pay both from the sea ($\sim 10^{11} tonnes$) that mined from earth mines ($\sim 10^8 tonnes$ and a cost of $\sim 0.02 euro/g$).

Last but not least, the environmental aspects are in favour of fusion reactors: there is no production of greenhouse gases; there is no direct radioactive waste and, unlike in the fission reactors, there is no risk of uncontrolled runaway of the reactions.

1.1.3. Thermonuclear fusion: the burning criteria

The aim of the fusion research is to obtain that the energy balance of a fusion reactor to be positive. This means that *the energy produced by fusion reactions has to exceed that required to create and sustain the plasma itself.*

One form of energy loss for a D-T plasma with electron density n_e, with $n_D = n_T = n_e/2$, and temperature T_i is *bremsstrahlung radiation* [14][15]. It is well known that bremsstrahlung refers to any radiation due to the acceleration of a charged particle and, in particular, that one produced by an electron when deflected by another charged particle (typically, a nucleus). The power lost per unit volume due to bremsstrahlung emission is

$$P_b = bn^2 T^{1/2} \tag{1.10}$$

where b is a function of the effective charge $Z_{eff} = n_j^{-1} \sum_j n_j Z^2$ in a plasma made up by j different species [14][15].

Note that in a pure D-T plasma, *line and recombination radiation* do not play an essential role except for the much cooler (10^4 times) plasma boundary region: in fact, in the bulk of the plasma all ions are fully ionized and the central plasma is too hot for the recombinations.

Also power losses due to the confinement degradation, like through *collisional and turbulent transport phenomena*, must be considered [21]. Without to go into details, a simple estimate of all of this mechanism bring to

$$P_t = \frac{3nT}{\tau_E} \tag{1.11}$$

by introducing the average energy confinement time τ_E.

The power generated by fusion reactions can be written as

$$P_n = \frac{1}{4} W_{DT} n^2 \langle \sigma v \rangle_{T_i} \tag{1.12}$$

where $W_{DT} = 17.6 MeV$ is the energy released after a single D-T reaction and $\langle \sigma v \rangle_{T_i}$ is the D-T fusion reaction rate, that is function of the temperature T_i.

It is crucial to estimate when a fusion reactor releases so much energy that it can run in a self-sustained way. For this purpose, the general approach is to assume that the reaction power P_n can be convert in electric power with an efficiency η and then re-injected in the reactor in order to balance the energy losses. So, the *self-sustainment condition* is:

$$P_b + P_t \leq \eta (P_b + P_t + P_n) \tag{1.13}$$

This relation can be rewritten as

$$n\tau_E \geq 3T \left(\frac{\eta}{1-\eta} \frac{W_D T}{4} \langle \sigma v \rangle_{T_i} - b\sqrt{T_i} \right)^{-1} \tag{1.14}$$

and it is known as *Lawson's criterion* [22]. It is trivial to observe that $n\tau_E = f(T)$ i.e. the r.h.s. of equation 1.14 depends only on temperature and this relation can be plotted. In figure 1.8 is reported this function, assuming $\eta = 30\%$.

The most probable reactor scenario is one in which the α particles produced by fusion reactions are confined by the magnetic field and replace all the energy losses by transferring their energy to the plasma, whereas neutrons escape the plasma volume and their energy is converted to electric energy. In this case the relation 1.13 must be modified in the following way:

$$P_b + P_t \leq P_\alpha \tag{1.15}$$

that it is named *ignition criterion*. This new relation can be written as

$$n\tau_E \geq 3T \left(\frac{W_\alpha}{4} \langle \sigma v \rangle_{T_i} - b\sqrt{T_i} \right)^{-1} \tag{1.16}$$

where $W_\alpha = W_{DT}/5$ is the energy of a single α particle after a fusion reaction.

The $n\tau_E$ curve that corresponds to the equality is shown in figure 1.8 again. As the Lawson's criterion curve, the ignition curve has a minimum at $T_i \simeq 20 keV$.

Isolating the temperature dependence in the right term of equation 1.16 we obtain the classical form of the so called *triple product*:

$$n\tau_E T_i \geq 3 \cdot 10^{21} m^{-3} s \cdot keV. \tag{1.17}$$

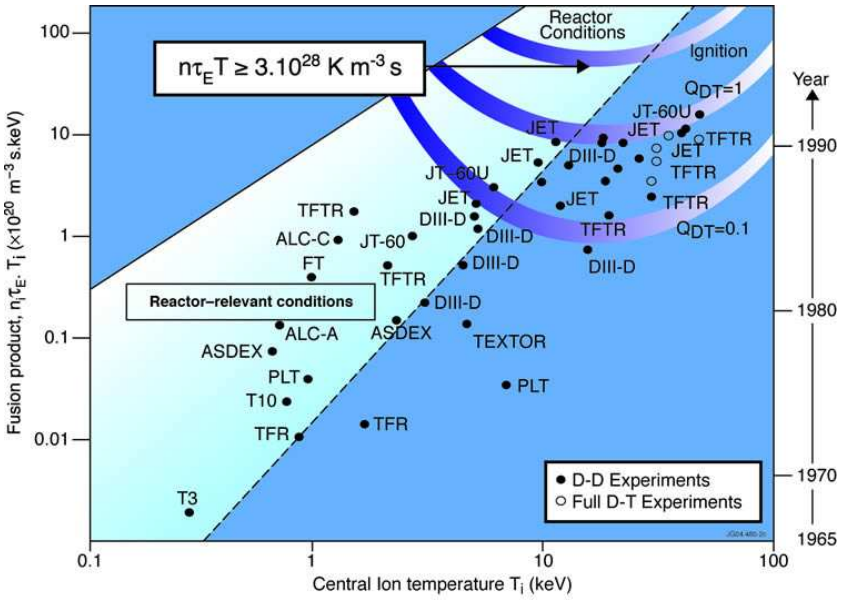

Figure 1.8: The triple product in fusion devices experiments, as a function of the central ion temperature. Let note the radiation limit (upper boundary).

The ignition happens for $P_{ext} = 0$, or $Q = \infty$. The equilibrium condition is achieved with $P_{ext} = P_{fus}$, or $Q = 1$.

Figure 1.8 shows the values of the triple product reached in fusion devices since the beginning experiment in plasma physics. The clear trend shows the improvement in confinement achieved up to now and the goal that the scientific community must reach to provide a fusion plant to the world [21][23].

ITER

All the experimental results in the last 30 years and the improving capability of numerical simulations have provided to the scientists the physics basis for the design of a burning plasma experiment based on the tokamak concept: ITER, acronym for *International Thermonuclear Experimental Reactor* [24][25]. The principal aims of ITER are:

- to achieve extended burn in inductively-driven plasmas with $Q = Q_{fus}/Q_{aux} \geq 10$ (at a nominal fusion power output of about 500MW) for a range of operating scenarios and with a duration sufficient ($\sim 400s$) to achieve stationary conditions;

- to aim at demonstrating steady state operation using non-inductive

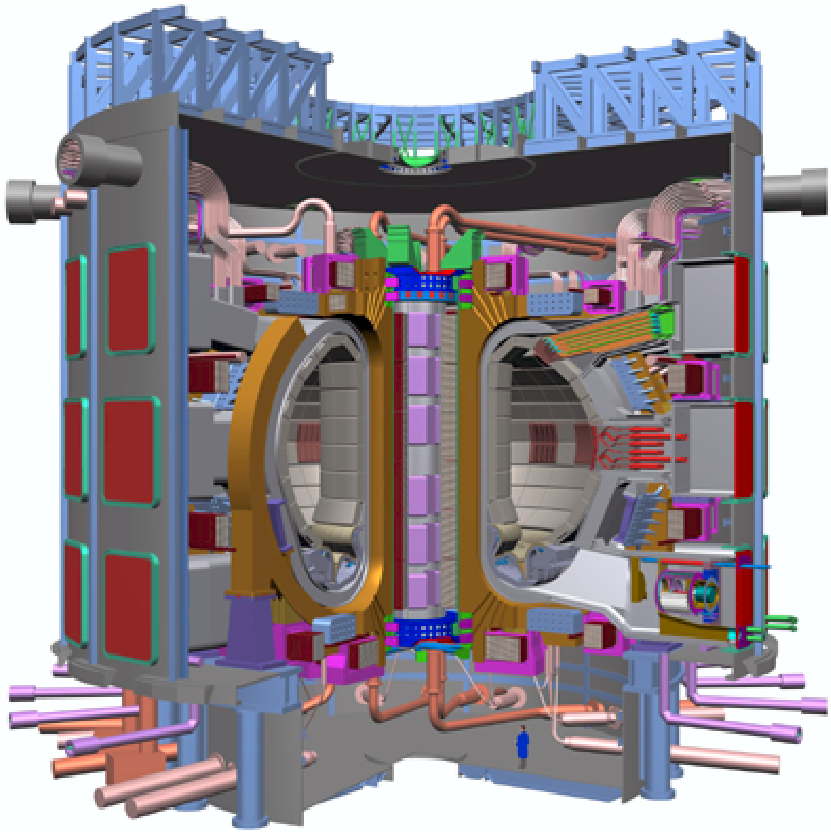

Figure 1.9: ITER. From [24].

current drive with a ratio of fusion power to input power for current drive of at least 5.

- the possibility of high Q operation will be explored if favorable confinement conditions can be achieved.

The main "numbers" of ITER are the following:

- $P_{out} = 500MW$ nominal;
- major radius $R_0 = 6.2m$;
- minor radius $a = 2m$;
- $B_{max} = 5.3T$;
- $I_p = 15MA$.

As we said, ITER is predicted to produce inductively driven D-T plasmas. These plasmas will be with density $n_e \approx 10^{20}m^{-3}$ and core electron and ion temperatures of $T_e \approx 8.8keV$ and $T_i \approx 8keV$.

New physical regimes and a variety of technological issues will be explored with ITER. For example, conditions in which the α particles contribute significantly to the plasma pressure, with a class of plasma instabilities which can be studied in depth only with this new device. Again, a variety of technological issues could also be studied in ITER, like for example the test of advanced materials facing very large heat and particle fluxes, the test of concepts for a tritium breeding module, the superconducting technology under high neutron flux and many others.

1.2 Magnetic confinement: MHD theory

1.2.1. Magnetic confinement and lines of field

Several magnetic field geometries have been investigated: magnetic mirrors, linear and toroidal configurations, and others. Up to now, the toroidal geometry has given the best confinement performances. We will dedicate this section to the principles of magnetic plasma confinement in toroidal devices.

First, we define in figure 1.10 the toroidal coordinates system (that will be used in the rest of the thesis) (r, θ, ϕ); r is the *radial coordinate* (said R_0 and a the major and minor radius of the torus, is $R = R_0 + a\cos\vartheta$), ϑ and φ are the *poloidal* and the *toroidal angle*, respectively. Magnetic field lines have both the poloidal and toroidal components, B_ϑ (or B_p) and B_φ (or B_t); the poloidal field is mainly generated by an external driven toroidal plasma current j_φ, whereas the toroidal field is generally produced by current flowing in external conductors (but in some configuration this is not totally true).

Thus, *the magnetic field lines are helixes*, which wind around the torus lying over toroidal surfaces, the *magnetic surfaces*. These lines are described by the so called *safety factor* q defined as follow:

$$q(r) = -\frac{r}{R_0}\frac{B_\varphi(r)}{B_\vartheta(r)}. \tag{1.18}$$

The name is due to the fact that q is crucial to determine several features of the plasma stability, as we will see better in the following. The inverse of this quantity represents the number of poloidal turns done by a helical field line per one toroidal turn, $1/q = 2\pi/\delta\varphi$, where $\delta\varphi$ is the toroidal angle that the magnetic line travels in $\delta\vartheta = 2\pi$. Again, q is linked to the pitch of the helix p by the relation $p(r) = 2\pi R_0 \cdot q(r)$.

1.2.2. MHD theory: the MHD-model

A large variety of plasma properties (e.g. equilibrium and stability) can be described using a fluid model called *magnetohydrodynamics model* (MHD

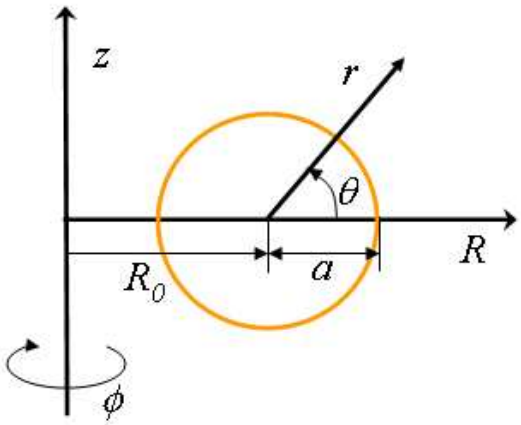

Figure 1.10: System of toroidal (r, ϑ, φ) and cylindrical (R, ϑ, z) coordinates.

model) [26], that consider a plasma as composed only by ions and electrons (two-fluid MHD). So, neglecting particle or momentum sources, the *mass* and the *momentum continuity equations* can be written as:

$$\frac{\partial \rho_\alpha}{\partial t} + \nabla \cdot (\rho_\alpha \overrightarrow{v}_\alpha) = 0 \tag{1.19}$$

$$\rho_\alpha \left(\frac{\partial \overrightarrow{v}_\alpha}{\partial t} + \overrightarrow{v}_\alpha \cdot \nabla \overrightarrow{v}_\alpha \right) = \sigma_\alpha \overrightarrow{E} + \overrightarrow{j} \times \overrightarrow{B} - \nabla p_\alpha + R_{\alpha\beta}. \tag{1.20}$$

The notation is the following: the greek letters α and β represent the species of particles (electrons or ions), $\rho_\alpha = m_\alpha n_\alpha$ is the mass density, σ the charge density of every species. $\overrightarrow{E}$, $\overrightarrow{B}$, $\overrightarrow{j}$, have the usual meanings of electrical and magnetic fields (the first two) and of current density. The r.h.s. of the equation 1.20 represents the balance between the electromagnetic forces (first two terms), the kinetic pressure force and the *collisional* term. The last one, $R_{\alpha\beta}$, is the rate at which momentum is varied (gained or lost) by the species α due to collisions with species β.

A plasma can be described as a single fluid by introducing the following variables: the *mass density* $\rho = \rho_i + \rho_e$, the *kinetic pressure* $p = p_i + p_e$, the *mass fluid velocity* $\overrightarrow{v}$ defined as $\rho \overrightarrow{v} = \rho_i \overrightarrow{v}_i + \rho_e \overrightarrow{v}_e$, the *charge density* $\sigma = e(n_i - n_e)$. With these new variables, and introducing also the resistivity η, it is immediate to obtain the subsequent *fluid equations*:

$$\frac{\partial \rho}{\partial t} + \nabla \cdot (\rho \overrightarrow{v}) = 0 \tag{1.21}$$

$$\rho \left(\frac{\partial \overrightarrow{v}}{\partial t} + \overrightarrow{v} \cdot \nabla \overrightarrow{v} \right) = \sigma \overrightarrow{E} + \overrightarrow{j} \times \overrightarrow{B} - \nabla p \tag{1.22}$$

$$\overrightarrow{E} + \overrightarrow{v} \times \overrightarrow{B} = \eta \overrightarrow{j} - \frac{\overrightarrow{j} \times \overrightarrow{B} - \nabla p_e}{ne} \tag{1.23}$$

They are, in sequence, the *mass continuity equation*, the *momentum continuity equation* (also called single-fluid equation of motion) and the *generalized Ohm's law* - note that the last one is not strictly a single-fluid equation, because of ∇p_e term.

The *resistive MHD model* can be derived from equations 1.21÷1.23 with the conditions of:

- quasi-neutrality of the charge, $n_i \simeq n_e$, so we can neglect the $\sigma \overrightarrow{E}$ term;
- small ion Larmor radius compared with the scale-length of the fluid motion, which permits to drop the Hall and diamagnetic terms in Ohm's law (fraction in the r.h.s. of equation 1.23).

By adding to the previous set of equations the Maxwell's equations

$$\nabla \times \overrightarrow{E} = -\frac{\partial \overrightarrow{B}}{\partial t} \tag{1.24}$$

$$\nabla \times \overrightarrow{B} = \mu_0 \overrightarrow{J} \tag{1.25}$$

$$\nabla \cdot \overrightarrow{B} = 0, \tag{1.26}$$

and the heat flux equation (the corresponding of the energy conservation), modeled for example by an equation of state for pressure

$$\frac{d(p/\rho^\gamma)}{dt} = 0 \tag{1.27}$$

we have the whole set of *resistive MHD equations*, that describe the behavior of the plasma in a magnetic field.

The exponent γ in the equation 1.27 is the ratio of the specific heats and is chosen depending on the phenomena to be modeled: $\gamma = 5/3$ for adiabatic compression, $\gamma = 1$ for isothermal compression.

From equations 1.24 and 1.27 we can obtain (assuming $\eta = constant$) the equation

$$\frac{\partial \overrightarrow{B}}{\partial t} = \nabla \times (\overrightarrow{v} \times \overrightarrow{B}) + \frac{\eta}{\mu_0} \nabla^2 \overrightarrow{B}, \tag{1.28}$$

that is able to describe the the coupled dynamics of the magnetic and fluid velocity fields.

1.2.3. MHD theory: the ideal MHD

The *ideal MHD model is a single-fluid model that describes, for a wide range of plasmas, the effects of magnetic geometry on the macroscopic equilibrium and stability properties of fusion plasma* [26]. The equations that constitute

the whole set of ideal MHD are the previously 1.24÷1.27, in the condition of low frequency and perfect conductivity.

From the equation 1.23 with $\eta = 0$ we can infer that in a reference frame moving with the plasma the electric field is zero, i.e. that the plasma is a perfect conductor ("ideal" case). Again, *the magnetic field line move like if they were frozen into the plasma*.

The three independent conditions that must be satisfied for ideal MHD to be valid are: (i) null resistivity, (ii) small gyroradius, (iii) high collisionality, specifically related to the assumption that the plasma is described by a maxwellian distribution with isotopic pressure.

For a typical fusion plasma, with

$$\begin{aligned} 10^{18}m^{-3} &< n < 10^{22}m^{-3} \\ 0.1keV &< T < 10keV \end{aligned}$$

the conditions (i) and (ii) are satisfied, while the third condition is not valid in general. But, following [26], the model is still trustworthy even *the point (iii) is not satisfied*: *"for problems involving MHD equilibrium and stability, the plasma motions of interest are incompressible"*. The conservation of mass and the perpendicular momentum equations are valid also in the collisionless limit; this is not true for the parallel momentum and the energy equations, but in the incompressibility regime neither of these equations is fundamental.

This is equivalent to said that in the fusion plasmas *the magnetic field plays the role of the collision*: perpendicular to the field, particles stay in the proximity of a given magnetic field line if their gyroradius is much smaller than the characteristic plasma length. This situation permit us *to consider fusion plasmas like ideal plasmas*, i.e. we can treat the perpendicular behavior of the plasma with a fluid model.

That just summarized is a modified MHD model known as, obviously, *collisionless MHD*: in general, it makes predictions similar to ideal MHD [26][27], but it does not depend on the collision-dominated assumption.

1.2.4. Magnetic surfaces

A *magnetic surface* is a surface which is ergodically[6] covered by a magnetic field line as it goes around the torus. A magnetic surface is everywhere

[6]We remember that *ergodicity* means that, over long periods of time, the time spent by a particle in some region of the phase space of microstates with the same energy is proportional to the volume of this region. In other words, all accessible microstates are equally probable over a long period of time. In this hypothesis on assume that the average of a process parameter over time is equal to the one over the statistical ensemble. This implies that it is as good to observe a process for a long time as sampling many independent realizations of the same process.

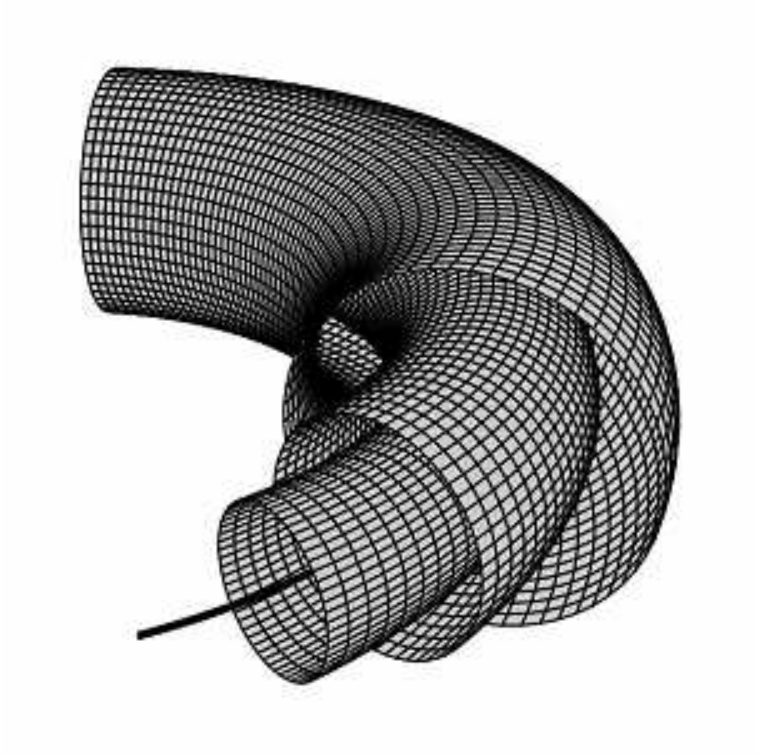

Figure 1.11: Magnetic surfaces. From [21].

tangential to the field, i.e. the normal of the surface is everywhere perpendicular to the magnetic field $\overrightarrow{B}$ [14]. There is special surfaces, the so called *rational surfaces*, characterized by the fact that their field lines close upon themselves after one turn (also one transit) around the machine. In toroidal geometry the magnetic surfaces are nested closed and smooth curves. A particular surface is the *magnetic axes*, the degenerate magnetic surface with the limiting zero values. Let see figure 1.11.

Well defined nested magnetic surfaces are usually taken to be a requirement for adequate plasma equilibrium as described by equation:

$$\overrightarrow{j} \times \overrightarrow{B} = \nabla p. \tag{1.29}$$

These magnetic surfaces are constant pressure surfaces, since $\overrightarrow{B} \cdot \nabla p = 0$, and the current-density lines lie on these surfaces because $\overrightarrow{j} \cdot \nabla p = 0$.

The beta of the plasma

A widely used figure of merit for magnetic confinement is the so called β parameter, a dimensionless number introduced to estimate how much kinetic

plasma pressure p is balanced by the magnetic field pressure $p_{mag} = B^2/2\mu_0$:

$$\beta = \frac{p}{p_{mag}}, \tag{1.30}$$

(In others words, the β says us how much plasma pressure is confined with respect the maximum than the magnetic field can contain.)

If $\beta \leq 0.1$ the internal and external magnetic fields are of the same order and the fields are determined by the conductors external to the plasma; when β is higher, the plasma currents contribute to determine the geometrical configuration of the plasma. For low β the confinement is not carried out in economy, but in general low β are necessary for the stability.

The toroidal or poloidal magnetic field separately can be used in the above definition, and in this case β is called poloidal β_ϑ or toroidal β_φ beta. Usually β_φ is indicated simply with β.

In the next section we will see like the β is an important parameter of the equilibrium.

1.3 Magnetic confinement: Equilibrium and stability

1.3.1. Equilibrium of a plasma

In fusion research have been investigated several configurations; in particular we are interested in magnetic confinement configuration[7], because the charged particles follow the magnetic field lines and the field lines are frozen into a perfect conducting fluid [14][29].

In *static equilibrium*, like in the fusion plasma condition, the isobar surfaces coincides with the magnetic surfaces and the current surfaces; the magnetic field lines must be to infinitive or must close themselves in nested torus (see figure 1.12).

The cylindrical pinches

Some of the simpler configurations that satisfy the equilibrium equation 1.29 are the cylindrical pinches, the analogues of the toroidal configuration. A *pinch* is a configuration (linear or toroidal) in which the plasma column squeezes and wrings radially, under the action of the magnetic field due to the current carried by the plasma itself [27][30]. This dynamical phenomenon ceases when the squeeze compensate the ∇p inner to the plasma; during the

[7] Here we totally omit the details about *inertial confinement fusion* [28]. In these experiments, small volumes of solid matter (*pellets*) are fired by high power lasers from many different directions. This treatment brings the pellets to sufficiently high temperatures and densities, with consequent compression and heating of the matter, till to reaching the critical conditions for fusion.

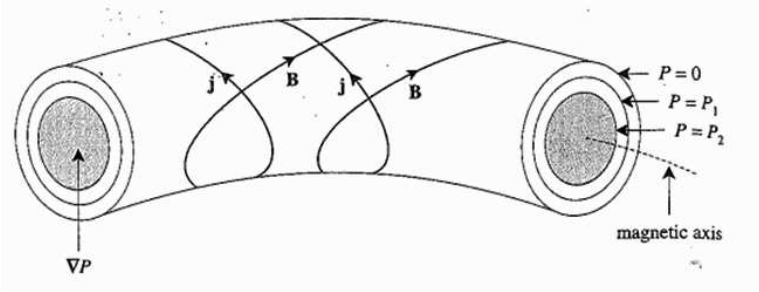

Figure 1.12: Nested isobaric surfaces. From [14].

pinch, the temperature increases till to equilibrium, that can be stable or not. Many of the more interesting toroidal configurations are pinches.

The analysis in the 1-dimension separates the radial pressure balance and the toroidal force balance problems. In cylindrical approximation all the variables are independent of ϑ and z and the lines of $\overrightarrow{B}$ and $\overrightarrow{j}$ lie on surfaces on constant r.

In the $\Theta-pinch$ an azimuthal current density j_ϑ is induced in the plasma by an external coil; consequently it is generated an axial magnetic field B_z that does not penetrate in the plasma, and remains confined in a narrow region between the plasma and the external coil. Vice versa, the $Z-pinch$ presents an axial current density and a poloidal magnetic field. The *screw pinch* is a flexible mix of $\Theta-$ and $Z-pinch$ [14][26].

The toroidal pinches

In cylindrical device the plasma will be implacably lost through the ends of the device. This motivation led to consider the *torus*: in a torus are used magnetic fields with closed geometry and thus it is possible to confine plasmas for relatively long times. In these cases there is a new equilibrium constraint, the *toroidal force balance*. Briefly, a toroidal plasma experiments a net outward force due to different physics phenomena: the effect of the plasma pressure; the $\overrightarrow{j} \times \overrightarrow{B}$ force due both to the poloidal and magnetic fields; the $\overrightarrow{E} \times \overrightarrow{B}$ drift due to toroidal field [14]. A perfectly conducting wall and external coils (in order to produce a vertical magnetic field) can provide toroidal force balance. Any configuration had advantage and disadvantage: for to say it with the words in [14, 4.3.2] *"the challenge is to find the optimal mix of poloidal and toroidal fields which can provide toroidal equilibrium without sacrificing radial stability"*.

In *tokamak* (like the *screw pinch*) $|B_\vartheta| \ll |B_\varphi|$: in particular, $|B_\varphi| > |B_\vartheta| \cdot R_0/a$, a magnetic field line makes several turn around the torus before completing one spiral of the minor axis and the toroidal current flows mainly

in the plasma column (whereas in the screw pinch the current flows mainly in a sheet surrounding the plasma column) [14]. In the *reversed field pinch* (whose acronym is RFP) $|B_\vartheta| \sim |B_\varphi|$ and the magnetic field lines spiral many times around magnetic axis in going once round to the torus. We discuss about RFP in the next section.

The equilibrium of the 2-dimensional configuration is described by the Grad-Shafranov equation, see page 27.

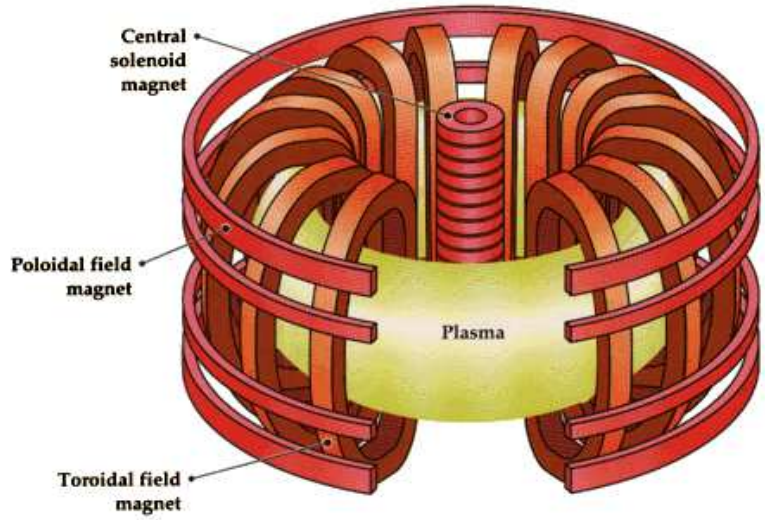

Figure 1.13: Sketch of a tokamak device. From [31].

The RFP configuration

The RFP configuration is an axisymmetric magnetic structure where the toroidal field B_φ reverses to the edge, from which the locution *reversed field*. The *reversal radius* is the radius at which $B_\varphi = 0$. The kinetic pressure at the ideal equilibrium is given by the equation 1.29. As we said, whereas in the tokamaks $B_\varphi \gg B_\vartheta$, in the RFPs the two fields are comparable.

Theoretically a RFP plasma is confined: the particles describe gyration orbits on the magnetic surfaces defined by the field lines, with a small probability to be spread orthogonally with respect these surfaces[8]. Such as all magnetic configurations, the kinetic pressure is ruled, at the equilibrium, by the ideal MHD equation 1.29.

In a RFP plasma, the plasma itself relaxes naturally and tends to a state of minimum energy. The first theory of the relaxed states had proposed

[8]This probability is proportional to the collisionality effects or magnetic drift orthogonal to the field lines.

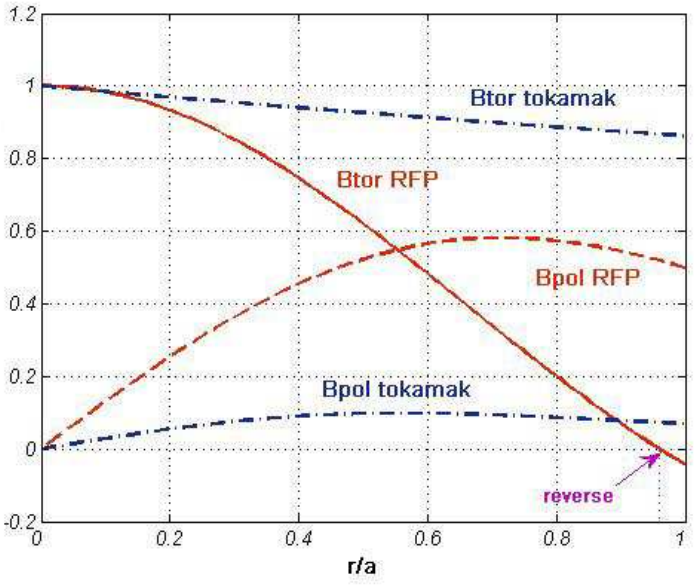

Figure 1.14: Relative magnitudes of the toroidal and poloidal magnetic fields for tokamaks and RFPs.

by Taylor in the 1974 [32] and subsequently improved. The condition of minimum energy for an RFP is described, when the *helicity* over the entire plasma volume is conserved, from the equation

$$\overrightarrow{J} = \nabla \times \overrightarrow{B} = \mu \overrightarrow{B} \tag{1.31}$$

where μ is constant and the conserved helicity is defined as:

$$K = \int_{vol} \overrightarrow{A} \cdot \overrightarrow{B} d^3 r \tag{1.32}$$

and $\overrightarrow{B} = \nabla \times \overrightarrow{A}$ (i.e. $\overrightarrow{A}$ is the vector potential of the magnetic field). Physically, K is a global quantity that measures how much the magnetic field "wraps around itself" and it was first introduced in studies on astrophysical plasmas [33]. In absence of dissipation magnetic energy, K is one of the quantities conserved into the plasma; in presence of dissipation (at short length scales, and related with the resistivity), magnetic energy is destroyed. This considerations can be translate in the variational principle

$$\delta \int_{vol} \Big(\frac{B^2}{2\mu_0} - \mu \overrightarrow{A} \cdot \overrightarrow{B} \Big) dV = 0 \tag{1.33}$$

that at least leads to the relation 1.31.

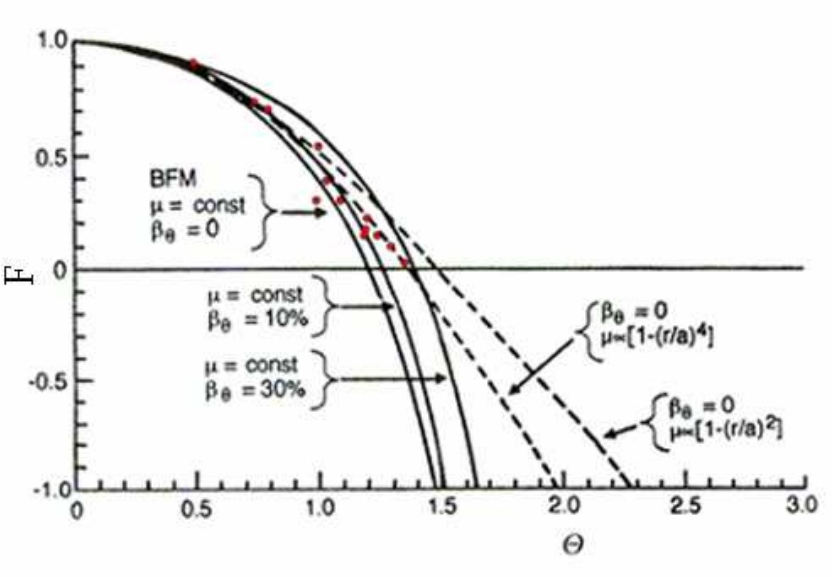

Figure 1.15: The F-Θ plane. Points: experimental data. Black line: Equilibrium curves by Bessel Function Model. Dashed line: Equilibrium curves by another model, named $\mu - p$ model. Tokamaks data are in the top right corner. From [36].

The parameter μ is a function of the radius r in the practical cases [34][35] whereas it is a constant following the Taylor relaxation theory. In the last case: B_φ is symmetric respect to the axis of the torus and follows the Bessel function $J_0(\mu r)$ while B_ϑ is antisymmetric and follows the Bessel $J_1(\mu r)$ (see the figure 1.15). This is the so called *Bessel Function Model* [30].

Macroscopically the RFP configuration is described by two parameters: the *pinch parameter*

$$\Theta = \frac{B_\vartheta(a)}{\langle B_\varphi \rangle} \tag{1.34}$$

and the *reversal parameter*

$$F = \frac{B_\varphi(a)}{\langle B_\varphi \rangle}. \tag{1.35}$$

The averages are extended over the cross section.

The BFM explains the experimental data for $\Theta \leq 1.5$ and gives a good approximation for the internal field profiles, but the external field profiles predicted by the theory don't match the observations. In any case, the BFM supplies an argument to explain why an experimental pinch is near a Bessel-like configuration: as observed, for $\Theta \geq 1.2$ a self-reversal of the toroidal

field occurs, with the consequently relaxation of the plasma (that tends to the minimum energy) to a stable configuration.

The Grad-Shafranov equation, the q and the shear s

If the 1-dimensional and cylindrically approximated magnetic configurations models the radial pressure balance problem, as mentioned previously, by adding one dimension we introduce the toroidal force balance problem. In particular, for these last magnetic geometries with the axisymmetric approximation, the toroidal equilibria are described by the Grad-Shafranov equation, GSE, a 2-dimensional non-linear elliptic partial differential equation. A large number of magnetic configurations are modeled by GSE, including tokamaks and RFPs[9].

The GSE is a form of 1.29 for toroidal configuration; it is derived by rewriting the components of the magnetic field $\overrightarrow{B}$ and of the current density $\overrightarrow{j}$ in term of the flux functions Ψ_p (poloidal magnetic flux) and F (proportional to the poloidal current density flux. Let not mismatched with the reversal parameter, in the equation 1.35 and figure 1.15). The nature of the equilibrium (tokamak, RFP, and so on) is determined by the choose of the free function $p(\Psi_p)$ and $F(\Psi_p)$ and from the boundary conditions; Ψ_p is treated as variable [14][26]. One form for the GSE is the following:

$$\Delta^* \Psi_p = -2\pi F \frac{dF}{d\Psi_p} - 2\pi\mu_0 R^2 \frac{dp}{d\Psi_p} \tag{1.36}$$

where we have used the operator

$$\Delta^* = R\frac{\partial}{\partial R}\Big(\frac{1}{R}\frac{\partial}{\partial R}\Big) + \frac{\partial^2}{\partial z} \tag{1.37}$$

In equilibrium definition, an important quantity is the safety factor q, introduced in the paragraph 1.2.1: we have seen yet that q gives us the number of poloidal turns done by a helical field line per one toroidal turn, in accordance with the relation 1.18. Starting from the field line equations, and writing it as a function of the toroidal flux χ, q can be expressed in general as [26]

$$q(\chi) = \frac{F(\chi)}{2\pi} \oint \frac{dl_\vartheta}{R^2 B_\vartheta} \tag{1.38}$$

where the integral is calculated on a poloidal circuit. For large aspect ratio configuration, i.e. in cylindrical approximation, q is expressed in the more simple form 1.18.

The tokamaks get the minimum of q on the magnetic axis, and the value increases with the radius; higher is q, greater is the stability. At the opposite, in the RFPs q decrease with the radius. See the figure 1.16.

[9] An equation similar to GSE but in helically symmetric equilibria is used to study the stellarators configurations.

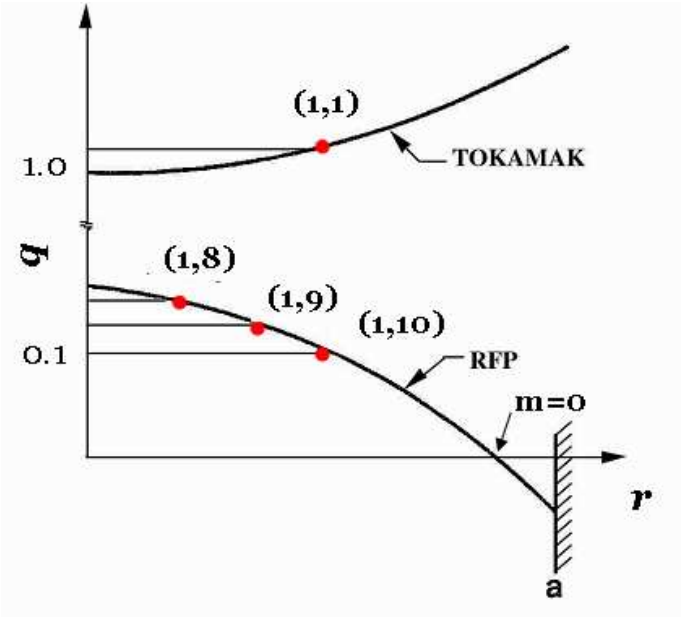

Figure 1.16: Safety factor for tokamak and RFP.

A quantity strictly related to q is the *shear*, that is a measure of the twisting of the field lines by changing radius:

$$s(r) = \frac{d[\ln q(r)]}{d[\ln r]}. \tag{1.39}$$

A dangerous helical magnetic perturbation are those which satisfies the *resonance condition*

$$\overrightarrow{k} \cdot \overrightarrow{B} = 0. \tag{1.40}$$

The shear stabilize in consequence of the stiff variation of q with the radius. In this way, an instability that grows around a resonance surface, defined by the relation 1.40, $\overrightarrow{k} \cdot \overrightarrow{B} = 0$, can not do this easily: its radial structure and the high shear push the mode out of resonance.

To explain better this fundamental concept, we expanded q in a neighborhood of r_{res}:

$$q(r) = q(r_{res}) + q'(r_{res}) \cdot (r - r_{res}).$$

In the vicinity of the resonance radius, the relation 1.40 is not more valid (since q is changed) and the perturbation must twist the equilibrium field lines. This simple example shows how high shear can help the stability.

The solutions of Grad-Shafranov equation can be obtained through asymptotic expansion considerations, given by simplifications due from a specific

ordering of fields and pressure characteristic of the different devices [14][26]. For example, for the RFP the asymptotic expansion is ensued in terms of the (very little) inverse aspect ratio $\epsilon \doteq a/R_0 \ll 1$: $B_\varphi/B_\vartheta \sim 1$, $\beta_\varphi \sim \epsilon$, $\beta_\vartheta \sim \epsilon$, $q \sim \epsilon$. So, the RFP is an high$-\beta$ and small q device with both poloidal and toroidal magnetic fields important in radial pressure balance. The GSE explicit solution is given in [26]: here we say only that the $0-th$ order solution gives the radial pressure balance, whereas the $1st$ *order* solution shows the toroidal effects. For the ohmically heated tokamaks, the asymptotic ordering in ϵ is: $B_\varphi/B_\vartheta \sim \epsilon$, $\beta_\varphi \sim \epsilon^2$, $\beta_\vartheta \sim 1$, $q \sim$ 1. The large vacuum toroidal field dominates the geometry, the plasma is heated and supported by the ohmic current; but this last is limited by the stability constraint. In *high-β regimes*, $\beta_\varphi \sim \epsilon$, $\beta_\vartheta \sim 1/\epsilon$ and $q \sim$ 1 [26].

1.3.2. Perturbations of the equilibrium state

It is clear that, like every dynamical system, plasma is subject to perturbations of its equilibrium, described by the relation 1.29 or the relation 1.36. The MHD equations (see the paragraph 1.2.2) predict that, under certain conditions, a small perturbation in a fluid quantity (for example the density or the magnetic field) can grow unstable in time [37]. These *MHD instabilities* are present in all the toroidal fusion devices, influencing the global plasma properties till they deteriorate the plasma confinement performances. For this motivation, an important task in fusion plasmas is to determine the properties of the stability of the configuration [26][38].

Introducing the poloidal and toroidal mode number, resp. m and n, each couple *(m,n)* represents a *mode*, or helical perturbation. A perturbation $\widetilde{\Psi}$ of a generic quantity Ψ in a toroidal plasma can be expanded in Fourier series

$$\widetilde{\Psi}(\overrightarrow{r};t) = \sum_k \widetilde{\Psi}_k(r) e^{i(\overrightarrow{k}\cdot\overrightarrow{r}-\omega t)} = \sum_k \widetilde{\Psi}_k(r) e^{i(m\vartheta+n\varphi-\omega t)} \tag{1.41}$$

where $\overrightarrow{r} = (r,\vartheta,\varphi)$ is the position vector and $\overrightarrow{k} = (k_r, k_\vartheta, k_\varphi) = (k_r, m/r, n/R_0)$ is the wavevector in toroidal coordinates. The angular frequency is in general a complex quantity, $\omega = \omega_R + i\omega_I$: the real part ω_R describes the propagation velocity of the wave while the imaginary part ω_I represents a damping ($\omega_I < 0$) or an exponential growth ($\omega_I > 0$) of the perturbation amplitude.

The condition 1.40 can be rewritten making $\overrightarrow{k}$ and $\overrightarrow{B}$ explicit:

$$\overrightarrow{k}\cdot\overrightarrow{B} = \frac{m}{r}B_\vartheta + \frac{n}{R_0}B_\varphi = 0 \tag{1.42}$$

that is

$$q(r) = -\frac{r}{R_0}\frac{B_\varphi(r)}{B_\vartheta(r)} = -\frac{m}{n}. \tag{1.43}$$

Each radial position where the safety factor q assumes rational values is called *rational radius* or *resonant radius*.

1.3.3. Plasma stability

It is well-known that the linear stability of a system is evaluated with respect to a pre-existent equilibrium condition. The equilibrium requests that there are not net forces that accelerate some portion of the plasma. Once that the equilibrium is established, the study of the stability asks if a small perturbation will grow or will be dumped.

To study the stability of the plasma the equation of motion 1.20 is linearized around the equilibrium state. The study is particularly easy in axial symmetry and cylindric approximation. We introduce for a generic quantity Ψ, naming Ψ_0 the equilibrium and $\widetilde{\Psi}_1$ the small perturbation ($\widetilde{\Psi}_1 \ll \Psi_0$), the following description:

$$\begin{aligned} \Psi(\overrightarrow{r};t) &= \Psi_0(r) + \widetilde{\Psi}_1(\overrightarrow{r};t) \\ &= \Psi_0(r) + \widetilde{\Psi_1}(r) \cdot e^{-\imath(\omega t - \overrightarrow{k}\cdot\overrightarrow{r})}, \end{aligned} \tag{1.44}$$

where $\overrightarrow{r} = (r, \vartheta, \varphi)$, $\overrightarrow{k} = (k_r, k_\vartheta, k_\varphi) = (k_r, m/r, n/R_0)$ and ω have the same meaning as in the 1.3.2 paragraph.

Classification of the MHD instabilities

The instabilities are in general classified according to the boundary or to the physical conditions, i.e. the sources of free energy.

In order to formulate in the right way an MHD problem, we must specify an appropriate set of *boundary conditions*, that couple the plasma with the externally applied magnetic field. So, the class of perturbations that we want to analyze must be consistent with the constraints of the system. We will study this topic in depth in the 2.1. Anyway, referring to the boundary conditions we have two kinds of perturbations. Preliminary, we name $\widetilde{\zeta}(a) = 0$ the displacement of the plasma column and $\overrightarrow{n_0}$ the normal to the unperturbed surface. The *internal (or fixed-boundary) modes*, $\overrightarrow{n_0} \cdot \widetilde{\zeta}(a) = 0$, don't require a displacement of the plasma-vacuum interface ($\delta W_s = \delta W_v = 0$). They are microinstabilities that don't upset the surface of the plasma column and don't give macroscopic effects, but degrade the plasma by altering the transport coefficients. The *external (or free-boundary) modes*, $\overrightarrow{n_0} \cdot \widetilde{\zeta}(a) \neq 0$, that require a displacement of the plasma-vacuum interface.

As seen in the paragraph 1.3.3, referring to free energy source we have pressure driven modes or current driven modes[10], where the names report

[10]But others sources of instabilities exist; for example, under certain conditions a ther-

to the normal and parallel components, respect to the magnetic field lines, of the plasma current density.

The *pressure driven modes* are exchange flux motion and so essentially hydrodynamic. The main of them are called *interchanges instabilities* and a their simple example is the case where a fluid of density ρ_1 lies horizontally over one of density ρ_2; if $\rho_1 > \rho_2$, perturbing the system the volumes of the upper fluid will go down. The respective instability is called *Rayleigh-Taylor instability*. In MHD, the analogue situation is a plasma supported against gravity by magnetic field [39]. In laboratory plasmas, where gravity is negligible, its role is hold by any other acceleration of the plasma, for example due to the magnetic field curvature. In the last case, because the unperturbed pressure gradient is generally directed towards the center of the plasma, for the stability the magnetic curvature must be directed outward: the combined interaction of pressure gradient and poloidal magnetic line stress originates the *sausage* or *flute modes* (see figure 1.17, left panel). The maximum stability is obtained when the plasma occupies the region where the average magnetic field is minimum [14][15].

In the 2- and 3-dimensional configurations there is a mixture of "good" and "bad" curvature. In a toroidal device, for example, there is the favorable curvature in the inner part of the torus and the unfavorable one in the outerside; perturbations tend to grow in the unfavorable regions, in this case the outer, originating a bump in the plasma column [14]. These *balooning modes* varying slower than the interchange instabilities and are inclined to accumulate in particular region. These kind of instabilities are important both for tokamak and for RFPs. A flat pressure profile and (for the RFP) the reversal of the toroidal magnetic field mitigate or suppress the pressure-driven instabilities. Because the balooning modes can not be controlled by a minimal magnetic field configuration, they are defused by reducing the plasma pressure. The stability thresholds for the baloonings select the maximum values of beta.

The *current driven modes* are large λ ($\lambda \approx a$) instabilities that produce a global displacement of the plasma column respect to the axis: p_{mag} on the concave region is increased, and the opposite behavior happens in the convex side. If we apply a longitudinal (toroidal) field, the force that originates tries to restore the pinch in its equilibrium position. These perturbations are called *kinks* (see figure 1.17, right panel) and arise when it is present a resonance of the mode (see equation 1.42); they are ideal instability with high growth rates, of the order of $1/\tau_A$ where τ_A is the Alfvén time. The ideal instabilities are the faster plasma instabilities. In fact we remember that the *Alfvén time* is defined as $\tau_A = a/v_A$, where a is the minor radius of the torus. $v_A \doteq B/\sqrt{\mu_0\rho_0}$ is the *Alfvén velocity*, that represents the

mal gradient can provide the necessary free-energy to a small perturbation to grow unstable.

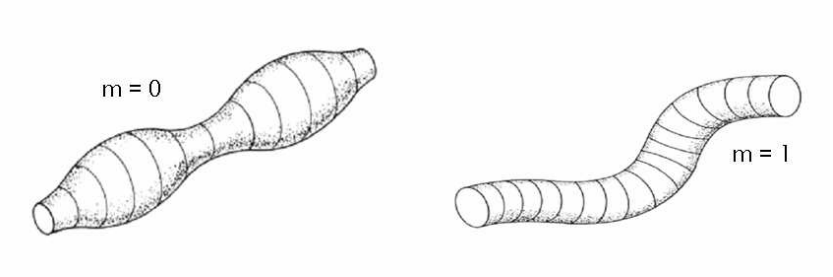

Figure 1.17: The $m = 0$ (left) and $m = 1$ (right) modes. From [21].

propagation velocity of the magnetic field lines, in order to restore the initial configuration. So, τ_A is the time it takes for an Alfvén wave to travel from the center of the plasma to the edge. Sometimes such instabilities can be mitigated by a conductive wall at the plasma edge: thanks to the eddy currents, it prevents the penetration of the magnetic field inside it for time shorter than the penetration time of the field in the material. Kinks can be either internal or external perturbations, depending upon the location of the singular surface. In the tokamaks, the *Kruskal-Shafranov condition* $q_a \doteq q(r = a) > 1$ defines the minimum limit for the kink stability; typically it is $q_a \geq 3$. For this reason the kinks are important essentially for the RFPs.

In terms of modal analysis, sausages are the $m = 0$ perturbations, i.e. a cyclical narrowing and widening of the plasma section that follows the increase or the reduction of the poloidal magnetic field. Kinks, that produces a global displacement of the plasma column respect to the axis giving to the plasma column a helix-like form, are the $m = 1$ perturbations.

The force operator and the Energy principle

The next step consist to express the linearized quantities in the MHD equations as functions of the already met plasma *displacement* from the equilibrium position $\widetilde{\zeta}$, $\widetilde{v}_1 = \partial\widetilde{\zeta}/\partial t$. It is obtained a single equation that describe the temporal evolution of $\widetilde{\zeta}$.

As already mentioned, to deduce the perturbed equation of motion we consider first an ideal stationary equilibrium

$$\overrightarrow{J_0} \times \overrightarrow{B_0} = \nabla p_0 \tag{1.45}$$

$$\mu_0 \overrightarrow{J_0} = \nabla \times \overrightarrow{B_0} \tag{1.46}$$

$$\nabla \cdot \overrightarrow{B_0} = 0 \tag{1.47}$$

$$\overrightarrow{v_0} = 0 \tag{1.48}$$

to which a small velocity $\overrightarrow{v_1}(\overrightarrow{r};t)$ is superimposed:

$$\frac{\partial\widetilde{\zeta}(\overrightarrow{r};t)}{\partial t} \equiv \widetilde{v_1}(\overrightarrow{r};t) \neq 0.$$

Under these conditions the equation of motion becomes:

$$\rho_0\frac{\partial^2\widetilde{\zeta}}{\partial t^2} = \underbrace{\widetilde{J_1}\times\overrightarrow{B_0}+\overrightarrow{J_0}\times\widetilde{B_1}}_{\overrightarrow{F}(\widetilde{\zeta})} \tag{1.49}$$

where $\overrightarrow{F}(\widetilde{\zeta})$ is the force for volume unit. In the case of exponential growth perturbations, $\widetilde{\zeta}=\widetilde{\zeta}(\overrightarrow{r})e^{\gamma}$, γ is the growth rate, we can translate our initial value problem in a normal modes eigenvalues problem:

$$\rho\gamma^2\widetilde{\zeta} = \widehat{F}(\widetilde{\zeta}). \tag{1.50}$$

The solution of both the equations 1.50 and 1.28 gives the evolution of the instabilities; in particular, referring to the equation 1.50, with $\eta=0$ we get the ideal instability, whereas for $\eta\neq 0$ we obtain the resistive instabilities.

We passed from the *vector* force $\overrightarrow{F}$ to the *operator* force $\widehat{F}$. For an ideal plasma without dissipative effects it can be shown that [26]:

- the operator $\widehat{F}$ is self-adjointed and this allow us to find eigenvalues and eigenfunctions with variational methods. The self-adjointness means that is $\left\{\omega_n^2\right\}\in\Re^n$, where the omegas are the eigenvalues
- the set of the self-function is orthogonal and complete[11].

By manipulating the equation 1.50 (see for instance [14]) we get the *energy integral*

$$\begin{aligned}\delta W &= -\int\overrightarrow{F}\cdot\, d\overrightarrow{\zeta} = \\ &= \delta W_s+\delta W_v+\delta W_p\end{aligned} \tag{1.51}$$

where the energy W is the sum of the surface, void and plasma contributes, and F is given by the equation 1.49.

The conclusion is that *there is instability if at least one of the ω_n is positive*. The spectral properties of the operator $\widehat{F}$ guarantee the existence of a first integral of the motion and the formulation of the stability problem through the *energy principle*: *necessary and sufficient condition for the MHD stability is that $\delta W\geq 0$*. Then, in cylindrical geometry the stability of the system can be determined (according to the energy principle) by analyzing the sign of the energy integral: if this is positive for all displacements

[11] The completeness is not a necessary hypothesis [40].

the system is *stable*; on the contrary, the system is *unstable* (there exists at least a ζ such that $W(\zeta) < 0$). For this reason it is important evaluate which terms in the expression 1.51 are positive, i.e. stabilizing, or negative, i.e. de-stabilizing.

The *surface energy*

$$\delta W_s = \frac{1}{2}\int (\widetilde{\zeta}\cdot\overrightarrow{n}_0)^2[\nabla p_{tot}]\cdot d\overrightarrow{S} \tag{1.52}$$

is an elastic-like term originates by the deformation of the interface surface itself. Because it is the work done by displacing the plasma boundary, it is null if the boundary is fixed ($\widetilde{\zeta}\cdot\overrightarrow{n_0} = 0$, where $\overrightarrow{n_0}$ is ever the normal to the unperturbed surface); this term is null also if there is not surface current (in this case, ∇p_{tot} is continuous across the boundary). δW_s provide a stabilizing contribute. $[\nabla p_{tot}]$ is the jump through the surface.

The *vacuum energy*

$$\delta W_v = \int \frac{\widetilde{B}^2}{2\mu_0} d\overrightarrow{r} \tag{1.53}$$

is the increase in the energy of the vacuum field and is positive (stabilizing).

The *plasma energy* is constituted by the increase magnetic energy (i), the work done against the perturbed force (ii) and the change of internal energy due to the plasma compression or expansion (iii).

$$\delta W_p = \frac{1}{2}\int \Big[\underbrace{\widetilde{B}^2/\mu_0}_{(i)}\underbrace{-\widetilde{\zeta}\cdot(\overrightarrow{j}_0\times\widetilde{B})}_{(ii)}\underbrace{-\widetilde{p}(\nabla\cdot\widetilde{\zeta})}_{(iii)}\Big] d\overrightarrow{r} \tag{1.54}$$

After further manipulation (see again [14]) the magnetized plasma term can be written highlighting the curvature of the equilibrium magnetic field $\overrightarrow{B_0}$ and separating any quantity in its parallel and perpendicular components, relative to $\overrightarrow{B_0}$. So, δW_p is a sum of sundry contributes. The stabilizing ones represents the variations of the potential magnetic energy of the fluid for to bend and compress the field lines, and for to compress the fluid[12] (the first kind variation originates the torsional Alfvén waves, whereas the second one originates the sound waves). The destabilizing terms are due to the different components of the plasma current and give raise to the so called *pressure driven instabilities* (driven by $\nabla p_0 = \overrightarrow{j_0}\times\overrightarrow{B_0} = \overrightarrow{j_{0,\perp}}\times\overrightarrow{B_0}$) and the *current driven instabilities* (driven by $\overrightarrow{j_{0,\parallel}}$).

From the Energy principle to the Newcomb's analysis

A general analysis of the energy principle has been given by Newcomb [41] (a good explanation of the analysis is given in [26] and [27]). The Newcomb's

[12] In this writing is clear that, because $\nabla\cdot\widetilde{\zeta} \neq 0$ is stabilizing, it is assumed for simplicity the incompressibility of the plasma.

analysis shows how the marginal stability differential equation associated with the variation of δW can be used to determine necessary and sufficient conditions for MHD stability of arbitrary internal modes. The stability of a given screw pinch profile is related to the solution for the plasma displacement $\widetilde{\zeta}$ of the corresponding Euler-Lagrange equation; for any specific configuration, one must solve this equation numerically. The energy integral can be rewritten so that in the integrance appear two functions of the radius which depend on the toroidal and poloidal number (m, n) and on the equilibrium profile [36]. Following what we said in the previously paragraph, by minimizing the energy integral we get a solution which corresponds to the radial profile of a marginally stable eigenfunction of the system. The minimization is done solving the *Newcomb's equation* [42]

$$\frac{d^2k}{dr^2} + Ak = 0 \tag{1.55}$$

where A depends on pressure and plasma density current profiles, on m and n and on equilibrium fields B_φ and B_ϑ; the function k is strictly related to the radial field perturbation [43]:

$$k = \frac{r^{3/2}\widetilde{b_r}}{(m^2 + n^2r^2)^{1/2}}. \tag{1.56}$$

The 1.56 can be solved for each (m, n) mode, but it is not defined at the resonant surface r_{res}, where $q = m/n$ [41]. So, the solution must be integrated by splitting into an *internal solution* (for $r < r_{res}$) and an *external solution* ($r_{res} < r < a$); moreover, one must impose a *continuity condition* at the resonant surface. The external solution is constrained by the boundary conditions at $r = a$, while the internal one is determined by imposing an asymptotic dependence on (m, n) at $r = 0$. The discontinuity of the $b'_r|_{r=r_{res}}$ characterizes the linear stability of tearing modes.

The Tearing Modes and the Magnetic Islands

An important kind of perturbation is given by the so called *tearing modes*, TMs, that are the dominant resistive instability in the RFP plasmas. The TMs are driven unstable by a gradient in the current density parallel to the magnetic field in presence of a finite plasma resistivity; so, a TM mode is the resistive form of the kink mode. The name originates from the fact that the magnetic field lines tear and reconnect during the evolution of the perturbation, see figure 1.18. When the current gradient is sufficiently high, a TM instability is triggered and this causes right the bending and reconnection of the magnetic field lines. The resultant magnetic configuration is characterized by the formation of a so called *magnetic island*.

We have already seen that in a perfectly conducting plasma, the plasma fluid moves with the magnetic field, i.e the field lines are "frozen" in the

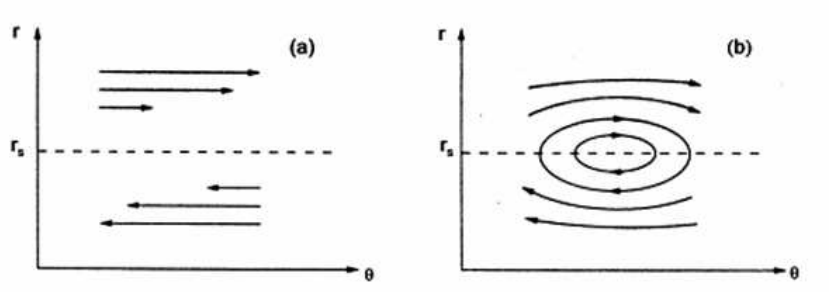

Figure 1.18: Topology of magnetic field lines. In *(a)* the ideal MHD case, in *(b)* the resistive MHD case, with the reconnection of the lines. r_s is the resonant radius.

plasma, and the Alfvén time τ_A (see in the paragraph 1.3.3) is the fundamental time scale and determines the growth rate of ideal modes. In resistive-MHD it is used a second time scale, the *resistive diffusion time*, $\tau_R = \mu_0 a^2/\eta$ (a is ever the minor radius of the torus, η the plasma resistivity). The TMs grow on a combined time scale $\tau_{tear} = \tau_A^{-2/5}\tau_R^{-3/5}$, $\tau_A \ll \tau_{tear} \ll \tau_R$. The ratio between the two fundamental time scale is the *Lundquist number* $S = \tau_R/\tau_A$ [44].

The growth of a TM is determined by the *tearing parameter*

$$\Delta'(w) = \frac{1}{b_r}\frac{\partial b_r}{\partial r}\Big]_{r_s+w/2}^{r_s-w/2}$$

where w is the size of magnetic island at the resonance radius r_s: the mode is unstable if $\Delta' > 0$. The size of the island varies according to the relation

$$\frac{dw}{dt} \cong \frac{\eta}{2\mu_0}\Delta'(w).$$

TMs affect the global confinement properties of the RFP and tokamak plasmas. The dominant TMs in RFP plasmas are the $m = 1$ core resonant modes, with resonant surfaces inside the reversal surface; the innermost resonant TM has toroidal mode number $n \sim 2R_0/a$. These modes are responsible for the dynamo sustainment of the RFP [14][45] and their number depends to the aspect ratio $A = R_0/a$ of the device; higher is A, higher is the number of the modes the tend to be unstable.

We will deal with more depth this important subject in the paragraph 1.3.4.

The Resistive Wall Modes

One important example of external modes (see paragraph 1.3.3) are the *resistive wall modes*, or *RWMs*. The resistive wall modes are slow, not-axial-

symmetric (toroidal mode number $n \neq 0$), kink-like, global instabilities that develop in plasma surrounded by a resistive wall. The RWMs have great λ and grow in the plasma in the time-scale penetration of the resistive wall: $\gamma_{RWM} \propto 1/\tau_w \propto \eta_w$. Here we indicate with η_w the resistivity of the wall. The wall penetration time τ_w is the longer decay time for an RWM in absence of the plasma and it is defined as:

$$\tau_w = \mu_0 \sigma r_w \delta_w \tag{1.57}$$

where μ_0 as usual is the vacuum permittivity, σ the wall conductivity, r_w the wall radius and $\delta_w \ll r_w$ the wall thickness. Let note that, being the RWMs resistive instabilities, it is $b_r|_{r=r_s} \neq 0$ (r_s is the rational surface where the mode occurs); consequently, it is permitted the possibility of reconnection of the field lines.

The spontaneous growth of the RWMs has been experimentally observed: they are $m = 1$ non-resonant current-driven modes in the RFPs [46][47][48] and $n \neq 1$ external pressure driven modes in the tokamaks. Their stabilization is a challenge, being one of the greater limiting factor for to reach high-β configuration in the advanced tokamak scenarios.

Resonant modes and ideal-MHD instabilities for a RFP

We already know that a resonant mode satisfy the condition 1.42 in some internal plasma surface; it can develop more easily than the non-resonant modes because it can grow without perturb the field lines and without undergo their force.

In a RFP the ideal instabilities are, in general:

- $m = 0$ resonant on the toroidal field reversal surface;
- $m = 1$, classified as follow:
  - *internally resonant* if $r_s < r_{rev}$
  - *externally resonant* if $r_s > r_{rev}$
  - *internally non-resonant* if $-m/n > q(0), n < 0$
  - *externally non-resonant* if $-m/n < q(a), n > 0$.

where, as usual, r_s is the resonant radius, r_{rev} the reversal one and $m/n = q(r)$. In general, the RFP stability depends on the current profile: peaker is it, higher is the probability to excite the unstable modes.

The plot 1.19 shows $q(r)$ for a RFP with aspect ratio $A = R_0/a = 4$. The four sectors correspond to different instability zones. From top to bottom: the first is the internally non-resonant RWMs zone ($m = 1, -7 < n < 0$); the second is the externally resonant TMs zone ($m = 1, n \leq -7$); the third is the externally resonant modes zone ($m = 1, n > 5$); the fourth is the

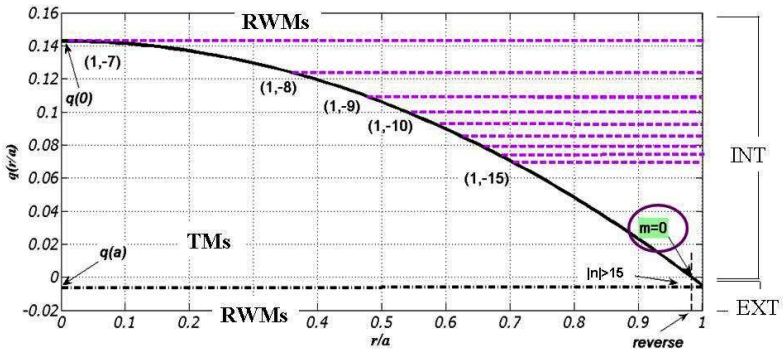

Figure 1.19: Safety factor q and instability zone (see text).

externally non-resonant RWMs zone ($m = 1, 2 \leq n \leq 5$). At the reversal radius we have the $m = 0$ modes. Another helpful visualization is the *mode spectrum*, in which is shown $\gamma_{m,n}\tau_w$, or simply $\gamma_{m,n}$, for any (m, n) mode with m given. The figure 1.20 shows the $m = 1$ instability spectrum for RFX-mod. We can compare with the previously figure. The $n > 0$ modes are the RWMs, whereas the modes with higher growth rates are the TMs. The external RWMs are influenced by the *shell proximity* value b/a, where b is the shell radius and a the minor radius of the torus. As b/a increases the γ of the RWM increases and at certain critical value the mode becomes ideal, i.e. $\gamma\tau_A \approx 1$.

In the RFP devices, a sufficiently close perfectly conducting wall permits to stabilize the $m = 0$ modes, the non-resonant $m = 1$ modes and the externally resonant $m = 1$ modes. Instead, the internal resonant stay usually unstables and contribute to the plasma relaxation; for this motivation they are named also *dynamo modes*.

1.3.4. Dynamo effect

We have already seen that the introduction of a resistive term allows the magnetic field lines to reconnect across the rational surfaces, forming magnetic islands. Again, the reconnection of magnetic field lines can trigger TM instabilities. Magnetic islands may grow and *overlap* with magnetic islands formed by other resistive modes. In this case, the magnetic field lines, not more restricted to a single rational surface, can fill the volume due to the overlapping magnetic islands: *the magnetic field lines are then stochastic in this volume* [49].

TMs are involved in the dynamo effect. The *dynamo effect* is a mechanism, not completely known, that rely on MHD turbulence (and related

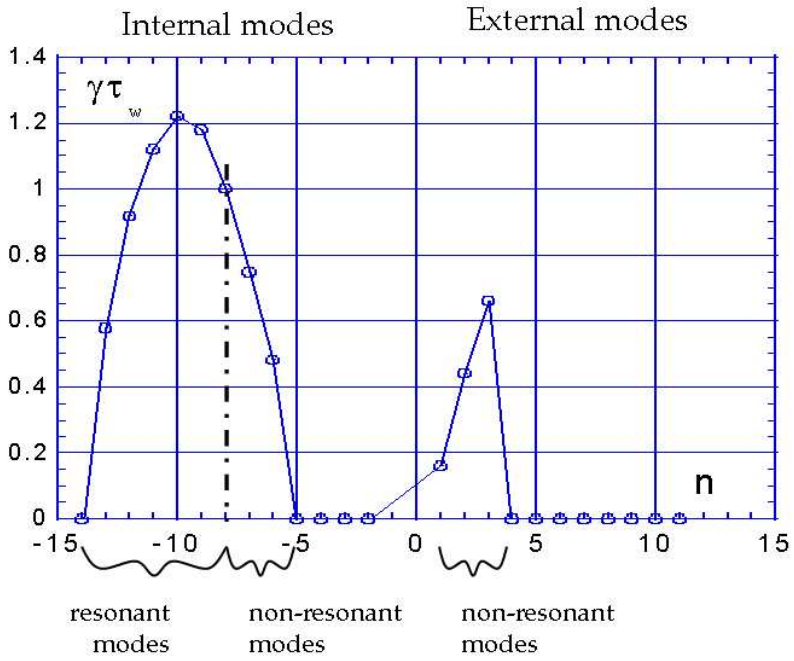

Figure 1.20: $\gamma\tau$ versus $(1, n)$ modes.

self-organization processes), and that is responsible for the persistence of strong magnetic fields for much longer period than the resistive diffusion time [50][51].

In particular, in a RFP laboratory plasma, if the resistive diffusion dominate the dynamic, the discharge would be limited in time. This is simple to proof, because a plasma described like a static conductor subjected to resistive diffusion is described by the equation 1.28. So, the poloidal and toroidal components of the magnetic field diffuse in a characteristic time τ (see [21]), each of them follows a low of the kind $B_i(t) = B_{i,0}e^{-t/\tau}$.

But, as we did say before, this not happened and it experimentally observed that the reversed field configuration is sustained as long as the toroidal current lasts. The dynamo effect is the mechanism that regenerate the magnetic field that is lost through the resistive diffusion.

The presence of the dynamo mechanism gives rise to an electric field, summed up in Ohm's law 1.23 to the externally applied electric field (see figure 1.21); again, this additional electric field contributes to drive a current density. Let decompose the magnetic and velocity fields as a sum of mean-field plus a fluctuation term, $\overrightarrow{A} = \overrightarrow{A}_0 + \widetilde{a}$ ($\overrightarrow{A}$ is a generic quantity). According to what we said above, considering the Ohm's law a new term E_d, the *dynamo electric field* given by the coherent interaction of the velocity

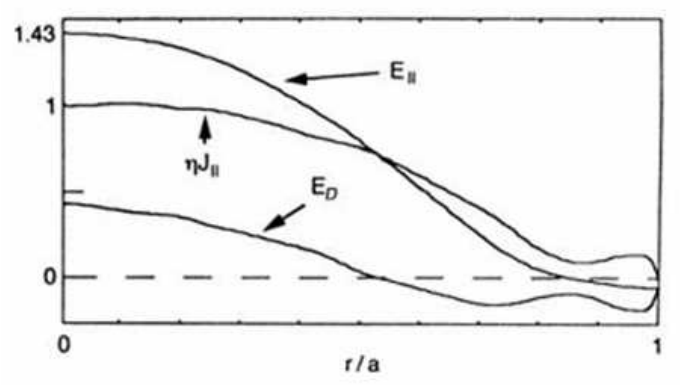

Figure 1.21: Radial profiles of parallel components of electric field and current density.

and magnetic field fluctuations[13], appears:

$$E_{\|} + E_d = E_{\|} + < \widetilde{v} \times \widetilde{b} >= \eta j_{\|}. \tag{1.58}$$

Multiple Helicity and Single Helicity

The high magnetic activity originates a well populated spectrum of $m = 0$ and $m = 1$ modes.

Standard RFP operations are called *multiple helicity (MH) regimes* because they are characterized by a *broad spectrum of helical magnetic modes resonant* throughout the plasma radius (see figure 1.22). This spectrum plays an important role in the standard MH dynamo. Again, because its richness, the spectrum implies that the many different magnetic islands associated with them, produces a *chaotic magnetic field*; in its turn, this chaos is a source for particle and heat transport [49]. This is a turbulent regime.

It is also possible a *spontaneous helically symmetric states*, called *quasi-single helicity (QSH) regime*, in which a single mode is dominant in the spectrum, but the amplitude of other modes (the *secondary modes*) is not zero, though very low. This regime have been measured in all existing RFP machines [52][53]. The QSH state is considered as an experimental evidence supporting the theoretical possibility for a helical *SH RFP state*. This a laminar regime.

The dynamo mechanism is described in several works. K. Kusano and T. Sato [54][55] clearly depicted the mechanism in terms of mode coupling. The RFP relaxation process resulting from the *non-linear* reconnection. Let consider two $m = 1$ unstable modes, $(1, n_1)$ and $(1, n_2)$, that rise up with

[13]For this reason the magnetic fluctuations are called also *dynamo modes*

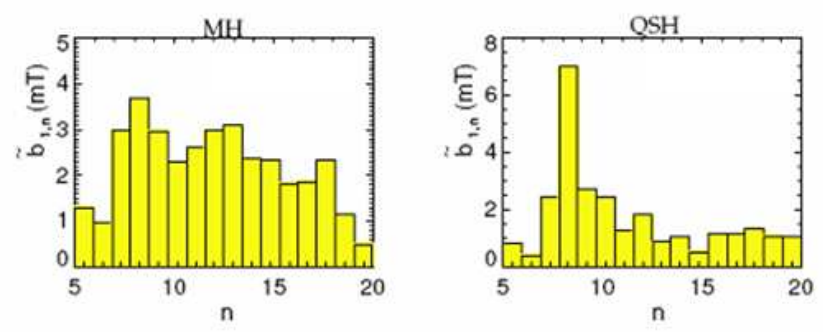

Figure 1.22: Typical $m = 1$ spectra for standard RFX discharge. In the left panel an example of MH spectra, in the right panel of QSH one.

natural growth rate γ_1 and γ_2 (as long as their amplitudes are much smaller than equilibrium magnetic field). Growing, the $m = 1$ modes coupling non-linearly and originate the $(0, n_1 - n_2)$ and the $(2, n_1 + n_2)$ modes. In its turn, the $m = 0$ mode form a magnetic island toroidally lined-up and yielding on the external side of the plasma column (at reversal radius $r_r ev$). Initially, the energies of the $m = 0$ and of the $m = 2$ mode are comparable; after than m=1 modes are non-linearly saturated, the energy of $m = 2$ mode is totally negligible with respect to the $m = 0$ energy.

All these $m = 0$ islands reconnect between them, generating a $m = 0$ *island chain*. With the reversal, the system stabilizes itself in its relaxed state. This picture implies an important role of the $m = 0$ modes for the production of the inverse field. But because the amplitude of the $m = 0$ dynamo electric field is one tenths respect to the $m = 1$ one, it could be that in fact the $m = 0$ effects are negligible. At least, Kusano and Sato deduced that the $m = 0$ mode not serve in presence of an initial highly unstable equilibrium, like an SH state; this means that any non-linear reconnection process is involved.

The transition from MH to QSH states, i.e between turbulent and laminar regimes, depending mainly on the *Hartmann number*, a dimensionless number defined as $H = (\eta\nu)^{-1/2}$ (η is the resistivity, ν is the viscosity) [56]; this is shown in the figure 1.23. The transition from MH state to SH state is smooth and the transition region describe the QSH states, with intermediate values of H and $m = 0$ amplitude.

Non-linear mode coupling and the Wall Locking

Mathematically, the modes are like the secondary terms of a Taylor expansion. So, the mode numbers of the resulting mode, due to the non-linear

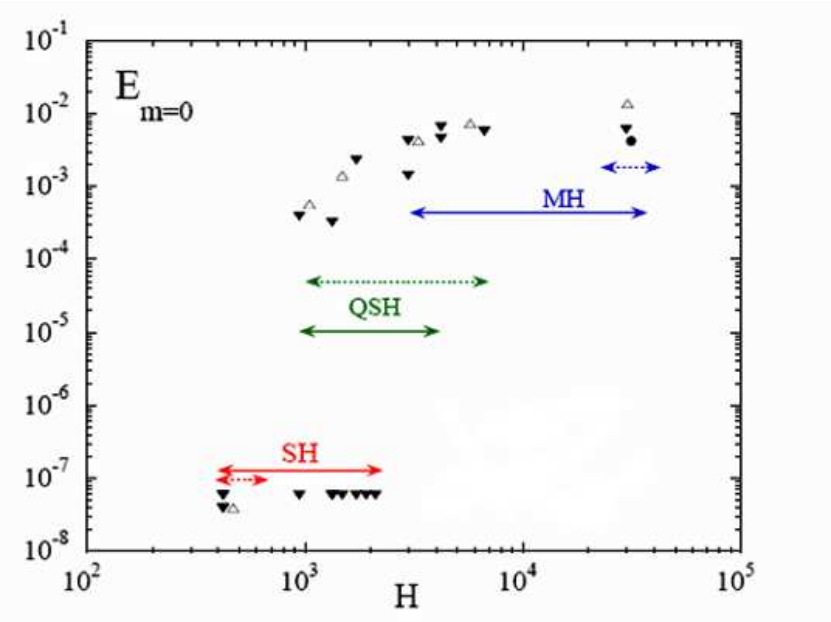

Figure 1.23: The time averaged magnetic energy of the $m = 0$ modes as a function of the Hartmann number. Adapted from [56].

coupling, are evaluated with the product of the periodical terms. Considering the coupling of two adjacent $m = 1$ modes, we have (without illustrate all the algebraic steps):

$$\begin{aligned} \cos \quad & [\vartheta - n\varphi] \cos[\vartheta - (n+1)\varphi] = ... = \\ = \quad & \frac{1}{2} \cos \varphi + \frac{1}{2} \cos[2\vartheta - (2n+1)\varphi]. \end{aligned} \tag{1.59}$$

This relation can be read as follow: *the non linear coupling of two adjacent* $m = 1$ *modes originates an* $(0, n)$ *mode and a* $(2, 2n + 1)$ *mode*. In general, if we have two modes (m_1, n_1) and (m_2, n_2), they not-linearly generate the modes $(m_1 + m_2, n_1 + n_2)$ and $(m_1 - m_2, n_1 - n_2)$. Actually, the modes generation is quite complicated: in fact, the progenitors interact with the generated modes in the same way, and so on. This is well shown in the figure 1.24.

The non-linear coupling is also crucial to produce mode phase lockings in RFPs devices, a phenomena both predicted from numerical simulations [57] and observed [58][59][60] in any experiment. Because to the viscous torque exerted on the mode rational surfaces by the flowing plasma, resonant modes often co-rotate with the plasma fluid [61][62]. Nevertheless, the mode rotation is generally not observed in resistive shell experiments and *the TMs are wall locked*. In the RFPs, $m = 0$ and $m = 1$ modes phase *lock together*

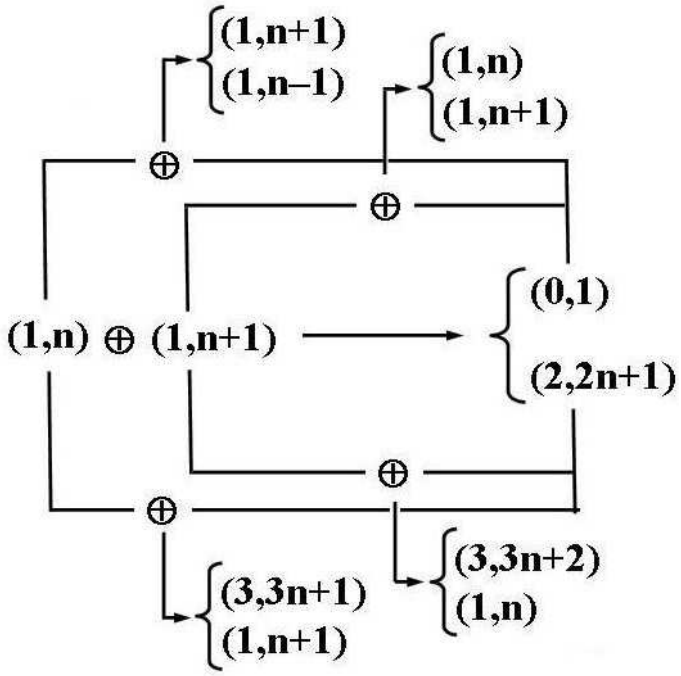

Figure 1.24: Cascade of modes originated by nonlinear way. Adapted from [30].

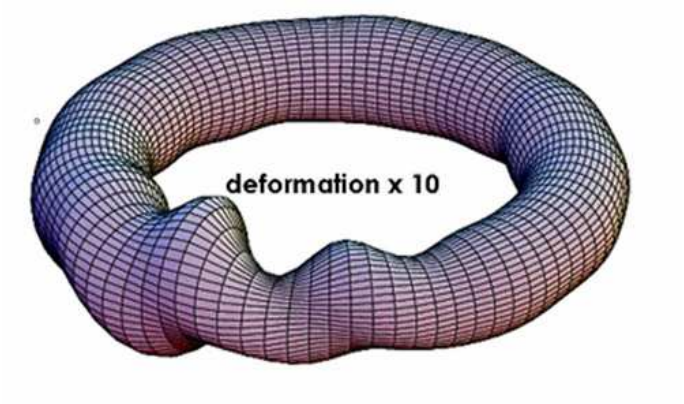

Figure 1.25: Deformation of the LCFS in a RFP owing to the locking in phase of $m = 0$ and $m = 1$ modes.

to form a toroidally localized structure in the perturbed magnetic field: the *slinky mode* [59][60][63]. If a slinky is stationary in the laboratory frame, it is referred as *wall locked mode* (LM).

The phase locking occurs as a result of *three wave nonlinear coupling* between $m = 0$ and $m = 1$ modes [64][65][66]. The mechanism of phase-locking is explained with the minimization of the electromagnetic torque exerted on the different resonant surfaces of the modes, in particular by static external field error, vacuum vessel (with its eddy currents), interacting with TMs [59][62][61][67][68], and it is detailed exposed in [69][70].

The LM is not negligible in amplitude and localized in nature: the distortion of the *last closed flux surface* (LCFS) is a non uniform, non-axisymmetric shift that follows a helical path (see figure 1.25). The LM brings evil effects for the discharge, leading the plasma-wall interaction and the subsequent production of impurities towards the plasma[58]. For instance, in the RFX machine the LM can extend for more than 40° in the φ coordinate and persists stationary during the discharge. The first wall facing to the wall locking is exposed to important thermal stresses ($\sim 100 MW/m^2$ in RFX). All in all, the TMs are dangerous instabilities that can lead to energy and plasma confinement losses [21].

An important relation of the mode phase locking physics, links the phases of adjacent modes [69][70]. The difference of these modes is constant, and should correspond to the position of the locking according to

$$\phi_{1,n+p} - \phi_{1,n+q} = (p - q)\phi_L \tag{1.60}$$

where $\phi_{1,n+p}$ and $\phi_{1,n+q}$ are the phases, respectively, of the $m = 1$ and $n = p, q$ modes, p, q natural numbers, ϕ_L is the locking position [69]. In the three-wave interaction between two adjacent $m = 1$ modes $(1, n + 1)$, $(1, n)$

and $(0,1)$ (the last one considered intrinsically stable), the electromagnetic torque is proportional both to the amplitudes of the $m = 1$ modes (for the viscous torque it is just the opposite) and to

$$\sin(\phi_{1,n+1} - \phi_{1,n} - \phi_{0,1}). \tag{1.61}$$

In the so-called *strong-locking condition* [67] the amplitude of the modes is high and 1.61 is small. In this limit is verified either the relation [69]

$$\phi_{1,n+1} - \phi_{1,n} - \phi_{0,1} \approx \begin{cases} 0 \\ \pi \end{cases} \tag{1.62}$$

If several $(1, n+p)$ modes are phase locked with the same $(0,1)$ mode, we obtain either

$$\phi_L \approx \begin{cases} \phi_{0,1} \\ \phi_{0,1} + \pi \end{cases} \tag{1.63}$$

The comparison between this model and the RFX data shows a good agreement for not too high Θ values. So it could be possible to that $m = 0$ are intrinsically unstable, because the vacuum space between plasma and conducting shell at $b/a = 1.18$ (that is a linear unstable condition for the $m = 0$ modes).

1.4 Magnetic confinement: RFPs experimental devices

1.4.1. RFX-mod

The RFX-mod experiment ($a = 0.459m$, $R_0 = 1.995m$, $I \leq 2MA$, plasma pulse length up to $350ms$), placed in Padua (Italy, near Venice), is a RFP device equipped with a sophisticated active control system composed by 192 active saddle coils, arranged in 4 toroidal arrays of 48 poloidal coils independently powered, each located on the external surface of the shell (average radius $r_c = 0.513m$, shell time constant for the penetration of the vertical field $\tau_w = 50 \div 60ms$). The corresponding magnetic sensors, able to measure the radial and toroidal components of the magnetic field, are positioned on the inner side of the shell at $r_w = 0.508m$. The system can interact with the typical broad perturbation spectrum of the RFP plasma, mainly modes with poloidal numbers $m = 0, 1$.

RFX-mod is the modification of RFX (**R**eversed **F**ield E**X**periment) experiment [71], operating in Padua in the period 1992-1999. The modifications were done to *improving the plasma boundary* (plasma facing components and passive magnetic boundary) and to introducing an *active MHD mode control capability* [72][73].

The system of sensors and active coils can be used to actuate different feedback schemes: e.g. the so called Virtual Shell (VS) is able to make the radial magnetic field b_r strongly reduced at r_w, with a stabilizing influence

on the unstable modes, a reduction effect on error fields and in general a strong beneficial effect on the plasma [74][75].

The saddle coils system is however not optimal for the generation of $m = 0$ low n's modes. For this reason, in some active experiments, the $m = 0$ perturbations are generated by the toroidal field coils, i.e. a set of 48 poloidally symmetric coils (average radius $r_c = 0.621m$), normally used to generate the axi-symmetric ($n = 0$) equilibrium toroidal magnetic field. The coils are arranged in 12 clusters of 4 coils each, so there are 12 currents determined by 12 independent power supplies. This system is able to generate non axi-symmetric $m = 0$ modes with n up to 6. Note the convention of assigning toroidal numbers $n < 0$ to the internally resonant magnetic perturbations.

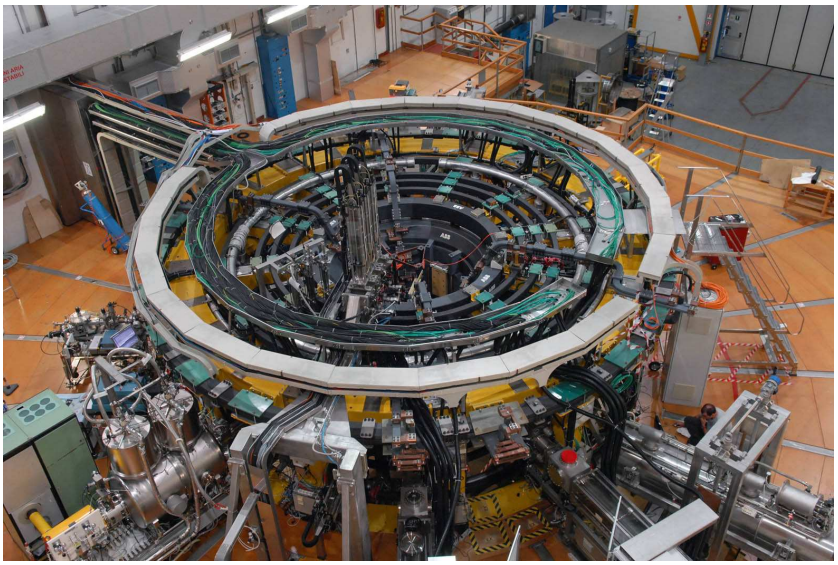

Figure 1.26: Picture of the RFX-mod device. From [76].

1.4.2. EXTRAP-T2R

The EXTRAP-T2R device ($a = 0.183m$, $R_0 = 1.240m$, I in the range $(100 - 300)kA$, plasma pulse length up to $25ms$) is an RFP placed in Stockholm. T2R has a resistive shell with magnetic penetration time for the vertical field of $\tau_w = 6.3ms$. As RFX-mod, the system can interact with the typical broad perturbation spectrum of the RFP plasma, mainly modes with poloidal numbers $m = 0, 1$. A typical $m = 1$ spectrum is shown in figure 1.28. The system for active control of RWMs installed includes a full-coverage, radial-field coil array located just inside the shell. The array get 64×4 coils (toroidal and poloidal, respectively); each coil covers a rectangu-

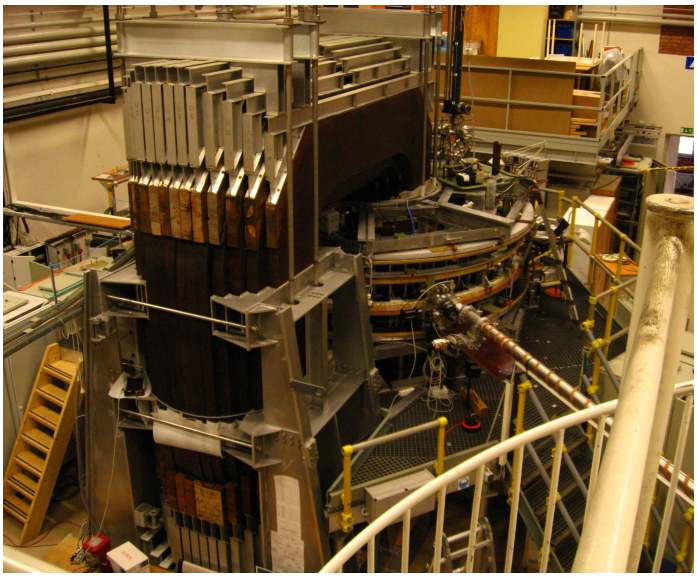

Figure 1.27: Picture of the T2R device.

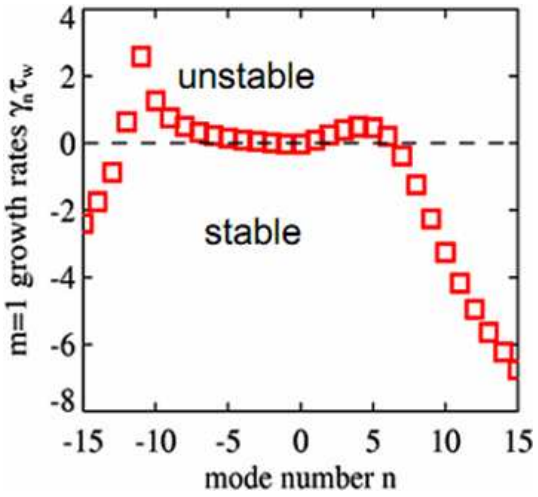

Figure 1.28: Typical spectra of EXTRAP-T2R machine.

lar area of $5.6° \times 90°$. There is also a 32×4 full-coverage saddle coil array, just outside the shell [77].

CHAPTER 2

A linear model for the feedback studies

In the previous paragraph we have seen that in fusion plasmas a wide range of MHD instabilities exist. These instabilities bring to a degradation of plasma confinement, on the loss of the plasma control with end of the discharge. Then it is clear that an important topic is to control these instabilities; in particular, by using feedback stabilization techniques[1]. Mode stabilization via the active feedback is therefore a method for increasing the global performance of the plasma in toroidal devices. Experiments and theoretical studies have shown MHD instability can be stabilized at least under certain conditions by active feedback [67][74][78][79][80][81].

The RFP physics is well approximated by the cylindrical MHD model with thin shell, simplifying the theoretical analysis. The magnetic field perturbation is expanded in Fourier harmonics (see the paragraph 1.3.2). The time-dependence is included in the model, by matching the solutions of both sides of the resistive wall.

The model follows reference [78], where a feedback control scheme is introduced, with a realistic geometrical description of the coils, for the RFP device. A theoretical cylindrical model for plasma response has been derived, considering a finite number of active coils and sensors. Besides, the model assumes a homogeneous thin shell (no gaps or holes) through which the solution is matched.

A feedback control scheme can be generally summarized as in the figure 2.3, where the active control structure is schematized. It works as follows (for more details see [75]). Let consider a plasma producing a magnetic

[1] This is a different problem with respect the fact that an elongated toroidal configuration is vertically unstable with respect a constant displacement along φ (i.e. with toroidal wave number n). The solution of this last problem has been faced and solved, by applying a vertical magnetic field B_v such as the Lorentz's force $q\overrightarrow{v} \times \overrightarrow{B_v}$ acting on the plasma itself, be direct towards the inside.

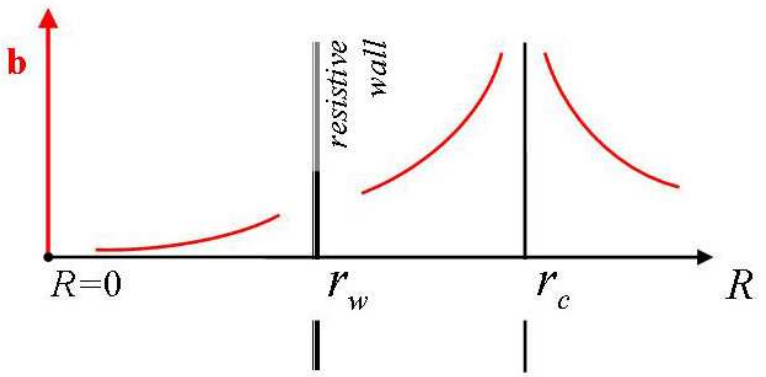

Figure 2.1: Scheme of the linear model. The boundary conditions determines the matching of the solutions between the plasma and the vacuum regions, through the resistive wall, at r_w, and the coils at r_c.

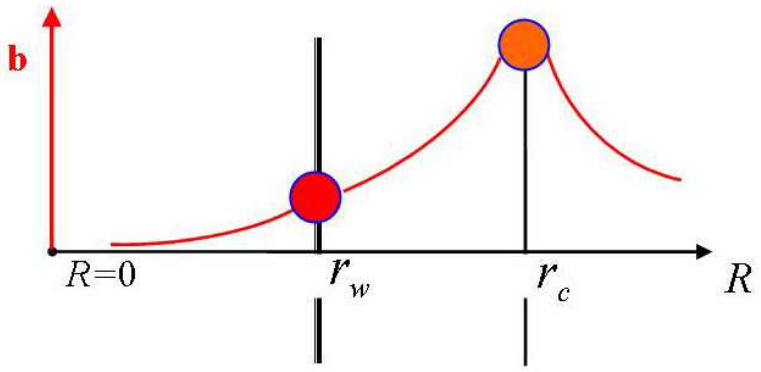

Figure 2.2: Like the previously sketch, highlighting the trend of the magnetic field and the region where must be satisfied the BCs.

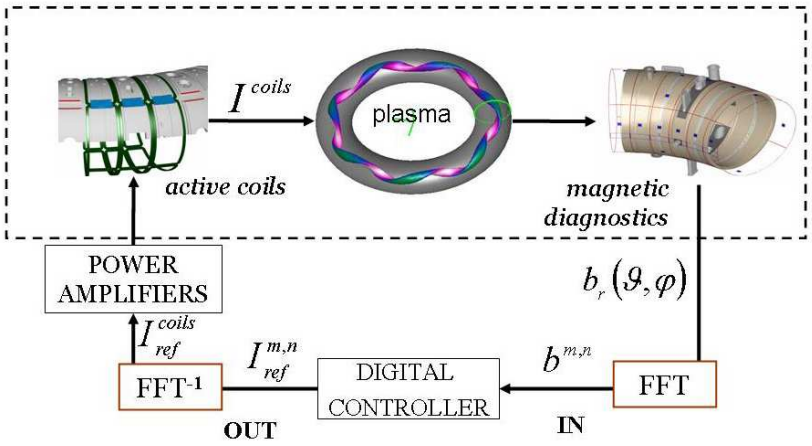

Figure 2.3: Feedback control scheme.

perturbation: it is measured by the magnetic sensors. Then the whole set of signals are Fourier decomposed REF SU FOURIER??? and converted, by the digital controller, into reference current signals for the active coils corresponding to each harmonic. The reference currents for each active coil (provided by the power supplies) is obtained by mean of an inverse FFT

2.1 The boundary conditions

To formulate in the right way an MHD problem, we must specify an appropriate set of boundary conditions, *BCs* hereafter, in order to couple the plasma with the externally applied magnetic field. Considering the problems that involve equilibrium and stability, there are mainly three class of BCs, see the figure 2.4.

In the case of *completely conductor wall* (case *(a)* of figure 2.4), used here, we put the wall itself at $r = R_w(\vartheta, z)$ and, said $\overrightarrow{n}$ the outward vector normal to the surface, the BCs are:

$$\overrightarrow{n} \times \overrightarrow{E}|_{R_w} = 0$$
$$\overrightarrow{n} \cdot \overrightarrow{B}|_{R_w} = 0$$

In case *(a)* of figure 2.4, where a metal wall surrounding the plasma is considered, the so called *thin shell* approximation can be used. In this case, the radial current density flowing in the wall is thought negligible, whilst the radial magnetic field and the others components of the current density are constant and proportional to the jumps in the magnetic field $\widehat{\vartheta}$ and $\widehat{\varphi}$ components. In fact the resistive wall is modelized like a thin and complete

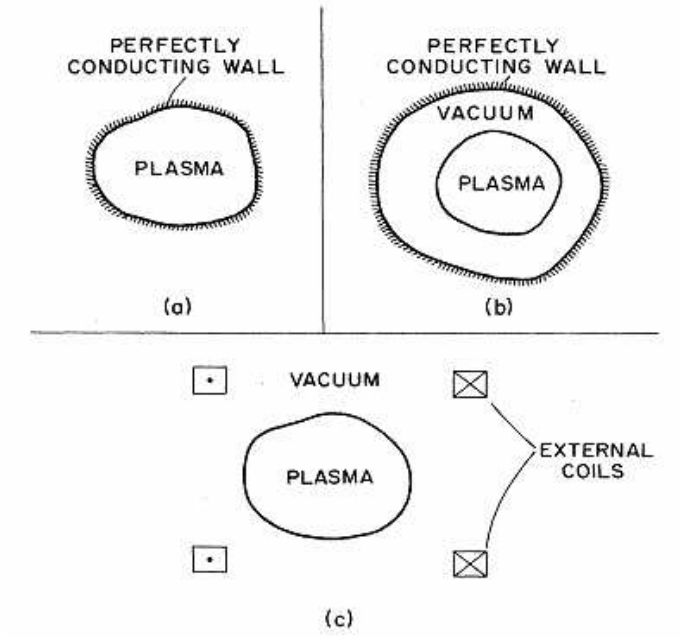

Figure 2.4: The three classes of boundary conditions more frequently used in ideal MHD. (a) Perfecting conducting wall; (b) Vacuum region that isolated plasma from wall; (c) Plasma surrounded by external coils and a metal wall. From [27].

shell; "complete" means that it is without gaps[2].

The thin shell approximation satisfies the following conditions:

$$\left[\overrightarrow{b_r}\right]_{r_w^-}^{r_w^+} = 0$$
$$\left[\frac{\partial}{\partial r}\left(r b_r\right)\right]_{r_w^-}^{r_w^+} = \tau_w \frac{\partial b_r}{\partial t}.$$

$[...]_{r_w^-}^{r_w^+} = 0$ is the *jump*, that is the difference among a quantity considered in the two side of the wall. τ_w is the *wall penetration time* of the field. In the case of a perturbation exponentially growing, denoting with $\gamma_{m,n}$ the natural growth rate of the mode (m,n) itself, $b_r = b_r^{(m,n)} \propto e^{\gamma_{m,n} t}$, the second condition becomes:

$$\left[\frac{\partial}{\partial r}\left(r b_r\right)\right]_{r_w^-}^{r_w^+} = \tau_w \gamma_{m,n} b_r. \tag{2.1}$$

In the outer vacuum region, a Laplace equation for the magnetic scalar potential defines the problem:

$$\nabla^2 \Phi = 0, \tag{2.2}$$
$$\overrightarrow{b} = \nabla \Phi. \tag{2.3}$$

Therefore (in a cylinder), the potential is a linear combination of the Modified Bessel Functions,

$$\Phi = A \cdot I_m(|n|\epsilon_r) + B \cdot K_m(|n|\epsilon_r) \tag{2.4}$$

where $\epsilon_r = r/R_0$; so, to obtain finite amplitude solution, for $r < r_w$is $B = 0$ and for $r > r_c$ is $A = 0$, whereas in $r \in [r_w, r_c]$ A and B are both non-zero. The resulting perturbed radial magnetic field is therefore the linear combination of the first derivatives (with respect to the radial coordinate) $I'_m(|n|\epsilon_r)$ and $K'_m(|n|\epsilon_r)$, in the three different spatial regions as explained above.

At least, we have a boundary condition for the coil region, considered like a layer of thickness δ_c. Let be $\overrightarrow{K} = (K_r, K_\vartheta, K_\varphi)$ the superficial density current of the coil. Observing that the radial field derivative has a jump at $r = r_c$, due to the current I_c associated to the coil, we have the condition (see appendix A.2):

$$\left[\frac{\partial}{\partial r}\left(r b_r\right)\right]_{r_c^-}^{r_c^+} = -\imath \frac{\mu_0}{2\pi r_c^2} \frac{m^2 + n^2 \epsilon_c^2}{m} I_c. \tag{2.5}$$

The coil current is linked to the superficial density current by the relation $I_c = 2\pi r_c \delta_c K_\varphi$.

[2]We remember that the error fields originate by different causes: the ripple of the toroidal magnetic field; the gaps and all the inhomogeneity and irregularities of the fields and of the conductors present around the plasma; the plasma-coils interactions.

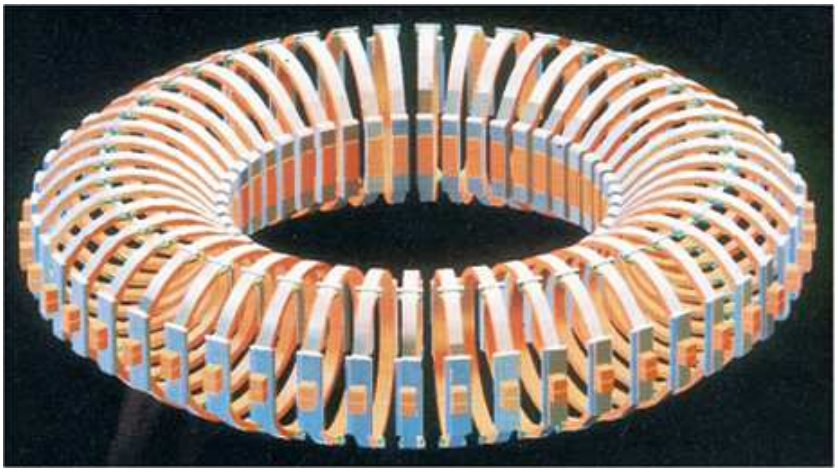

Figure 2.5: Schematic representation of the RFX-mod toroidal field coils system. From [82].

2.2 Current contributions from discrete coils

First, we must remember again that we consider a cylindrical model for a RFP, with a minor radius of the plasma and periodicity on the axis $f(R, \vartheta, z) = f(R, \vartheta, z + 2\pi R_0)$. In our model we assume two arrays of coils: the sensor loops array and the feedback coil loops array. The sensors, able to measure the components of the magnetic field, just inside the wall, are located at the wall radius $r_w > a$. The feedback coils are located at the radius $r_c > r_w$, forming a $M_c \times N_c$ array, where M_c and N_c are, respectively, the number of poloidal and toroidal coils.

Now, we must characterize the coils system. Let us assume that these coils are equidistant in ϑ and φ with angular width, respectively, $\delta\vartheta_c$ and $\delta\varphi_c$. We must calculate the shape factor in Fourier space in two different cases: for the toroidal field coils used to produce the $m = 0$ toroidal field perturbation and for the 192 saddle coils system (4 poloidal $\times$ 48 toroidal) mainly to produce m=1 perturbation (figure 2.6).

The shape factor for an array of ring coils

The shape factor for an array of N_c coils modelized as rings, each of them of radius r_c, can be calculated in the following way.

Let consider N_c rings, infinitely narrow along r and toroidal angular width $\delta\varphi$, of poloidal current I_k (control currents), in toroidal position $\varphi_k = 2\pi(k-1)/N_c$, with $k = 1, ..., N_c$. For each of these currents one can associate

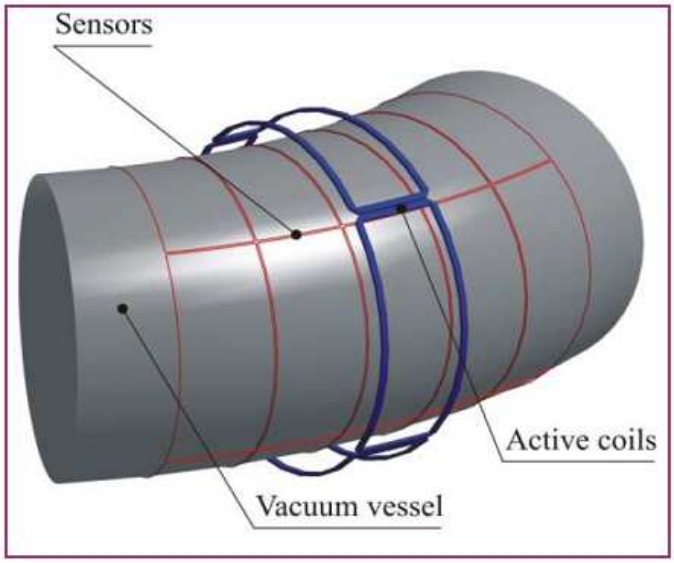

Figure 2.6: Sketch of the RFX-mod structure, with in evidence a saddle coil, some sensors and the vacuum vessel section.

a superficial density current (Ampere/meter)

$$K_\vartheta = \frac{I_k}{R_0 \cdot \delta\varphi}\Theta_\pm \tag{2.6}$$

where R_0 is the major radius of the torus,

$$\begin{aligned}\Theta_- &= \Theta\left(\varphi - (\varphi_k - \frac{\delta\varphi}{2}\right), \\ \Theta_+ &= \Theta\left(\varphi + (\varphi_k - \frac{\delta\varphi}{2}\right)\end{aligned}$$

and (see figure below)

$$\Theta_\pm = \Theta_- - \Theta_+. \tag{2.7}$$

For a thin shell the eddy currents in the shell itself have not important variations along the direction of its thickness and so we can express the current density by means of a flow function [83]; then we introduce the *current stream function* $J_f(\vartheta, \varphi)$ with its Fourier transform [78]

$$FT\,(J_f) = J_f^{m,n} = \frac{1}{(2\pi)^2}\int_{-\infty}^{+\infty}\int_{-\infty}^{+\infty} J_f e^{-\imath\pi\vartheta} e^{-\imath\pi\varphi} d\vartheta d\varphi. \tag{2.8}$$

Let consider for simplicity a rectangular coil of dimension $\Delta\vartheta \times \Delta\varphi$ centered in (ϑ, φ); by defining the current path as clockwise and observing that the

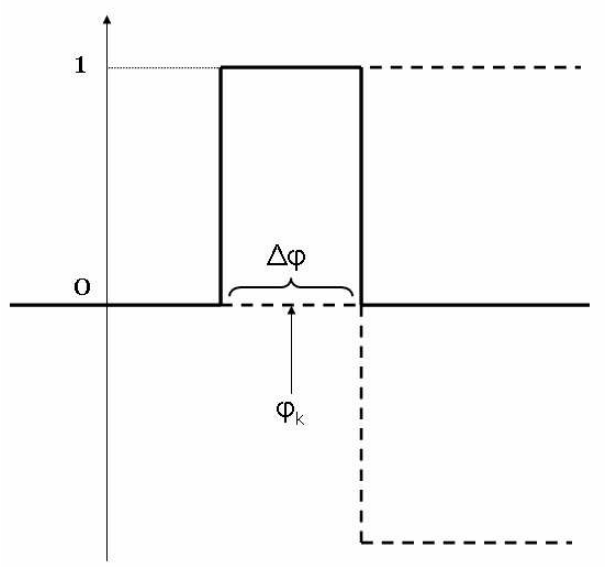

Figure 2.7: Heaveside's theta composition.

line-elements are

$$\begin{aligned} ds_\varphi &= R_0 \tan\Delta\varphi \approx R_0\Delta\varphi, \\ ds_\vartheta &= r_c \tan\Delta\vartheta \approx r_c\Delta\vartheta \end{aligned}$$

(see figure 2.8), and by defining $\overrightarrow{K} = \nabla J_f \times \widehat{e}_r$, we can write:

$$\begin{aligned} K_\vartheta(\vartheta,\varphi) &\cong \frac{J_f(\vartheta,\varphi+\Delta\varphi) - J_f(\vartheta,\varphi)}{R_0\Delta\varphi}, \\ K_\varphi(\vartheta,\varphi) &\cong \frac{-J_f(\vartheta+\Delta\vartheta,\varphi) + J_f(\vartheta,\varphi)}{r_c\Delta\vartheta}. \end{aligned}$$

In the approximation of J_f continue, we obtain just

$$\overrightarrow{K} \cong \left(0, \frac{1}{R_0}\frac{\partial J_f}{\varphi}, -\frac{1}{r_c}\frac{\partial J_f}{\vartheta}\right) = \nabla J_f \times \widehat{e}_r. \tag{2.9}$$

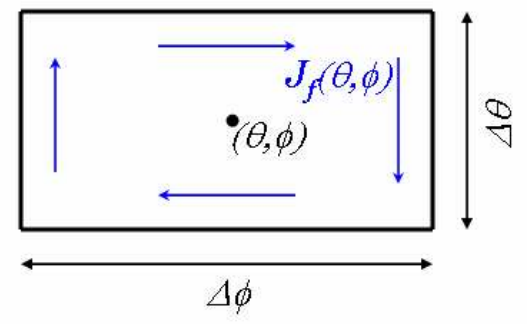

Figure 2.8: Direction of the currents for the derivation of relation 2.9.

Now,

$$\begin{aligned} FT\left(K_\vartheta\right) &= FT\left(\frac{1}{R_0}\frac{\partial J_f}{\partial\varphi}\right) = \\ &= \frac{1}{2\pi}\int_{-\infty}^{+\infty}\left[\frac{1}{R_0}\frac{\partial J_f}{\partial\varphi}\right]e^{-\imath n\varphi} = \\ &= \frac{1}{2\pi}\left\{\left[-J_f\frac{\imath n}{R_0}e^{-\imath n\varphi}\right]_{-\infty}^{+\infty} + \frac{\imath n}{R_0}\int_{-\infty}^{+\infty} J_f e^{-\imath n\varphi}d\varphi\right\} = \\ &= \frac{\imath n}{R_0}FT\left(J_f\right). \end{aligned}$$

Since it is, by definition, $FT\left(K_\vartheta\right) = \frac{1}{2\pi}\int_{-\infty}^{+\infty} K_\vartheta e^{-\imath n\varphi}d\varphi$, the Fourier transform of the stream function will be:

$$J_f = -\frac{\imath R_0}{2\pi n}\int_{-\infty}^{+\infty} K_\vartheta e^{-\imath n\varphi}d\varphi.$$

Substituting to K_ϑ the expression in 2.8, the one for the $k-th$ current will be

$$J_f = -\frac{\imath I_k}{2\pi n\cdot\delta\varphi}\int_{-\infty}^{+\infty}\Theta_\pm e^{-\imath n\varphi}d\varphi$$

that, using the Fourier transform for (2.8), leads[3] to:

$$J_{f,k} = -\frac{jI_k}{2\pi n\cdot}\frac{\sin\left(n\delta\varphi/2\right)}{n\delta\varphi/2}e^{-\imath n\varphi}. \tag{2.10}$$

[3]See appendix A.1.

Now we must sum over all the currents $k = 1, ..., N_c$, obtaining

$$\begin{aligned} J_f^n &= -\frac{\imath}{2\pi n\cdot}\frac{\sin(n\delta\varphi/2)}{n\delta\varphi/2}e^{-\imath n\varphi}\sum_{k=1}^{N_c} I_k e^{-\imath n\varphi_k} = \\ &= \underbrace{-\frac{\imath N_c}{2\pi n\cdot}\frac{\sin(n\delta\varphi/2)}{n\delta\varphi/2}}_{F_n}\cdot\underbrace{\frac{1}{N_c}\sum_{k=1}^{N_c} I_k e^{-\imath n\frac{2\pi}{N_c}(k-1)}}_{I_n}. \end{aligned}$$

F_n is the shape factor for the $(0, n)$ mode and I_n the respective coil current. For infinitely thin coils $\delta\varphi \to 0$ is trivial to deduce the result:

$$F_n \longrightarrow_{\delta\varphi\to 0} -\imath\frac{N_c}{2\pi n}. \tag{2.11}$$

This is the relation used in the code for the active coils in the case of $m = 0$ mode applied.

The shape factor for a rectangular coil in an array of $M_c \times N_c$ similar coils

In the case of rectangular shaped coils by recalling that the Fourier transform of a rectangular box with base L and unit hight is the function $L\text{sinc}(\pi sL)$, with s independent variable in the Fourier space and $\text{sinc}(x) = \sin(x)/x$. By extending the calculation in two dimension and specializing it for an array of $M_c \times N_c$ rectangular coils (M_c in the ϑ direction, N_c in the φ direction), where any coil has dimension $\delta\vartheta \times \varphi$, the shape factor for each of them, referred to a (m, n) mode and supposing thin wires, is [78]:

$$F_{m,n} = \frac{M_c N_c}{(2\pi)^2}\,\text{sinc}(m\delta\vartheta/2)\,\text{sinc}(n\delta\varphi/2) \tag{2.12}$$

The sideband effect

We obtain that the (m, n)-th Fourier component in the real space of the current potential 2.8:

$$J^f_{m,n} = F_{m,n}\sum_{\lambda=-\infty}^{+\infty}\sum_{\nu=-\infty}^{+\infty} I_{m',n'} \tag{2.13}$$

with $m' = m + \lambda M_c$, $n' = n + \nu N_c$. This equation points out the so-called *sideband effect* produced by the discrete set of coils: *an externally produced (m, n)-th component of the current in the coils generates an infinitive number of harmonics in J^f, each of them separated by multiples of M_c and N_c.* Actually, this is a general characteristic of each system based on a finite

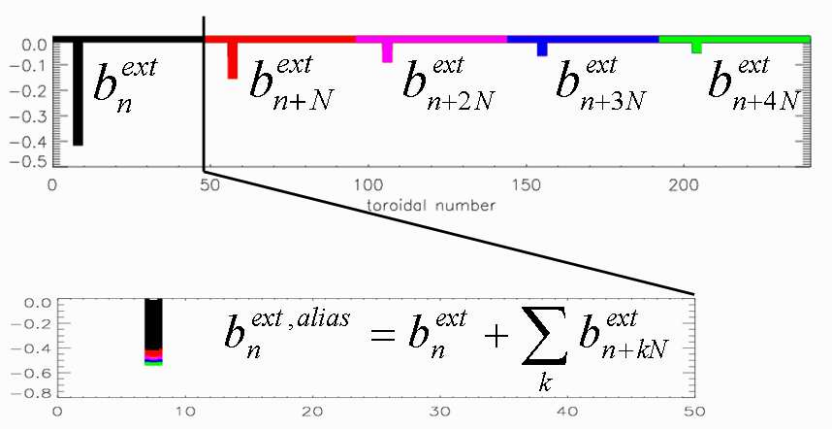

Figure 2.9: Sidebands aliasing. (Courtesy of L. Marrelli.)

number of dimensionally finite coils, and it corresponds to the well known phenomenon of the *aliasing* (see [84]).

This effect introduces difficulties for the control system. In particular, in the magnetic confinement system as the RFPs it is present the problem of the simultaneous stabilization of the modes. The main complication is about the possible coupling of the unstable modes through the feedback coils: due to the coils generation of the sidebands harmonics.

So, the main limitation for an effective control of the RWMs or others MHD instabilities is the finiteness of the number of the feedback coils, that doesn't permit the independent control of any unstable mode. The requirement of to avoid the mode coupling imposes restriction on the minimum number of the coils in the arrays. For avoiding the sideband coupling, the minimum on number of feedback coils along the toroidal direction must be

$$\begin{cases} N_c > n_{max} - n_{min} \\ M_c > m_{max} - m_{min}, \end{cases} \tag{2.14}$$

which means for typical spectra in the RFX device, $N_c > 20$ and $M_c > 1$. For safety, $N_c = 48$ and $M_c = 4$ was chosen.

Against the number of sidebands, virtually infinite, we have a finite number of sensors. For a better clarity, let look figure 2.9 where we consider the array of coils only in the φ direction, with the sensor number $N = 48$ equal to the active coils number.

2.3 The complete relations

As we said at page 51, the model is completed by suitable BCs, e.g. the continuity of the radial magnetic field (thin shell approximation) and jump

conditions for its first radial derivative at r_c and at r_w. The fluctuating fields are expanded in Fourier series, like in the equation 1.41:

$$\widetilde{\psi}(r,\vartheta,\varphi;t) = \sum_{m,n} \widetilde{\psi}(r;t)\cdot e^{-\imath(m\vartheta+n\varphi)}, \tag{2.15}$$

The jump condition at the conductive wall for each Fourier harmonics reads as (see the appendix A.2):

$$r_w \left[\frac{\partial b^{rad}_{m,n}}{\partial t}\right]_{r_w^-}^{r_w^+} = \tau_w \frac{\partial b^{rad}_{m,n}}{\partial t} \tag{2.16}$$

where the +/- signs refer to the inside and outside of the wall. At r_c, in general a jump condition for the radial magnetic field can be deduced (see 53).

The response of the system depends noticeably by the type of sensor used. In [79] and [78] is described the method used for to calculate currents and magnetic fields. The radial magnetic field $b^{fc}_{m,n}$ generated by the coils depends, through the Modified Bessel functions (see 26) and the geometry of the array, to the surface current density J^{fc} flowing in the coils themselves. The (m,n)-th component of J^{fc} is

$$J^{fc}_{m,n} = F_{m,n} \sum_{l=-\infty}^{+\infty} \sum_{p=-\infty}^{+\infty} I_{m+lM_c,n+pN_c} \tag{2.17}$$

where $F_{m,n}$ is the shape factor. In fact, first is introduced a basic shape function for each single coil, $f(\vartheta,\varphi)$, such as $f=1$ in the coil are and zero outside it. Let be $I_{m,n}$ a generic control current harmonic and considering a generic lk-th coil centered in ϑ_l, φ_k, with $\vartheta_l = 2\pi l/M_c$ and $\varphi_k = 2\pi k/N_c$. Then, the current potential at $r = r_c$ is

$$\begin{aligned} J^f(\vartheta,\varphi) &= I_{m,n}\cdot \\ &\cdot \sum_{l=0}^{M_c-1}\sum_{k=0}^{N_c-1} f(\vartheta-\vartheta_l,\varphi-\varphi_k)\exp[-\imath(m\vartheta_l+n\varphi_k)] \end{aligned} \tag{2.18}$$

The (m',n') Fourier component of $J^f(\vartheta,\varphi)$ is:

$$J^f_{m',n'} = \frac{1}{2\pi^2}\oint\oint J^f(\vartheta,\varphi)\exp[-\imath n'\varphi]\exp[-\imath m'\vartheta]d\varphi d\vartheta.$$

Considering the definition of the Fourier transformed shape function for a generic single coil,

$$F_{m,n} = \frac{M_c N_c}{(2\pi)^2}\oint\oint f(\vartheta,\varphi)\exp[-\imath(m\vartheta,n\varphi)]d\varphi d\vartheta \tag{2.19}$$

(of which the relation 2.12 is a particular expression), at last we obtain 2.17.

After all it results [78]

$$b^{fc}_{m,n} = \frac{\mu_0}{\pi a} c_{m,n} J^{fc}_{m,n} \tag{2.20}$$

where we can make the coefficient explicit,

$$c_{m,n} = -\pi n^2 \epsilon_a \epsilon_c K'_m(|n|\epsilon_c) I'_m(|n|\epsilon_c). \tag{2.21}$$

The final relation links the harmonics of the toroidal magnetic field at the sensor position to the harmonics of the radial component of the magnetic field generated by the coils $b^{fc}_{m,n}$ in absence of the plasma and the wall:

$$\{b^{rad}_{m,n}, b^{pol\pm}_{m,n}, b^{tor\pm}_{m,n}\} = \{1, a^{pol\pm}_{m,n}, a^{tor\pm}_{m,n}\} M_{m,n} b^{fc}_{m,n} \tag{2.22}$$

These relations ask for a better explanation. According to what we said in the previously paragraph, there is a sidebands generation effect:

$$b^{fc}_{m,n} = -\frac{\mu_0}{\pi a} \cdot \left[-\pi n^2 \epsilon_c \epsilon_w K'_m(|n|\epsilon_w) \cdot I'_m(|n|\epsilon_w)\right] \cdot F_{m,n} \sum_{\lambda=-\overline{m}}^{+\overline{m}} \sum_{\nu=-\overline{n}}^{+\overline{n}} I^{coils}_{m',n'} \tag{2.23}$$

where $m' = m + \lambda M_c$, $n' = n + \nu N_c$ and the indexes λ and ν are spanning over the sidebands. The coil shape factor $F_{m,n}$, relative to the (m,n)-mode, is related to the geometry.

The coefficients a and M are defined as:

$$a^{pol-,tor-}_{m,n} = s_0 \frac{d_{m,n} - 1 + 2\tau_w \gamma_{m,n}}{m^2 + |n|^2 \epsilon_w^2}, \tag{2.24}$$

$$a^{pol+,tor+}_{m,n} = s_0 \frac{d_{m,n} - 1 + 2\tau_w (\gamma_{m,n} - s)}{m^2 + |n|^2 \epsilon_w^2}, \tag{2.25}$$

$$M_{m,n} = -\frac{1}{2\tau_w \left(s + \Gamma^w_{m,n}\right)} \cdot \frac{1 + \frac{m^2}{n^2 \epsilon_w^2}}{K'_m(|n|\epsilon_w) \cdot I'_m(|n|\epsilon_c)} \tag{2.26}$$

$$\tag{2.27}$$

where

$$d_{m,n} = 1 - \left(1 + \frac{m^2}{n^2 \epsilon_w^2}\right) \frac{|n|\epsilon_w K_m(|n|\epsilon_w)}{K'_m(|n|\epsilon_w)}; \tag{2.28}$$

$\epsilon_c = r_c/R_0$ (and $\epsilon_w = r_w/R_0$) and $\Gamma^w_{m,n}$ is a quantity related to the "natural" penetration rate of the mode through the wall in absence of feedback, while s is the Laplace transformed time variable. $M_{m,n}$ is the radial transfer function, i.e. the ratio $b^{rad}_{m,n}|_{r_{sens}}/b^{fc}_{m,n}$, with poles at the basic mode growth (or damping) rates $s = \Gamma_{m,n}$. Physically, $M_{m,n}$ represents the effective self-inductance, calculated assuming that sensors and coils are equally-spaced, both in ϑ and φ, as we said previously. The quantities $a_{m,n}$ are the ratios

between the selected component of the magnetic field, in the inner (sign +) or the outer (sign −) side to the wall, with respect to the radial field at the wall. The adimensional quantity $d_{m,n}$ is the ratio $r\ b'_r/b_r$ for the external magnetic field in the absence of feedback currents. The *sign factor* $s_0 = \pm 1$ that depends to the mode (m, n) that we want to stabilize (we must choose the sign of m or of n, respectively, for the poloidal sensors and the toroidal sensors).

Contribute of the sensors

We already pointed out that, in the case of saddle coils, sensors and actuators are in the same number and, then, the sidebands are the same for construction. With a treatment similar to that for the feedback coils, for each component of the field at the sensors we obtain the equation **??** with the shrewdness to replace $M_{m,n}$ in 2.24 with the factor

$$M_{m,n} \rightarrow \sum_{m'} \sum_{n'} S_{m',n'} M_{m',n'}$$

where S is the shape factor for the sensor and the summations are above the terms $m' = m + lM_c$ and $n' = n + pN_c$ [78].

2.3.1. The m=0 case

Particular interest covers the the poloidally symmetric case, that is we apply the $m = 0$ perturbation, the radial field is instead radially continuous. The final relation 2.22 now is:

$$b^{calc}_{0,n} = a_{0,n} M_{0,n} b^{fc}_{0,n} \tag{2.29}$$

where only $m = 0$ modes generated by the poloidally symmetric toroidal field coils are considered. $M_{0,n}$ and the coefficients $a_{0,n}$ are defined as:

$$M_{0,n} = \frac{1}{2\tau_w \left(s + \Gamma^w_{0,n}\right)} \cdot \frac{1}{K'_0(|n|\epsilon_w) \cdot I'_0(|n|\epsilon_c)}, \tag{2.30}$$

$$a_{0,n} = \frac{\mathrm{sgn}(n)}{|n|\epsilon_w} \cdot \left[\frac{2\tau_w \Gamma^w_{0,n}}{|n|\epsilon_w} - \frac{K_0(|n|\epsilon_w)}{K'_0(|n|\epsilon_w)}\right] \tag{2.31}$$

where any quantity has the same significance that in the equation 2.22.

In our model a cluster of four coils is supplied with the same current, therefore the number of independent currents is limited to $N_c = 12$ and there is a sidebands generation effect:

$$b^{fc}_{0,n} = -\frac{\mu_0}{\pi a} \cdot \left[-\pi n^2 \epsilon_c \epsilon_w K'_0(|n|\epsilon_w) \cdot I'_0(|n|\epsilon_w)\right] \cdot F_{0,n} \sum_{\nu=-\overline{n}}^{+\overline{n}} I^{coils}_{0,n'} \tag{2.32}$$

where $n' = n + \nu N_c$ and the index ν is spanning over the sidebands. Note that, for circular (poloidally symmetric) coils only toroidal sidebands are produced and therefore we don't have summation in m's. The coil shape factor $F_{0,n}$, relative to the $(0, n)$-mode, is related to the geometry and for infinitely thin coils can be simply calculated through the relaiton 2.11.

Infinitely thin coils have been assumed since their thickness is much smaller than the electromagnetic skin depth. The model through equations 2.29 and 2.32 is able to predict the "vacuum" field generated by the system of 48 toroidal coils (having only 12 independent currents) accounting for the effect of the conductive shell and of the sidebands.

2.4 The gain and the feedback

As well known [85], the control chain can be of two kinds. In the *open loop systems* the arbitrary $I(t)$ is pre-programmed (such situation is used for to estimate τ_w). In the *closed loop systems* $I(t)$ is determined by the feedback law.

There are essentially two models for the control. In the *intelligent shell control* the feedback law has the same gain for each harmonic. In practice, however, in the Intelligent Shell scheme the control system doesn't calculate harmonics. What is done is that each active coil tends to react to the measured radial field at the corresponding sensor in order to vanish it. It must be clear that the feedback system can cancel the measure of the mode, not the mode itself! In the RFPs the active feedback schemes are complicated because of the big number of MHD modes potentially unstable. In the *mode control* (*wide-shell control* or *targeted-mode control*) different gains for different set of modes are used; the sideband effect is partially mitigated.

2.4.1. The current control

We define the non-dimensional open-loop transfer function P_1 from the feedback current to the sensors (i.e from the "control current", that is the input signal, to the normalized field at the sensor), for each Fourier component:

$$P_1 = P_1^{m,n}(s) = \frac{b_{m,n}}{2b_{m,n}^{rad}} = \frac{\pi a}{\mu_0} \cdot \frac{b_{m,n}^{sens}(s)}{I_{m,n}}. \tag{2.33}$$

P_1 describes the response of the plasma-wall system to the current harmonic; s is the Laplace variable in the frequencies domain. For each Fourier component we have

$$P_1^{m,n}(s) = \sum_{m'=m+lM_c} \sum_{n'=n+pN_c} \frac{R_{m',n'}(s)}{s - \Gamma_{m,n}}. \tag{2.34}$$

The $\Gamma_{m,n}$ are the open loop growth rates for each mode, whereas the residuals R are functions of the geometry of the system (i.e shape coils and their

arrangement; this can be easily view utilizing the relation from 2.29 to 2.32). Let note that *the summations include all the sideband mode coupled by the system coils to the* (m, n)*-mode that we want to stabilize.* When the stabilization is restricted in a window narrower than $M_c \times N_c$ the different Fourier modes of the feedback system decouple. In this condition we can write the transfer function as

$$P_1^{m,n}(s) = \sum_{l=-\infty}^{+\infty} \sum_{p=-\infty}^{+\infty} S_{m',n'} M_{m',n'} a_{m',n'} c_{m',n'} \tag{2.35}$$

with $m' = m + lM_c$, $n' = n + pN_c$.

The harmonic $I_{m,n}$ of the control current is defined by $I_{j,k}$, that are the currents flowing in the feedback coils:

$$I_{m,n} = \sum_{j,k} I_{j,k} e^{-\imath(m\vartheta_j + n\varphi_k)} \tag{2.36}$$

where the summation includes all the coils and the coordinates (ϑ_j, φ_k) are referred to the center of the (j, k)-th feedback coil. In the current control system the field at the sensors is amplified by the controller $K(s)$ and then fed-back in order to obtain

$$I_{m,n} = -K_{m,n} \frac{\pi a}{\mu_0} b_{m,n}^{sensor}. \tag{2.37}$$

Said $K_{m,n}(s)$ the gain, it can study the stability properties of the transfer function in the complex field,

$$1 + K_{m,n}(s) P_1^{m,n}(s) = 0 \tag{2.38}$$

through standard control techniques [85][86].

2.4.2. The voltage control

A limitation of the current control is that the currents flowing in the coils are not influenced by the plasma behavior; on the contrary, the currents are determined by the control system. One can adjoint an internal feedback loop that control the voltage through the feedback coils, in order to produce the desired current. But is more convenient to plan a system that control directly the coils voltage (*volt control*), that is that really considers the self-inductance of the coils.

In the voltage control the relation between the voltage and the current in the coil is determined [47]. If the controller produce a voltage through the coil, included a resistance R, it is suitable to introduce a second transfer function $P_2(s)$. P_2 is defined by following:

$$P2 = \frac{L_f^c + L_f^{ext}}{L_f^0} \tag{2.39}$$

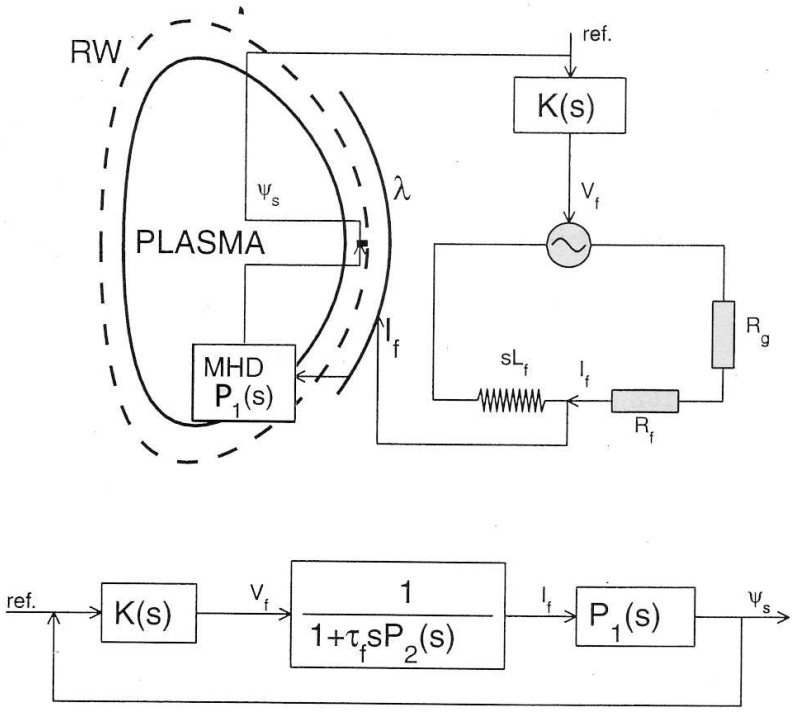

Figure 2.10: Representation of the geometry with the main feedback variables, taken from [79] (here is lacking).

where L_f^c is the inductance of the coils system, L_f^{ext} is the external inductance that also takes into account currents induced in the plasma and in the wall, L_f^0 is the standard self-inductance of a single coil [47].

The P_2 is introduced for every Fourier harmonic (m, n), $P_2^{m,n}(s)$. The properties of stability are given by 2.38 with $P_{tot}^{m,n}(s)$ instead of $P_1^{m,n}(s)$:

$$P_{tot}^{m,n}(s) = \frac{s\tau_f P_1^{m,n}(s)}{1 + s\tau_f P_2 m, n(s)}. \tag{2.40}$$

is the voltage control open-loop transfer function of the plasma-wall system, considering of the inductive voltage of the coils. The quantity τ_f is the temporal response of the feedback system (see also figure 2.10).

The inductive effects are important for the system response only for the modes that grow quickly enough(compared to the characteristic time of the coils[4]): only the more unstable modes, with $\gamma_{m,n}^{-1} \approx \tau_w$, are affected

[4]An actual coil corresponds exactly to a RL circuit, because of its internal resistance r; said l its inductance, the characteristic time $\tau_c = r/l$ is the time for which the current flowing in the coil and the voltage between the both ends of it reach full value, like the magnetic energy stored.

of it. For the slowly growing modes, $\gamma_{m,n}^{-1} \gg \tau_w$, the coils behave like simple resistance. Besides, the width of the windings influences weakly the coils-plasma coupling (that is: P_1), whereas is strong the influence on the self-inductance (that is: on P_2).

2.4.3. An example: application to the RWMs

It is important that the sideband effect not couple two unstable modes, for example RWM and TM. Considerations about stability and geometry [87] imply the conditions $M_c \geq 3$ and $N_c \geq \delta n = n_{max} - n_{min}$ for to avoid unstable couplings. If the number of feedback coils is equal or lower to the half of the number of the sensors is not possible to control independently each field harmonic. For example, if we have $\delta n = 16$, for a RFP with aspect ratio $A = 4$ the mode $(1, 15)$ will be coupled with the modes $(1, -11)$ and $(1, +21)$. Besides, with only an unstable mode the stabilization can be reached fed-backing only the signal of the unstable mode. A way for to "not disturb" the more unstable TMs, that is the mode with $-2 \leq n \leq +2$ for the RFPs with $A = 4$, is that to apply a null gain over them and fed-bach all the others.

CHAPTER 3

Results and conclusions

Now we propose, through the model developed and explained in the previously chapter, an analysis of the experimental data obtained in the RFX-mod device to shed some light in the mode coupling among magnetic perturbations. The model was implemented in Matlab®language.

3.1 Behavior of the $m = 0$ modes

Several experiments have been done in the past in the attempt of quantitatively determine the mode coupling in RFPs [63][88][66][89][90]. The peculiarity of our results is that this coupling is estimated by actively applying an m=0 perturbation to the plasma[1]. In this sense the experiments are similar to those performed in RFX, before its modification, and oriented at establishing the effect of mode coupling on the torque exerted on the plasma by an external perturbation [92].

3.1.1. Results in vacuum

To verify and validate the model, we first apply it to a set of vacuum shots, i.e. shots without plasma where however a non axi-symmetric current distribution over the toroidal field coils generates a non axi-symmetric toroidal field. For these experiments we compare the model calculated toroidal field with that measured by the 192 sensors, both in cases of applied rotating or non-rotating perturbations along the toroidal angle, as shown in the scheme of figure 3.1.

The analytical expression for the *growth rate* of a generic (m, n) mode implemented in our code, is that one defined by C. G. Gimblett in [93] and

[1]Part of this work was presented at 34^{th} EPS Conference on Plasma Physics hold in Warsaw, July 2007, and it is shown in [91].

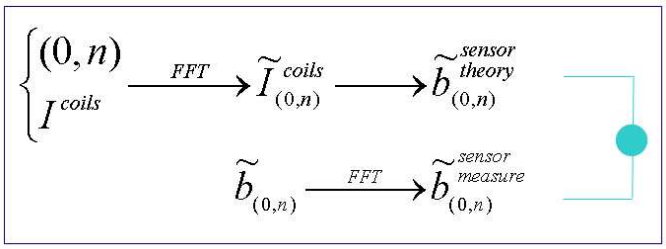

Figure 3.1: Work principle of the code for the vacuum shots.

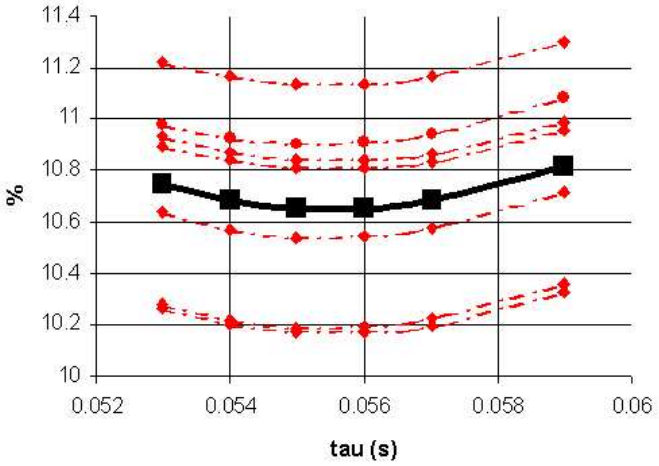

Figure 3.2: Δ_b vs. τ_w for different vacuum rotating shots in a selected experimental run session (circles are experimental data, squares is the average).

then used by R. Fitzpatrick [67] and by R. Paccagnella and P. Zanca [94]:

$$\Gamma_{m,n} = \frac{1}{2\tau}\frac{m^2 + n^2\epsilon_w^2}{n^2\epsilon_w^2}\frac{1}{K'_m(|n|\epsilon_w)I'_m(|n|\epsilon_w)}. \tag{3.1}$$

where I' and K' are the first derivative of Modified Bessel Functions. For the $m = 0$ modes it becomes:

$$\Gamma_{m,n} = -\frac{1}{\tau}\frac{1}{K_1(|n|\epsilon_w)I_1(|n|\epsilon_w)} \tag{3.2}$$

(I and K are the Modified Bessel Functions).

Another preliminary work is the *smoothing* of coil currents signals for the first parte of the discharge for each shot, because of the electrical noise and the initial spikes. For this purpose, we use the *Matlab*® function `polyfit`; we choose a polynomial polynomial of degree 6 for the data fit.

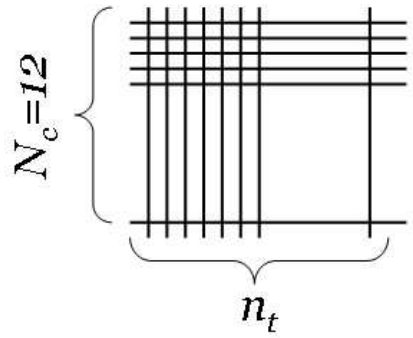

Figure 3.3: Grid for the Δ_b calculation, eq. 3.3.

As first step, we have determined the "effective" penetration time of the wall (which we leave as a free parameter in the model) by looking the minimum reconstruction error, that we called Δ_b (see below). In figure 3.2, the Δ_b versus τ_w is shown for different vacuum cases with an applied $(0, 4)$ slowly (10 Hz) rotating perturbation (the continuous thick curve represents the average). We found τ_w depending also on frequency (time) and not only on harmonics. In fact, for a fast rotating mode ($\omega\tau_{w,0} > 1$, where $\tau_{w,0}$ is τ_w calculated at $\omega = 0$) *the wall acts as a perfect conductor and the mode could not penetrate at all.* So it is not strange that the measured penetration time depends on rotation frequency, increasingly with it. In particular, we found a value of about $56ms$ for τ_w ($\omega = 10Hz$), while for a static perturbation this constant is around $36ms$. The perturbation applied are $(0, 4)$ modes. We defined the reconstruction error as follow:

$$\Delta_b = \frac{\sqrt{\frac{1}{\widetilde{n}-1}\sum_k \left(b_k^{meas} - b_k^{calc}\right)^2}}{b_0^{meas}} \tag{3.3}$$

where the sum is done over $\widetilde{n} = 12$ toroidal positions. The other quantities are the following: b^{calc} is the amplitude of the field generated by the coils; b^{meas} is the amplitude of the local field measured by the sensors; b_0^{meas} is the average amplitude of the measured field.

Let note that, because we have a matrix of values, i.e. the amplitudes of the magnetic field at any fixed times and any fixed spatial positions in φ like shown in figure 3.3, we must calculate the error 3.3 first along one direction and then along the other. The values obtained following the two different paths are very similar, as expected, and we use as effective value the average between them.

The error estimated by the equation 3.3 is similar for non-rotating and rotating perturbations and it is about 10-15% (for the best shots it is less

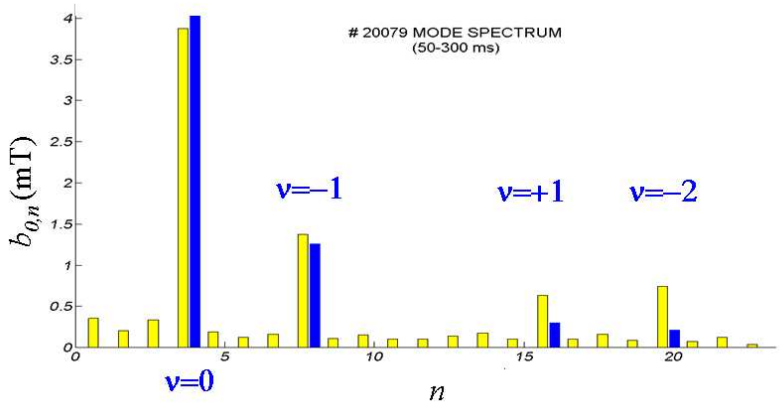

Figure 3.4: ♯20079 $m = 0$ mode spectrum. Toroidal components amplitudes averaged in the range $50 - 300ms$. Light bars: measured amplitudes; dark bars: calculated amplitudes. Indexes: ordering numbers of the geometrical sidebands.

than 10%, see figure 3.6). We think that this error is mainly related to the wall non homogeneities (gaps and pipes) and also to the aliasing effect, as will be discussed later. In figure **??** is depicted the three-dimensional comparison between the calculated toroidal magnetic field with the measured one. In the figure 3.1.1 we show the averaged amplitudes of harmonics in the time window of application of $(0, 4)$ mode: the clear effect of sideband generation due to the limited number of independent coils, as already discussed, is shown. Measured (light bars) and calculated amplitudes (dark bars) are compared. The indexes shown in the figure represent the sidebands (see equation 2.32). Note that $\nu = +2$ corresponds to the sideband $(0, 28)$ which is not measured and therefore, due to the aliasing, it folds up on the $(0, 4)$ mode, as explained in the paragraph 2.2.

Both measures and model calculate all sidebands, included the aliasing effects, produced by the finite number of measurements; this suggests that the differences between the measured and the calculated values in each harmonics can be understood as due to inhomogeneities. As to be expected, the error is stronger for high n's.

In figure , for the same shot of figure , the toroidal fields calculated by the model and measured by the sensors (left panels) and also Δ_b are plotted in the real space and in time. Note also that, as expected, in correspondence to the gap (at 112° in the toroidal angle) the calculated Δ_b is higher. Therefore we can conclude that the discrepancies between the calculated and measured values can be attributed on one side to the $n = 8$ and $n = 16$ aliasing, and secondly to the localized error at the gap.

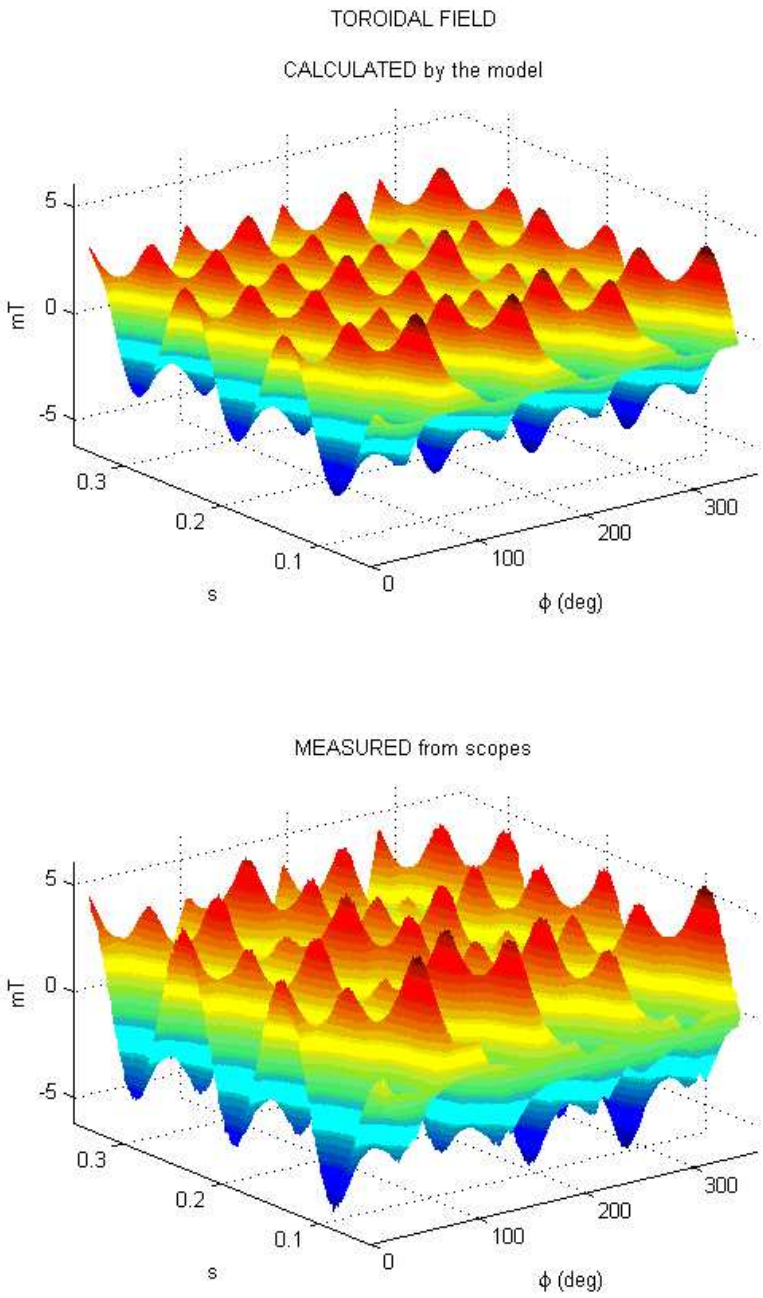

Figure 3.5: ♯20079: measured (bottom) and calculated (top) toroidal magnetic field.

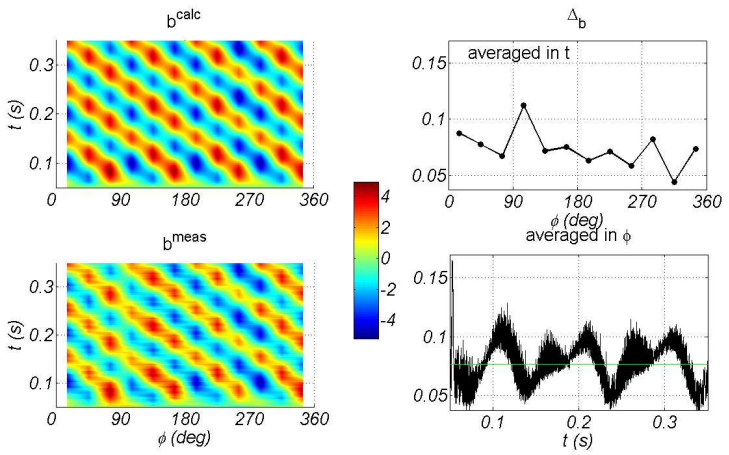

Figure 3.6: ♯20079 toroidal fields (left panels) calculated by the model and measured from the sensors, and Δ_b (right panels) vs. angle (top) and time (bottom).

By comparing the cylindrical model with the data we can in principle extract information about the effects induced by the toroidicity. We can estimate the last one observing that the amplitudes must be corrected by a factor R_0/R, where, we remember, R_0 is the major radius of the torus (see figure 1.10). Because $R = R_0 + a \cdot \cos\vartheta$, the corrective factor can be written as

$$\frac{R_0}{R} = \frac{R_0}{R_0 + r\cos\vartheta} = \frac{1}{1 + \epsilon\cos\vartheta} \tag{3.4}$$

with $\epsilon = r/R_0$. Developing in Taylor series, we obtain:

$$\begin{aligned} \frac{R_0}{R} \quad &\longrightarrow_{\epsilon\ll 1} \quad 1 - \epsilon\cos\vartheta + \frac{\epsilon^2}{2}\cos^2(\vartheta) - \frac{\epsilon^3}{4}\cos^3(\vartheta) + ... = \\ &= \quad 1 - \epsilon\cos\vartheta + \frac{\epsilon^2}{2}\left[\cos(2\vartheta) + 1\right] + \\ &- \quad \frac{\epsilon^3}{4}\left[\cos(3\vartheta) + 3\cos(\vartheta)\right] + ... \end{aligned} \tag{3.5}$$

Considering a generic (m, n) mode, equation 3.5 means that the toroidal geometry gives rise to the following corrections: at the 1st order on the $(1, 0)$ mode (main toroidal field correction); at the 2nd order both on the (m, n) and the $(2, 0)$ mode; and so on. The non-linear interactions between these modes and the (m, n) one, originate a correction at the 2nd order on the $(m + 1, n)$ and $(m - 1, n)$ modes, a correction at the 3rd order on the $(m+2, n)$ and $(m-2, n)$ modes, and so on. In our case, the $(0, 4)$ mode generates by coupling with the dominant $(1, 0)$ toroidal field correction, a $(0, 8)$

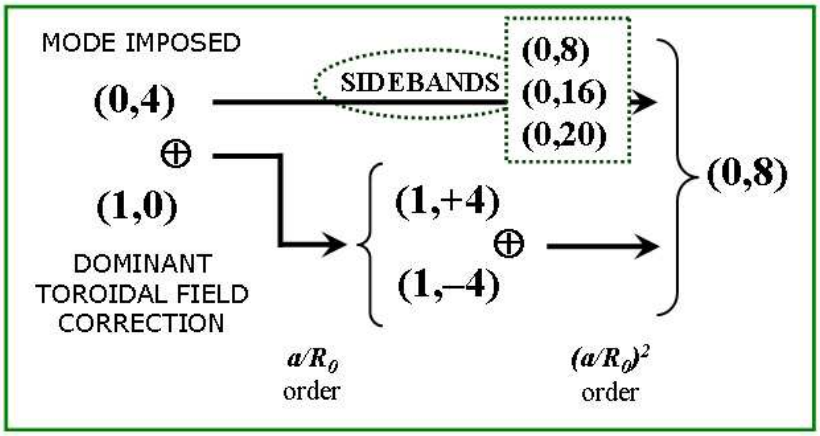

Figure 3.7: Coupling scheme of the modes with a (0,4) mode applied. It is highlighted both the production of sidebands and the toroidal effects.

mode with amplitude $(a/R_0)^2$ of the progenitor. Due to the choice of the applied perturbation ($n = 4$) and because of the already discussed sideband effect, the toroidally generated harmonic being much smaller than the $n = 8$ sideband, is however almost negligible. Coupling scheme is summarized in figure 3.7.

At this point, we have seen that the toroidal field and its geometrical sidebands are well reconstructed by the model; this allow us to apply it to the plasma shots.

3.1.2. Results with plasma

After validation, the model is applied to cases with plasma in order to extract information about the plasma generated $m = 0$ component in response to the applied perturbations. By calculating with the model the contribution of the coils and the sidebands effect, we can obtain the plasma response subtracting the calculated field to the measured sensor field. As an example, figure 3.8 shows the full $m = 0$ mode spectrum (averaged in a time interval which includes the current flat-top phase, in general between 100 and $200ms$) for a shot with an applied $(0, 1)$ rotating mode, before (top frame) and after (bottom frame) the subtraction of the coil and wall contribution, i.e. the net plasma response to the applied field. In the top frame the time measured averaged amplitudes are the light bars, whereas the calculated ones are the dark bars. The calculated $(0, 2)$ harmonic is the pure toroidal sideband in this case; it is, as expected (and already discussed) very small.

In figure 3.9, for this shot, the time-evolution of the coils generated field (dotted line) and the plasma calculated temporal response at the sensor

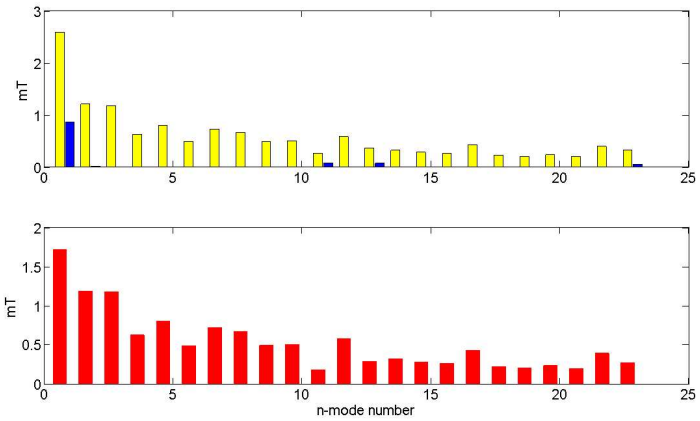

Figure 3.8: ♯19305 $m = 0$ mode spectrum, toroidal component amplitudes averaged in the range $10 - 192ms$. Top panel: light bars are measured amplitudes, dark bars are calculated ones. Bottom: net plasma response.

positions (continuous line), are shown. In the bottom panel of figure 3.9, the plasma $(0, 1)$ response (dotted line) is compared with the signal obtained from the difference between the $m = 1$ dominant modes, i.e the $m = 1, n = -7$ and the $m = 1, n = -8$ (dark thick curve). We subtract the amplitudes according to what we said about the wall locking in the paragraph 1.3.4, i.e. for the existence of a relation 1.63 between the two $m = 1$ phases.

It is seen that a good correlation in time between these two signals exists. This correlation can be expressed by calculating the *linear correlation coefficient*, defined in general as

$$\rho = \frac{\sigma_x y}{\sqrt{\sigma_{xx}\sigma_{yy}}}.$$

σ_{xy}, σ_{xx} and σ_{yy} are the usual covariance matrixes [95]. We know from the statistics that, for each defined ρ_0, $P_N(|\rho| \geq |\rho_0|)$ is the probability that N measures of two uncorrelated variables give a coefficient ρ as big as ρ_0. Obtaining ρ_0 such as $P_N(|\rho| \geq |\rho_0|)$ is small, then is improbable that our variables are uncorrelated, i.e. is indicated a correlation. This *no-correlation hypothesis test* indicates that we are in presence of a strong correlation between the two data sets considered; e.g., for the shot discussed above and the signals in figure 3.9, $\rho = 0.71$ with $\rho_0 = 0.05$.

Let note that for most of the shots, also the $m = 1$ with $n = -9 \div -12$ have a smaller but not completely negligible amplitude; this means that a full reconstruction of the $(0, 1)$ response should receive contributions also from other $m = 1$ modes.

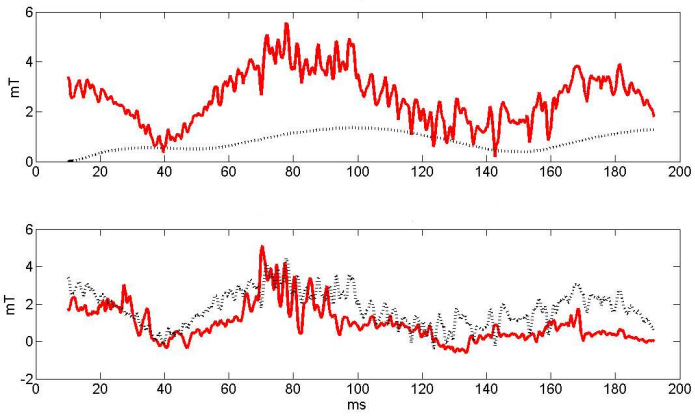

Figure 3.9: ♯19305, time-evolution of the toroidal component amplitudes. Top panel: $(0, 1)$ coils generated harmonic (dotted line); $(0, 1)$ measured harmonic (continuous line). Bottom: $(0, 1)$ plasma response (dotted line); $(1, -7) - (1, -8)$ difference (continuous line).

For comparison, we have also analyzed shots without any applied perturbation. In figure 3.10 for one of these shots the evolution of the $(0, 1)$ signal and the difference between the $m = 1$ dominant modes are compared; it can be seen that even in this case, the two curves are well correlated. This bring us to the conclusion that the $(0, 1)$ field is mainly due to the non-linear interaction of the $m = 1$ modes, with or without the applied $(0, 1)$ perturbation. Therefore we can conclude, not only that the $m = 0$ plasma response is stable, but also that the indirect action of the applied $m = 0$ field has no destabilizing effect on $m = 0$ and $m = 1$ modes.

In many shots peaks, in the trace obtained from the difference of the two $m = 1$ dominant modes, due to the sawtooth activity of the $n = -7$ mode, are present (figure 3.12), while the $(0, 1)$ response does not show these sharp peaks, since the $m = 1, n = -8$ mode does not oscillate in time following the $n = -7$. In any case, even for these shots, the $(0, 1)$ plasma response fits reasonably well the envelope of the difference of the two dominant $m = 1$ modes, as seen in figure 3.12.

Some of the harmonics of the $m = 0$ spectrum (see figure 3.8) can be related (at least in part) to the coupling of the two $m = 1$ modes with the dominant $(1, 0)$ toroidal correction, which generates two $m = 0$, $n = 7, 8$ modes with amplitudes of the order (a/R_0) of their progenitors. Finally, the interaction with the applied $(0, 1)$ of the toroidicity generated modes, can also produce (but in this case only at the second order in the inverse aspect ratio expansion) the $(0, 6)$ and $(0, 9)$ harmonics (see figure 3.8). All these

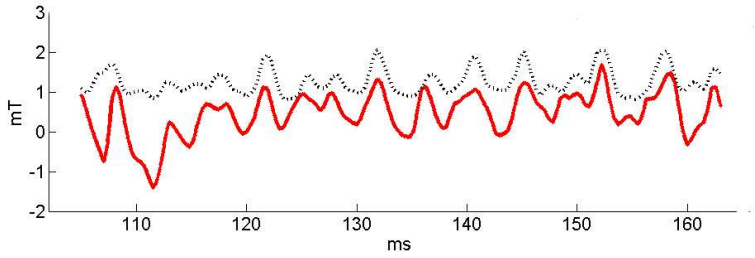

Figure 3.10: ♯19353, time-evolution of the toroidal component amplitudes: the dotted line is the $(0, 1)$ mode ,continuous line represents the $(1, -7) - (1, -8)$ difference.

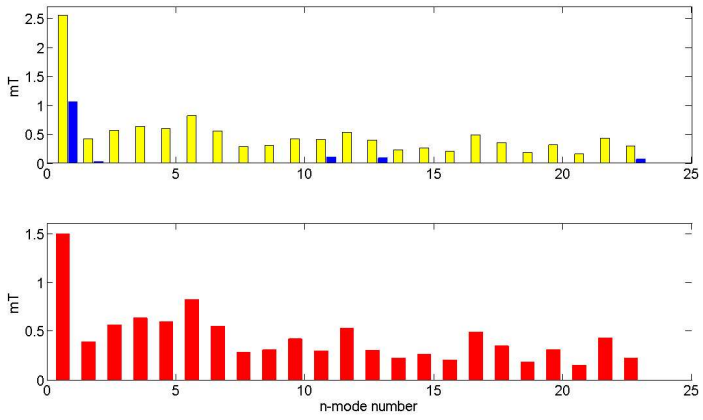

Figure 3.11: ♯19318 $m = 0$ mode spectrum, toroidal component amplitudes averaged in the range $10 - 260ms$. Top panel: light bars are measured amplitudes, dark bars are calculated ones. Bottom: net plasma response.

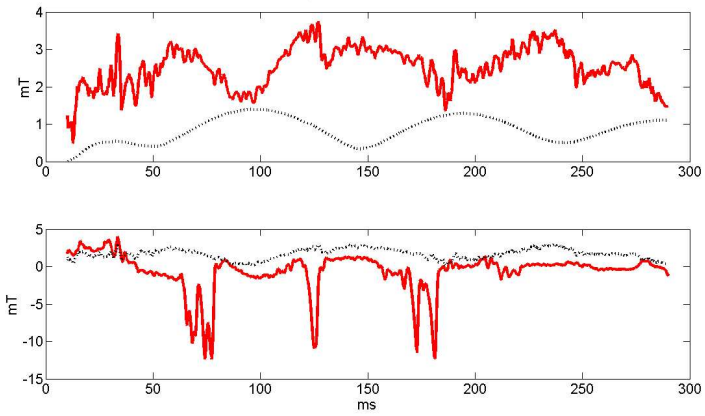

Figure 3.12: ♯19318, time-evolution of the toroidal component amplitudes. Top panel: $(0,1)$ coils generated (dotted line); $(0,1)$ measured mode (continuous line). Bottom: $(0,1)$ plasma response (dotted line); $(1,-7)-(1,-8)$ difference (continuous line).

interactions are better summarized in the figure 3.13.

It is clear from the comparison of the above scheme with the measured spectrum of $m = 0$ modes (see figure 3.8 bottom frame) that there are many other harmonics that can not be accounted for by the interactions of the dominant $m = 1$ modes with the applied $m = 0$, for example the modes in the range $2 \leq n \leq 5$, which are of comparable amplitude with the $n = 1$. The amplitudes of these secondary modes have been related in [52], to the strong non-linear coupling of $m = 1$ modes. However we note that in our cases it is difficult to justify the relatively high amplitude of these modes only as a result of the $m = 1$ non-linear interaction. A possible alternative/additional explanation could be the development of these modes during the RFP formation phase, where relatively high $m = 0$ fluctuations are generally measured [96].

3.2 Discussion and conclusions

3.2.1. Discussion of the m=0 model

In this thesis we have described a model for calculating the plasma response to an applied $m = 0$ perturbation in the RFX-mod device. Initially the model has been validated for vacuum shots with applied static and rotating perturbations. The model reproduce perfectly the $m = 0$ spectrum, with all the sidebands observed (except to the background noise). Again, a simple

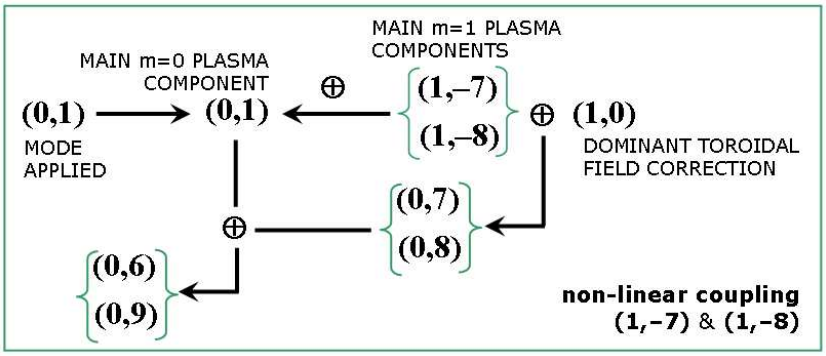

Figure 3.13: Coupling scheme of the main modes, with a (0,1) mode applied.

estimation permit to consider the so-called "toroidal sidebands" (sidebands due to the curvature effect) negligible. Also the main gap of the mechanical structure of the device is noticed by the model (this can seen by the reconstruction error curve). Last, for this first part, we have observed a frequency-dependence of the wall penetration time.

Next, we analyzed plasma pulses, in the attempt of obtaining information about the plasma response to the imposed $m = 0$ non axi-symmetric field. The analyzed data have allowed to extract important information.

First, the $m = 0$ response, once that the externally generated field has been subtracted from the measurements, can be interpreted mainly as the result of the non-linear coupling between the two adjacent $m = 1$ dominant modes. This outcome is expected to the theoretical study in [55] and also agrees with similar experiments reported in [92]. This also confirms the expectation of no intrinsic $m = 0$ unstable response [97], at least for the shallow F values (where, we remember, F is the reversal parameter) in the range $-0.1 < F < -0.05$ considered in these analysis. In fact if F is shallow, the reversal surface of the mean toroidal magnetic field, which corresponds to the $m = 0$ resonance radius, is very close to the wall. In agreement with the predictions, these modes are therefore very efficiently stabilized.

An experimental confirmation of this stable $m = 0$ response has been recently obtained in MST, the Madison RFP device. For this purpose see the S. C. Prager's work [98], where the $m = 0$ mode is considered responsible of the edge dynamo current: despite such mode mediate the non-linear coupling between different $m = 1$ that did generate itself, it is found linearly stable. We should however mention that m=0 modes have been found unstable during the plasma setting up [96].

An unstable response of the $m = 0$ modes is expected possibly at deeper F values. In this case the model (particularly the function $M_{0,n}$) should be

modified to take into account the $m = 0$ modes growth rates. Since however, as we have shown in this thesis, $m = 0$ and $m = 1$ modes are, in many cases, very well coupled together, it is not guaranteed that a linear response model, as that presented here, could be used to predict the behavior of the unstable $m = 0$ modes. This subject will be left for future studies.

Regarding the physical relevant dynamo problem, we have shown that in the MH case, when many modes are simultaneously present at relatively large amplitude (this correspond to the fully non-linear case), a big contribution to the $(0, 1)$ mode is produced by the non-linear interaction of the two dominant on-axis resonant $m = 1$ modes. This is inferred by the correlation between the $(0, 1)$ plasma signal and the signals of the dominant $(1, n)$ adjacent modes.

On the basis of this result one could speculate that the dynamo electric field (needed especially near the reversal of the mean toroidal magnetic field [30] where the $m = 0$ modes have their resonance) can be linked to this interaction. This conclusion was reached in several papers [88][66][89][99] where different mechanisms of interactions were also formulated, even with the contribute of the first wall.

Moreover, for experimental cases where a single mode dominates the spectrum (in most cases in an oscillatory quasi periodic way), the non-linear $m = 1$ coupling seems not to explain satisfactorily the observed $(0, 1)$ behavior (and the correlation index between $(0, 1)$ signal and the signal difference of the adjacent main $m = 1$, is very low). In this cases the observations seem to suggest a dynamo activity where the $(0, 1)$ mode plays a modest or no role at all, as found also in non-linear simulations [54]. This conclusion is in agreement with A. K. Hansen's experiments [65] where the $m = 0$ mode response has been made very weak by changing the plasma equilibrium. In this case no difference on the behavior of the dominant m=1 mode (and in general on the dynamo) has been found, apart from the beneficial effect of the absence of mode deceleration at the crash of the dominant $m = 1$ mode, indicating again the $(0, 1)$ as an important "player" in the torque balance [92][69] more than as a driver of the dynamo. In particular, in [69] the electromagnetic torque is considered as produced by a non-linear coupling of the modes.

We underline again that *in any case, the action of the applied* $m = 0$ *field on the* $m = 1$ *modes has no destabilizing effect*, or, in other words, we have not amplification of the $(0, 1)$ applied field (and in fact the "plasma response" is stable).

Anyhow, it remains open the following crucial question: what is the role of the $(0, 1)$ mode for the dynamo activity?

3.2.2. About $m = 1$ model and Final remarks

At present, a wider version of this code, extended also to $m = 1$ modes, is carrying out. This extension involves:

- different shape factor for the coils (see page 54 and followings);
- the presence of both poloidal and toroidal sidebands (contrary to the $m = 0$ case, where we have only toroidal sidebands);
- different transfer function, ever also with respect to the $m = 0$ case.

For this purpose, a large set of data form EXTRAP-T2R (Stockholm) has been collected.

With regard the $m = 0$ model, we can say that by means of a relatively simple model, interesting physical information can be extracted from the analysis of MHD experiments, where external perturbations are actively applied to the plasma.

It is clear that more systematic experiments are needed (and auspicated) to firmly establish a conclusion on the dynamo problems and the role of the different modes. In particular: experiments with more deeper F (i.e with more deeper reversal); homogeneus sets of vacuum and plasma shots for a better validation; application to different experiments. About the last point, we must remark the impossibility to test this model on EXTRAP-T2R machine, where the author spent a short mobility period, because its control system can not generates $m = 0$ modes.

Another interesting application could be the use of this code to estimate the relative phases between the modes. This can be do putting together the main result obtained in this work (i.e that the $m = 0$ has no effect, under our operative condition, to the $m = 1$ modes) with the phase locking relation existing in the RFP devices. The idea is still in the embryo stage, but could be promising.

CHAPTER A

Appendixes

A.1 The Fourier transform for $\Theta_{\pm}$

For to obtain the equation 2.10 we must calculate the Fourier transform for the quantity $\Theta_{\pm}$. We have:

$$\begin{aligned}
&\int_{-\infty}^{+\infty} \Theta_{\pm} e^{-\imath n\varphi} d\varphi = \\
&= \int_{\varphi_k-\delta\varphi/2}^{\varphi_k-\delta\varphi/2} e^{-\imath n\varphi} d\varphi = \\
&= -\frac{1}{\imath n}\left[e^{-\imath n\varphi}\right]_{\varphi_k-\delta\varphi/2}^{\varphi_k-\delta\varphi/2} = \\
&= -\frac{1}{\imath n}\left[e^{-\imath n\varphi_k}\left(e^{-\imath n\varphi/2} - e^{+\imath n\varphi/2}\right)\right] = \\
&= -\frac{1}{\imath n} e^{-\imath n\varphi_k}(-2\imath)\sin\left(n\delta\phi/2\right) = \\
&= \delta\varphi \frac{\sin\left(n\delta\varphi/2\right)}{n\delta\varphi/2} e^{-\imath n\varphi}.
\end{aligned}$$

A.2 The jump condition for b_φ and b'_φ

Let consider a cylindrical reference frame (r, ϑ, φ) with $\varphi = z/R_0$ simulated azimuthal angle. Let be all the quantities expanded in Fourier series, like in the equation 2.15:

$$\psi(r, \vartheta, \varphi; t) = \sum_{m,n} \psi^{m,n}(r; t) \cdot e^{-\imath(m\vartheta + n\varphi)},$$

where ψ is a generic quantity. For to make easier the reading further, hereafter the indication of m and n will be understood [1].

[1] Again, called x a generic quantity, r a generic radius (r^+ and r^- are the outer and

A.2.1. The jump in r_c

Let consider a current wire with thickness $\delta_c = r_c^+ - r_c^-$, where the current flows only along ϑ, and resistivity $\eta \equiv \eta_\vartheta$ ($E_\vartheta = \eta j_\vartheta$ whereas $E_r = E_\varphi = 0$). Let suppose, as well, that such current is constant ($j_\vartheta = constant$).

From Faraday's law $\partial\overrightarrow{B}/\partial t = -\nabla \times \overrightarrow{E}$ we have:

$$\begin{aligned}
\frac{\partial b_r}{\partial t} &= \imath\frac{n}{R_0}\eta j_\vartheta \\
\frac{\partial b_\vartheta}{\partial t} &= 0 \\
\frac{\partial b_\varphi}{\partial t} &= -\eta\left[\frac{j_\vartheta}{r} + \frac{\partial j_\vartheta}{r}\right] = -\eta\frac{j_\vartheta}{r}.
\end{aligned}$$

From Ampère's law $\nabla \times \overrightarrow{B} = \mu_0\overrightarrow{J}$ we have:

$$\begin{aligned}
\frac{m}{n}b_\varphi &= \frac{r}{R_0}b_\vartheta \\
\imath\frac{n}{R_0} - \frac{\partial b_\varphi}{\partial r} &= \mu_0 j_\theta \\
\frac{\partial\left(r b_\vartheta\right)}{\partial r} &= \imath m b_r.
\end{aligned}$$

At last, the conservation of charge, $\nabla \cdot \overrightarrow{B} = 0$, gives:

$$\frac{\partial\left(r b_r\right)}{\partial r} + \imath\frac{nr}{R_0}b_\varphi = 0.$$

---

the inner side) and δ the width of a thickness placed in r, we can consider the following 1st order approximation:

$$\begin{aligned}
\Big[rx\Big]_{r^-}^{r^+} &= r^+x^+ - r^-x^- = \\
&= \ r^- + \delta\ \ x^+ - r^-x^- = \\
&= \ r^-\ \ x^+ - x^-\ \ + \delta\cdot x^+ \cong \\
&\cong \ r\Big[x\Big]_{r^-}^{r^+}.
\end{aligned}$$

The case $m = 0$

The whole set of equations, for the modes $(0, n)$, give us:

$$\begin{aligned}
&\frac{\partial b_r}{\partial t} = \imath \frac{n}{R_0} \eta j_\vartheta \\
&\frac{\partial b_\varphi}{\partial t} = -\eta \frac{j_\vartheta}{r} \\
&\frac{r}{R_0} b_\vartheta = 0 \rightarrow b_\vartheta = 0 \\
&\imath \frac{n}{R_0} b_r - \frac{\partial b_\varphi}{\partial r} = \mu_0 j_\vartheta \\
&\frac{\partial (r b_r)}{r} = -\imath \frac{nr}{R_0} b_\varphi.
\end{aligned} \tag{A.1}$$

By integrating A.1 from r_c^- to r_c^+ and remembering that the current flowing in the coil is related to the current density by the relation

$$j_\vartheta = \frac{I_c}{2\pi r_c \delta_c} \tag{A.2}$$

we obtain:

$$\begin{aligned}
\int_{r_c^-}^{r_c^+} \frac{\partial b_\varphi}{\partial r} dr &= \imath \frac{n}{R_0} \int_{r_c^-}^{r_c^+} b_r dr - \mu_0 \int_{r_c^-}^{r_c^+} j_\vartheta dr; \\
\Big[b_\varphi \Big]_{r_c^-}^{r_c^+} &= \underbrace{\imath \frac{n}{R_0} \int_{r_c^-}^{r_c^+} b_r dr}_{0} - \mu_0 \frac{I_c}{2\pi r_c \delta_c} \delta_c; \\
\Big[b_\varphi \Big]_{r_c^-}^{r_c^+} &= -\mu_0 \frac{I_c}{2\pi r_c}.
\end{aligned} \tag{A.3}$$

For the condition on the field's derivative, we obtain:

$$\begin{aligned}
\Big[b_\varphi \Big]_{r_c^-}^{r_c^+} &= -\mu_0 \Big[j_\vartheta \Big]_{r_c^-}^{r_c^+} = -\mu_0 \left[-\frac{\imath R_0}{n} \frac{\partial b_r}{\partial t} \right]_{r_c^-}^{r_c^+} = \\
&= \frac{\imath R_0 \mu_0}{n} \frac{\partial \Big[b_r \Big]_{r_c^-}^{r_c^+}}{\partial t} = 0.
\end{aligned} \tag{A.4}$$

A.2.2. The jump in r_w

Let consider a resistive shell with thickness $\delta_w = r_w^+ - r_w^-$, where the current flows along both ϑ and φ; η_ϑ and η_φ are the resistivities ($E_\vartheta = \eta j_\vartheta$, $E_\varphi = \eta j_\varphi$ whereas $E_r = 0$).

Besides to the previously equations, we must consider that $\nabla \cdot \overrightarrow{j} = 0$:

$$\frac{\partial (r j_r)}{\partial r} + \imath m j_\vartheta = 0 \rightarrow j_\vartheta = -\frac{nr}{mR_0} j_\varphi. \tag{A.5}$$

It is clear that for $m = 0$ the last equation diverges and so, in that case, it is not used. Moreover, we remember the condition for the radial field's derivative [**?**]:

$$\left[b_r'\right] = \frac{\tau_w}{r_w} \frac{\partial b_r}{\partial t} \tag{A.6}$$

where τ_w is the wall penetration time of the field, defined in 1.57.
From Faraday's law we have:

$$\begin{aligned}
\frac{\partial b_r}{\partial t} &= \imath \frac{m}{r} \eta_\varphi j_\varphi + \imath \frac{n}{R_0} \eta_\vartheta j_\vartheta \\
\frac{\partial b_\vartheta}{\partial t} &= \eta_\varphi \\
\frac{\partial b_\varphi}{\partial t} &= -\eta_\vartheta \frac{j_\vartheta}{r}.
\end{aligned}$$

From Ampère's law we have:

$$\begin{aligned}
\imath \frac{n}{R_0} b_r - \frac{\partial b_\varphi}{\partial r} &= \mu_0 j_\theta \\
\frac{1}{r} \frac{\partial (r b_\vartheta)}{\partial r} - \frac{\imath m}{r} b_r &= \mu_0 j_\varphi
\end{aligned}$$

and the equation

$$\frac{m}{n} b_\varphi = \frac{r}{R_0} b_\vartheta$$

that is not usable in the case $m = 0$ because it produces a singularity.
At last, the divergence of $\overrightarrow{B}$ is ever:

$$\frac{\partial (r b_r)}{\partial r} + \imath \frac{nr}{R_0} b_\varphi = 0.$$

The case $m = 0$

The whole set of equations, for the modes $(0, n)$, is similar to the one obtained for the jump in r_c [2]. In particular, we consider the equation A.1 and the equation

[2] It is clear that for $m = 0$ the resistivity is uniquely that poloidal one.

$$\frac{\partial\left(rb_r\right)}{r} = \imath\frac{nr}{R_0}b_\varphi. \tag{A.7}$$

From the relation above we can link the jump of the radial magnetic field to that of the toroidal magnetic field:

$$\begin{aligned}
\frac{\partial\left(rb_r\right)}{r} = b_r + rb'_r &= \imath\frac{nr}{R_0}b_\varphi; \\
\underbrace{\Big[b_r\Big]_{r_w^-}^{r_w^+}}_{0} + \Big[rb_r\Big]_{r_w^-}^{r_w^+} &= i\frac{n}{R_0}\Big[rb_\varphi\Big]_{r_w^-}^{r_w^+}; \\
\Big[b_r\Big]_{r_w^-}^{r_w^+} &= i\frac{n}{R_0}\Big[b_\varphi\Big]_{r_w^-}^{r_w^+}.
\end{aligned} \tag{A.8}$$

By substituting for $\Big[b_r\Big]_{r_w^-}^{r_w^+}$ the condition obtained in [**?**], we can link the variation in time of the radial field to the jump of the toroidal field:

$$\tau_w\frac{\partial b_r}{\partial t} = \imath\frac{nr_w}{R_0}\Big[b_\varphi\Big]_{r_w^-}^{r_w^+}. \tag{A.9}$$

We can express $\partial b_r/\partial t$ as function of j_ϑ and j_ϑ, in its turn, as function of $\partial b_\varphi/\partial t$. So, at the end, we obtain the condition for the jump of the toroidal magnetic field:

$$= \Big[b_\varphi\Big]_{r_w^-}^{r_w^+} = \tau_w\frac{\partial b_\varphi}{\partial t}. \tag{A.10}$$

In order to obtain the jump condition for the radial derivative of the toroidal magnetic field, we start from the equation A.1, and we calculate the jump of the quantities through the shell:

$$\imath\frac{n}{R_0}\underbrace{\Big[b_r\Big]_{r_w^-}^{r_w^+}}_{0} - \Big[b'_\varphi\Big]_{r_w^-}^{r_w^+} = \mu_0\Big[j_\vartheta\Big]_{r_w^-}^{r_w^+}.$$

For a poloidal current density constant in the shell, the last equation leads to the continuity of the radial derivative of the toroidal magnetic field, $\Big[b'_\varphi\Big]_{r_w^-}^{r_w^+} = 0$.

In other way, we can utilize again the relation A.7 and the relation that links the poloidal current density to the temporal derivative of the toroidal magnetic field,

$$\frac{\partial b_\varphi}{\partial t} = -\eta_\vartheta \frac{j_\vartheta}{r}.$$

From this, and some simple but boring algebra, we find again the continuity of b'_φ.

List of Figures

List of Figures

Bibliography

[1] `http://www.energy.gov`.

[2] J. Ongena and G. van Oost. *Transactions of Fusion Science and Technology*, 53:3, 2008.

[3] `http://www.unibg.it/dati/corsi/9415/6319`.

[4] `http://www.fusion-eur.org`.

[5] World Energy Council. *2007 Survey of Energy Resources*. WEC, 2008.

[6] `http://www.aspo.it`.

[7] `http://www.eia.doe.gov/international`.

[8] M. Westra and S. Kuyvenhoven. *Energy, Powering Your World*. EFDA-FOM, 2002.

[9] World population prospects: the 1994 revision. Technical report, United Nations Population Division, 1994.

[10] `http://www.ipcc.ch`.

[11] F. Joos. *Europhysics News*, 27:213, 1996.

[12] M. E. Mann, R. S. Bradley, and M. K. Hughes. *Geophys. Res. Lett.*, 26:213, 1999.

[13] `http://antwrp.gsfc.nasa.gov/apod/archivepix.html`.

[14] T. J. M. Boyd and J. J. Sanderson. *The Physics of Plasmas*. Cambridge University Press, 2003.

[15] R. J. Goldston and P. H. Rutherford. *Introduction to Plasma Physics*. Institute of Physics, 1995.

[16] A. Ünsold and B. Baschek. *The New Cosmos*. Springer-Verlag, 4th edition, 1991.

[17] V. Castellani. *Astrofisica stellare*. Zanichelli, 1985.

[18] R. R. Weynants. *Transactions of Fusion Science and Technology*, 53:37, 2008.

[19] `http://www.kayelaby.npl.co.uk/`.

[20] G. van Oost and E. Rebhan. *Transactions of Fusion Science and Technology*, page 16, 2008.

[21] F. Auriemma. *Particle transport in Reversed Field Pinch plasmas*. PhD thesis, Università di Padova, Scuola di Dottorato di Ricerca in Ingegneria Industriale - Indirizzo Energetica - Ciclo XX, 2007.

[22] J. D. Lawson. *Proc. Phys. Soc. B*, 70:6, 1957.

[23] J. Wesson. *Tokamaks*. Claredon Press, 1987.

[24] `http://www.iter.org`.

[25] D. J. Campbell. *Phys. Plasmas*, 8:2041, 2001.

[26] J. P. Freidberg. *Plasma Physics and Fusion Energy*. Cambridge Press, 1987.

[27] J. P. Freidberg. *Reviews of Modern Physics*, 64:801, 1982.

[28] W. K. Hogan. *Nucl. Fusion*, 44, 2004.

[29] H. Alfvén. *Cosmical Electrodynamics*. Oxford University Press, 1951.

[30] S. Ortolani and D. D. Schanck. *Magnetohydrodynamics of Plasma Relaxation*. World Scientific, Singapore, 1993.

[31] `http://www.upei.ca/home/`.

[32] J. B. Taylor. *Phys. Rev. Lett.*, 33:1139, 1974.

[33] L. Woltjer. *Rev. Mod. Phys.*, 32:914, 1960.

[34] B. Alper et al. *Plasma Phys. Control. Fusion*, 31:205, 1989.

[35] R. Paccagnella. *Nucl. Fusion*, 38:1067, 1998.

[36] A. Cravotta. *Magnetic topology around the $q = 0$ surface in the Reversed Field Pinch and its influence on transport*. PhD thesis, Università di Padova, Scuola di Dottorato di Ricerca in Fisica - Ciclo XVIII, 2005.

[37] H. Ji et al. *Phys. Rev. Lett.*, 73:668, 1994.

[38] G. Bateman. *MHD instabilities*. The MIT Press, 1978.

[39] M. D. Kruskal and M. Schwarzschild. *Proc. Roy. Soc.*, A223:348, 1954.

[40] C. Mercier G. Laval and R. Pellat. *Nucl. Fusion*, 5:156, 1965.

[41] W. A. Newcomb. *Annals of Physics*, 10:232, 1960.

[42] D. C. Robinson. *Plasma Phys.*, 13:439, 1971.

[43] D. C. Robinson. *Nuclear Fusion*, 18:939, 1978.

[44] S. Lundquist. *Ark. F. Fys.*, 5:297, 1952.

[45] E. J. Caramana D. D. Schnack and R. Nebel. *Phys. Fluids*, 28:321, 1985.

[46] J. R. Drake. Experiments on feedback control of multiple resistive wall modes comparing different active coil arrays and sensor types. Technical report, Alfven Laboratories, Stockholm, 2006.

[47] D. Gregoratto, R. Paccagnella, and Y. Q. Liu. *Nucl. Fusion*, 44:1, 2004.

[48] D. Gregoratto et al. *Phys. Plasmas*, 12:092510, 2005.

[49] A. B. Rechester and M. N. Rosenbluth. *Phys. Rev. Lett.*, 40:38, 1978.

[50] D. Biskamp. *Magnetohydrodynamic Turbulence*. Cambridge University Press, 2003.

[51] P. Piovesan et al. *Physics Rewiev Letters*, 93:235001, 2004.

[52] P. Martin et al. *Phys. Plasmas*, 7:1984, 2000.

[53] P. Martin et al. *Nucl. Fusion*, 43:1855, 2003.

[54] K. Kusano and T. Sato. *Nucl. Fusion*, 27:821, 1987.

[55] K. Kusano and T. Sato. *Nucl. Fusion*, 30:2075, 1990.

[56] S. Cappello. *Plasma Phys. Control. Fusion*, 46:B313, 2004.

[57] K. Kusano et al. *Nucl. Fusion*, 31:1923, 1991.

[58] A. Buffa et al. In *21st EPS Conference on Controlled Fusion and Plasma Physics, Montpellier*, volume 18B, page 458, 1994.

[59] A. F. Almagri et al. *Phys. Fluids B*, 4:4080, 1992.

[60] G. Hedin et al. *Plasma Phys. Control. Fluids*, 40:1529, 1998.

[61] R. Fitzpatrick. *Nucl. Fusion*, 33:1049, 1993.

[62] D. J. Den Hartog et al. *Phys. Plasmas*, 2:2281, 1995.

[63] K. Hattori et al. *Phys. Fluids*, B3:3111, 1991.

[64] R. Fitzpatrick. *Phys. Plasmas*, 6:1168, 1999.

[65] A. K. Hansen et al. *Phys. Rev. Lett.*, 85:3408, 2000.

[66] J. S. Sarff et al. *Physics of Fluids B*, 7:2540, 1993.

[67] R. Fitzpatrick and E. P. Yu. *Phys. Plasmas*, 6:3536, 1999.

[68] R. Fitzpatrick and E. P. Yu. *Phys. Plasmas*, 7:3610, 2000.

[69] P. Zanca et al. *Physics of Plasmas*, 8:516, 2001.

[70] R. Fitzpatrick and P. Zanca. *Phys. Plasmas*, 9:2707, 2002.

[71] G. Rostagni. *Fusion Eng. Des.*, 25:301, 1995.

[72] P. Sonato et al. *Fusion Eng. Des.*, 25(301), 2003.

[73] S. Martini et al. *Nucl. Fusion*, 47:783, 2007.

[74] R. Paccagnella et al. *Phys. Rev. Lett.*, 95:075001, 2006.

[75] S. Ortolani and the RFX team. *Plasma Phys. Control. Fusion*, 48:B371, 2006.

[76] `http://www.igi.cnr.it/`.

[77] P. R. Brunsell et al. *Phys. Plasmas*, 10:3823, 2003.

[78] R. Paccagnella, D. Gregoratto, and A. Bondeson. *Nucl. Fusion*, 42:1102, 2002.

[79] A. Bondeson et al. *Nucl. Fusion*, 41:455, 2001.

[80] R. Fitzpatrick. *Phys. Plasmas*, 4:2519, 1999.

[81] Y. Q. Liu and A. Bondeson. *Phys. Rev. Lett.*, 84:907, 2000.

[82] G. Marchiori et al. *Fusion Engineering and Design*, page 691, 2003.

[83] J. D. Jackson. *Classical Electrodynamics*. John Wiley and Sons, 1998, 3rd edition.

[84] A. Falaschi. *Elementi di Trasmissione dei Segnali e Sistemi di Telecomunicazioni*. eBook, 2006.

[85] G. F. Franklin, J. D. Powell, and A. Emami-Naeini. *Feedback Control of Dynamic Systems, IV edition*. Prentice-Hall, 2002.

[86] J. Bechhoefer. *Review Modern Physics*, 77:783, 2005.

[87] A. H. Boozer. *Review Modern Physics*, 76:1071, 2004.

[88] S. Hoking et al. *Phys. Fluids B*, 3:2241, 1991.

[89] D. J. Den Hartog et al. *Phys. Plasmas*, 6:1813, 1999.

[90] P. Nordlund and P. Mazur. *Phys. Plasmas*, 1:4032, 1994.

[91] A. Pizzimenti and R. Paccagnella. *Plasma Phys. Control. Fusion*, 50:065006, 2008.

[92] R. Bartiromo et al. *Physical Review Letters*, 83:1779, 1999.

[93] C. G. Gimblett. *Nucl. Fusion*, 26:617, 1986.

[94] R. Paccagnella and P. Zanca. Technical Report FC/57, Consorzio RFX, Padova, June, 20 2001.

[95] P. R. Bevington and D. K. Robinson. *Data Reduction and Error Analysis for the Physical Sciences*. McGraw-Hill, 2003.

[96] P. Zanca et al. *Plasma Phys. Control. Fusion*, 48:407, 2006.

[97] Z. X. Jiang, A. Bondeson, and R. Paccagnella. *Phys. Plasmas*, 2:442, 1995.

[98] S. C. Prager et al. *Nucl. Fusion*, 45:S276, 2005.

[99] B. E. Chapman et al. *Physics of Plasmas - Letters*, 3:709, March 1996.